A STUDY OF ENHANCED ENERGY CAPTURE BY A VERTICAL AXIS WIND TURBINE IN AN URBAN/SUBURBAN ENVIRONMENT

by

Lam Trung Nguyen

A dissertation submitted to the faculty of
The University of Utah
in partial fulfillment of the requirements for the degree of

Doctor of Philosophy

Department of Mechanical Engineering

The University of Utah

August 2017

The University of Utah Graduate School

STATEMENT OF DISSERTATION APPROVAL

The dissertation of **Lam Trung Nguyen**

has been approved by the following supervisory committee members:

Meredith Metzger	, Chair	**1 May, 2017** Date Approved
Eric Pardyjak	, Member	Date Approved
Marc Calaf	, Member	**1 May, 2017** Date Approved
Amanda Smith	, Member	**1 May, 2017** Date Approved
Steven Burian	, Member	**1 May, 2017** Date Approved

and by **Timothy A. Ameel** , Chair/Dean of

the Department/College/School of **Mechanical Engineering**

and by David B. Kieda, Dean of The Graduate School.

ABSTRACT

Wind conditions within the urban environment have been found to be more turbulent than that in rural areas, due to the increased surface roughness caused by the presence of buildings, houses, and trees. Furthermore, winds in the urban environment are typically characterized by gusts with large fluctuations in magnitude/direction that contain a substantial amount of energy. Development of a vertical axis wind turbine (VAWT) to exploit this turbulent wind energy could yield a significant increase in the total amount of energy captured annually, thus making VAWTs a viable renewable energy technology in urban areas. One challenge in the implementation of VAWTs in the built environment stems from the lack of knowledge regarding the transient response behavior of a wind turbine operating in unsteady winds. The overall goal of this research is to investigate the conditions under which enhanced energy capture is possible by a VAWT operating in gusty winds representative of an urban/suburban environment.

The transient response behavior of a Darrieus-type VAWT was modeled using Blade Element Momentum theory applied to the conservation of angular momentum equation about the turbine rotor. This allowed the power generated by the turbine to be calculated as a function of input wind speed. Time-resolved wind data acquired over a full year were used as input to the numerical model. Two different common turbine controllers were investigated, namely the constant rotational speed and the ideal tip speed ratio. The constant rotational speed controller drives the turbine rotor at a fixed speed regardless of variations in the incoming wind speed while the ideal tip speed ratio controller provides active control of the turbine, allowing the turbine to respond instantaneously to the variation of the wind speed. The efficiency of the VAWT was found to be strongly dependent on the mean wind speed and turbulence intensity of the wind. For the case of the constant rotational speed controller, the

turbine should be operated at an overspeed setting (ω_{opt}) based on the turbulence intensity of the incoming wind in order to harvest as much energy as possible. For the ideal tip speed ratio controller, the turbine efficiency was observed to plateau to a maximum value when the nondimensional turbine response parameter ζ drops below the critical value ζ_c.

The research also sought solutions for improving turbine energy efficiency by investigating four different methods of wind forecasting for use with the constant rotational speed controller. The methods examined were the persistence method (PM), modified persistence method (MPM), autoregressive moving average (ARMA), and weather research and forecasting (WRF). Results showed that the forecasting models allow the VAWT to harvest approximately 78% to 85% of the ideal amount of energy that could be harvested assuming the actual wind data were known in advance. The modified persistence model outperformed the persistence model, autoregressive moving average model, and weather research and forecasting model by capturing as much as 6% more energy. When compared to the case of no forecasting, the MPM improved the total amount of energy captured over the full year of operation as much as 17.3%.

Finally, a parameter study was performed to determine the optimal VAWT design configuration that yields the maximum amount of energy captured during operation in realistic gusty wind conditions. The turbine design configuration studied in this work is a straight blade Darrieus wind turbine that has three blades. Four design parameters were varied including the height-to-diameter aspect ratio, blade airfoil shape, turbine solidity, and turbine moment of inertia. The optimal turbine design that harnessed the most amount of energy from the wind was the one with the following features: H/D = 1.2, NACA 0015 airfoil blades, S = 12%, and c = 8 cm. The results also suggest that for the case of operation in unsteady winds, the optimal power coefficient (Cp) versus tip speed ratio (TSR) curve is not necessarily the one exhibiting the highest peak Cp value, but rather the broadest shape. The economic analysis suggested that a VAWT is economically viable when it is deployed at locations where the local annual average wind speed is 4.2 m/s or greater.

Thank you for always believing in me and encouraging me through the hardest times

I dedicate this to my wonderful parents,

Hoa and Hieu Nguyen

CONTENTS

LIST OF FIGURES

LIST OF TABLES

ACKNOWLEDGMENTS

This research project would not have been possible without the guidance, help, and support of several individuals who in one way or another contributed and extended their valuable assistance to the completion of this research. First and foremost, I would like to thank my advisor, Professor Meredith Metzger, for her advice, patience, motivation, and encouragement throughout this research project and all the freedom she gave me to pursue my own ideas. I have thoroughly enjoyed the research experience working with her and her support has been greatly appreciated. Furthermore, I would like to thank my graduate committee advisory members, Dr. Eric Pardyjak, Dr. Marc Calaf, Dr. Amanda Smith, and Dr. Steven Burian, for their support and guidance. A special thank you goes to Dr. Prathap Ramamurthy and Dr. Eric Pardyjak for providing the sonic anemometry data in Salt Lake Valley in 2006. This research would not have been where it is now without the help of Dr. Jeff Basara of the University of Oklahoma for providing the Micronet wind data in Oklahoma City in 2009. I would like to express my great appreciation to the help of Marcela Loria-Salazar and Dr. Heather Holmes of the University of Nevada, Reno for providing the WRF model results for Salt Lake City in 2013. In addition, I would like to thank a number of my friends and colleagues for their friendship, help, and support with this research and classes throughout the course of my Ph.D. program here at the University of Utah. This includes Emina Maric, Derek Jensen, Chaoxun Hang, Nathan Miller, and many others. Last but not least, I would like to thank my family for their continuous spiritual support throughout my Ph.D. program.

Part of this research was funded by a Graduate Research Fellowship from the University of Utah. In addition, some travel grants to North Carolina for the ASME Energy and Power Conference were funded by the Global Change and Sustainability Center (GCSC) at the University of Utah.

CHAPTER 1

INTRODUCTION

This research project stems from our vision of an energy-neutral sustainable city, where the demand for energy is supplied by local renewable sources. We imagine the idea of an urban wind farm as a means toward balancing the local energy budget in urban areas, at least within the residential and commercial sectors as illustrated in Figure 1.1. Ideally, this would be coupled with other renewable energy alternatives where appropriate, such as solar, hydropower, geothermal, and biofuels-based on sustainably produced biomass. This vision is not too far-fetched. In fact, the city of Vaxjo, Sweden generates 51 percent of its energy today from non-fossil-based fuel sources and has reduced its emissions of CO_2 by 24 percent, relative to 10 years ago, on a per capita basis (Oliver, 2007).

Wind energy harvesting has increased rapidly in the past few decades due to the considerable advancement in wind turbine technologies (Ackermann and Söder, 2002; Kaldellis, 2002; Leung and Yang, 2012). Along with the increasing number

Figure 1.1: Envisioned urban wind farm (adapted from Green-Blog (2015)).

of wind farms containing large horizontal axis wind turbines (HAWTs), an upsurge in small-scale wind turbines including vertical axis wind turbines (VAWTs) has also occurred in recent years (Azau, 2010; Stefan Gsnger, 2015). Although small-scale wind turbines are certainly limited in the amount of overall energy that can be produced due to size constraints, one major benefit of locating technology where the demand is highest stems from reduced capital investment on transmission lines. Another potential benefit stems from the hypothesis that the presence/visibility of renewable energy technologies in the urban environment will encourage better energy conservation practices by the people living in those areas. This idea serves as the underlying motivation for the present work. According to a technical report by the U.S. Energy Information Administration EIA (2017), approximately 11% of total energy was consumed by the residential and commercial sectors in 2014 and within this consumption, approximately about 82% of the energy came from burning fossil fuel, 8% came from nuclear power, and only 10% came from renewable energy resources. The purpose of bringing renewable energy into an urban/suburban area is not only to increase the amount of energy supplied by a clean renewable energy resource but also to promote better conservation practices in high-density areas. By bringing renewable energy into the urban/suburban environment in any form (i.e., wind energy, solar energy, or geothermal), it is hoped that the renewable energy resources could provide some percentage of the consumed energy while reducing the supplied energy from burning fossil fuel. Most importantly, it is hoped that an additional percentage of energy consumption could be conserved from an increased awareness and better conservation practices by energy consumers.

The wind condition within typical urban/suburban environments has been found to be more turbulent than that in rural areas, due to the increased surface roughness caused by the presence of houses and buildings (Roth, 2000; Klipp, 2007; Bertényi et al., 2010). Wind flow over houses/buildings is highly turbulent with rapid fluctuations in both magnitude and direction, making it challenging to harvest wind energy in urban/suburban areas (Bertényi et al., 2010). Compared to the HAWT, the VAWT is a promising wind energy harvesting device for application in the urban area because of its simple structure, high efficiency, and most importantly, insensitivity to

wind direction. Common types of VAWTs include the eggbeater Darrieus turbine, straight-blade Darrieus turbine, Savonius turbine and helical wind turbines (McIntosh et al., 2007; Islam et al., 2008; Mahmoud et al., 2012; Bedon et al., 2013). Figure 1.2 illustrates the eggbeater and straight-blade Darrieus wind turbine types. Each wind turbine type poses its own advantages and disadvantages. The eggbeater Darrieus wind turbine provides lower bending stress on the blades; however, due to the high manufacturing cost, this wind turbine is less preferable compared to the straight-blade Darrieus wind turbine. The objectives of this research study are to investigate the condition under which the Darrieus vertical axis wind turbine could enhance the amount of energy captured available from the wind gust when the turbine is operated in gusty wind conditions representative of an urban/suburban environment. This research examines several different aspects of the VAWT design in order to improve the aerodynamic performance and enhance the amount of energy harvesting from the wind.

Understanding the transient response of a VAWT operating under gusty wind is critical in order to improve the performance of the turbine. The wind turbine's ability to respond to fluctuations in wind speed depends on the aerodynamics of the blades, the inertia of the turbine, and the time lag of the controller. Several research studies

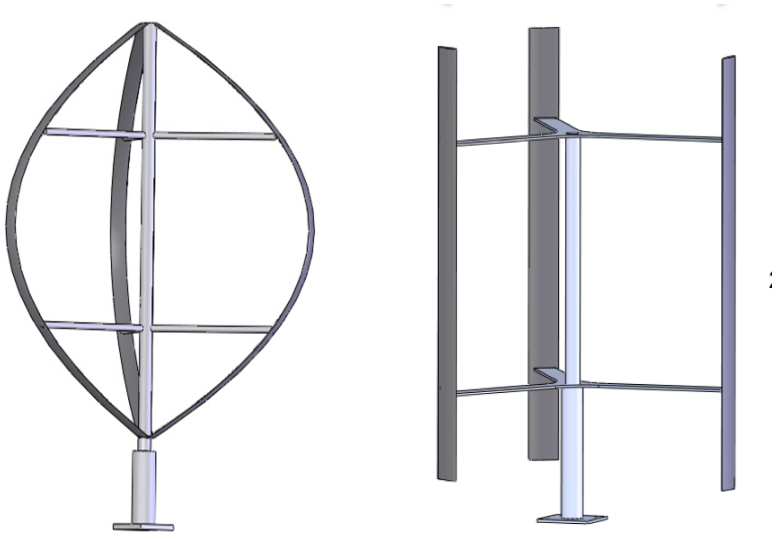

Figure 1.2: Two common types of vertical axis wind turbine (i) Eggbeater Darrieus wind turbine and (ii) Straight-blade Darrieus wind turbine.

have been done to investigate the impact of unsteady wind on the performance of a VAWT (Hara et al., 2012; Danao et al., 2013; Shahzad et al., 2013). Danao et al. (2013) performed CFD simulations of the performance of a VAWT under a sinusoidal wind with 12% fluctuating amplitude and 0.5 Hz fluctuation frequency. Shahzad et al. (2013) performed CFD simulations to analyze the performance behavior of a VAWT under an accelerating and decelerating incoming flow. Their results show that the power output varied significantly with the accelerated/decelerated flow; however, the net effect on overall performance due to a cyclic combination of accelerated/decelerated flow was not clear. Recently, experiments and simulations were performed by Hara et al. (2012) to study the effect of turbine inertia on the performance of a VAWT in a sinusoidally pulsating wind with amplitude ΔV and period T. Their results implied the energy efficiency decreased as the fluctuating amplitude ΔV increased. Further work is needed to determine whether this finding is universal and holds in the case of realistic winds having a wide range of amplitudes and frequencies.

The response time of the turbine and degree of unsteadiness of the wind have shown to be important terms of the amount of energy captured by a VAWT during unsteady wind conditions (McIntosh et al., 2007, 2008; Kooiman and Tullis, 2010). McIntosh et al. (2008) used a characteristic time scale based on the frequency corresponding to 99% of the total energy in the wind. It remains to be seen whether this is the most relevant time scale for a gusty wind. Higher frequency turbulent motions in the atmospheric surface layer do not contain significant energy; therefore, a time scale based on the dominant frequency in the wind spectrum may be more appropriate. Kooiman and Tullis (2010) found the unsteadiness of the wind, quantified in terms of turbulent intensity (I_v), has a significant impact on the overall performance of the wind turbine, especially for high I_v. In their recent study, McIntosh et al. (2007) suggested that in order to increase the energy captured during unsteady wind using a turbine operated at a constant rotational speed, an overspeed control technique should be applied. It remains to be determined how the optimal overspeed setting varies with turbulence intensity and whether enhanced energy capture is possible as the turbulence intensity increases.

Another important aspect that is worth considering to improve the wind turbine performance is wind forecasting. Forecasting of the wind condition plays a critical role in the optimization of the amount of energy captured by a wind turbine (Sanchez, 2006; Lei et al., 2009). Accurate wind speed prediction provides valuable information for the wind turbine operation controller (Cadenas and Rivera, 2007). Over the last few decades, considerable research has been conducted on forecasting the wind speed for wind turbine applications (Watson et al., 1992; Cadenas and Rivera, 2007). Several wind speed forecasting techniques have been developed and reported over the years with the two most common techniques being (1) Physical Approach and (2) Statistical Approach. The "Numeric Weather Prediction (NWP)" model uses parameterization based on the physical descriptions of the atmosphere such as terrain, pressure, temperature, etc. to estimate the future wind speed (Soman et al., 2010). The NWP is often rendered on supercomputers and is computational expensive. This model does not provide accurate results in short-term prediction (Lei et al., 2009).

One common model that uses the physical approach is the Weather Research and Forecasting (WRF) model. Recently, the WRF model has been used to forecast wind speed and wind power for wind turbine applications (Clifford, 2011; Deppe et al., 2013). The WRF model is an efficient and flexible simulation program, with grid resolutions from 1–10 km, that has been designed for a wide range of weather forecast and research applications (Klemp, 2005; Michalakes et al., 2005). The WRF model is maintained and supported for broad community use with over 30,000 users in over 150 countries (WRF, 2016). Clifford (2011) used the WRF model to forecast the near-surface wind speed and available wind power in the Altamont Pass wind farm near Livermore, California. The results indicate that the WRF-modeled wind speeds were close to those observed.

The statistical approach is based on a training procedure that uses the difference between the actual data and the predicted data in order to determine coefficients in the mathematical model. This approach is easy to model, inexpensive, and provides fairly accurate results, especially for short-term forecasting (Lei et al., 2009; Soman et al., 2010). Based on the Box-Jenkin methodology (Box et al., 2011), some of the common models have been developed and reported over the years such as autore-

gressive model (AR), moving average model (MA), autoregressive moving average (ARMA), and autoregressive integrated moving average (ARIMA). The ARMA and ARIMA have been widely used for short-term forecasting of wind speed (Lei et al., 2009; Soman et al., 2010). In addition, a simple method named "Persistence Method" has been used for predicting wind speed for very short-term forecasting. This method is surprisingly accurate compared to most of the physical and other statistical methods for very short-term forecasting (Soman et al., 2010). Accurate wind speed forecasting has significant economic and technical advantages in maximizing the amount of energy captured by a wind turbine. In their studies, Fabbri et al. (2005) suggested that the error prediction costs could be as much as 10% of the total income from selling wind energy. One of the goals of the present study is to determine whether forecasting can increase the amount of energy harvested during conditions of gusty winds, and to quantify (in economic terms) the benefit of forecasting during gusty winds.

Accurate performance modeling of vertical axis wind turbines poses a significant challenge for scientists and engineers. Over the years, a considerable amount of theoretical, computational, and experimental research has been conducted with the intention of optimizing wind turbine performance (Templin, 1974; Blackwell et al., 1976; Paraschivoiu, 2002; Beri et al., 2011; Danao et al., 2013). Most wind turbine designers use numerical models based on the Blade Element Momentum theory (BEM theory) to predict wind turbine performance (Templin, 1974; Strickland, 1975; Paraschivoiu and Delclaux, 1983; Beri et al., 2011). BEM theory is a common feature underlying many existing numerical models of VAWTs, including, for example, the single stream tube model (Blackwell et al., 1976), the double multiple streamtubes model (Strickland, 1975; Beri et al., 2011; Chong et al., 2013), and the 2D vortex model (McIntosh et al., 2008). All of these numerical models are relatively inexpensive with low computational effort, compared to Computational Fluid Dynamics (CFD) models. The majority of numerical models that use BEM theory incorporate static airfoil data in the model to predict wind turbine performance. It is well known that lift and drag forces acting on an airfoil undergo hysteresis in unsteady wind conditions. Initial work performed by Schuerich and Brown (2011) showed that at moderate tip speed ratio, the use of dynamic stall data is more adequate to capture the behavior

of the airfoil. It remains to be answered whether including dynamic stall data in the model will improve the prediction of wind turbine performance in gusty winds, as it better represents actual operating conditions.

Wind turbine design optimization poses a significant impact on turbine performance and the amount of energy captured (Tirkey et al., 2014). It is well known that each turbine design configuration has its own characteristic power performance curve that is typically referred to as a C_p-TSR curve. Over the years, efforts have been made in order to optimize this C_p-TSR curve by varying turbine design parameters such as airfoil shape, solidity, turbine height, and diameter (Blackwell et al., 1976; Paraschivoiu et al., 1983; Fiedler and Tullis, 2009; Brusca et al., 2014; Tirkey et al., 2014). Most of these turbine configurations were modeled/tested either at constant incoming velocity or constant rotational speed (Blackwell et al., 1976) that does not well represent the actual wind condition in the urban environment. Even though a particular turbine configuration may result in slightly better power performance curve C_p-TSR at a fixed incoming velocity, it is not guaranteed that turbine design will yield the most energy efficiency in realistic gusty wind conditions. It remains to be seen whether slight adjustments in the C_p-TSR curve can result in significant differences in the amount of energy captured by the turbine while operating in the gusty wind conditions of an urban environment.

1.1 Research Objectives

Wind conditions within the urban environment have been found to be more turbulent than those in rural areas, due to the increased surface roughness caused by the presence of buildings, houses, and trees (Roth, 2000; Klipp, 2007). Winds in the urban environment are characterized by gusts with large fluctuations in magnitude and direction that contain a large amount of energy within the gust component. Development of a VAWT that could exploit this turbulent wind energy would yield a significant increase in the total amount of energy captured. The overall goal of this research project is to investigate the conditions under which enhanced energy capture is possible by a vertical axis wind turbine operating in gusty winds representative of an urban/suburban environment. An economic analysis is performed to evaluate the cost

benefits and the practical feasibility of the different control strategies investigated.

The first aim of the research is to better understand the transient behavior of a VAWT during gusty wind conditions. It was hypothesized that the turbulent intensity and characteristic time scale of the gusty wind in the urban environment would have a significant impact on the overall performance of the wind turbine, thus affecting the amount of energy captured by the turbine. To assess this hypotheses, the following scientific questions were addressed:

- How much excess energy is contained within the gusty wind compared to the steady wind?
- What is the relationship between the turbulence intensity and the excess energy contained within the gust?
- How do the turbulence intensity and characteristic gust time scale affect the amount of energy captured by the VAWT using two different control strategies: (i) constant rotational speed (ii) ideal tip speed ratio?
- How much more energy can be captured by a VAWT using the two aforementioned controllers?

Several numerical models were utilized to address the proposed scientific questions in the first aim. Actual wind data acquired from cup/vane and sonic anemometers located in urban areas were used as input to the numerical models. Sonic anemometry data collected in June 2005 from a tower located in Murray, Utah, a suburban neighborhood in the Salt Lake Valley, was obtained from the study of Ramamurthy and Pardyjak (2011). Cup/vane anemometry data collected during 2013 from a wind monitor located on the roof of the William Browning Building (WBB) on the University of Utah campus was obtained online from the MesoWest Project. The optimal operating point of the turbine was determined for two different control strategies: (i) constant rotational speed controller (constant–ω) and (ii) ideal tip speed ratio (ideal–TSR) controller. The effect of turbulence intensity, gust frequency, and turbine inertia on the overall performance of of the turbine was explored. The total energy captured by the VAWT for the two controllers was examined and compared.

Detail descriptions of the numerical models, analysis, and results of the first aim are reported in Chapter 2 of this dissertation.

The second aim of the research is to better understand the benefits of accurate forecasting on the amount of energy harvested by a vertical axis wind turbine. It was hypothesized that accurate forecasting of the wind condition would allow for better control of a VAWT, leading to enhanced energy captured and resulting in significant economic benefits. To assess this hypotheses, the following scientific questions were addressed:

- How does the sensitivity of forecasting accuracy affect the overall energy captured by a VAWT?
- How much energy can be captured by a VAWT if the future wind condition is forecasted using the "Persistence Method" compared to the Modified Persistence Method (MPM), Autoregressive Moving Average (ARMA) model, and Weather Research, and Forecasting model (WRF)?
- What is the most accurate forecasting model between the four examined methods?
- What is the economic benefit of wind forecasting on the wind turbine in terms of electricity price?

Several numerical models were utilized to address the proposed scientific questions in the second aim. Sonic anemometer data collected in 2009 at different sites in Oklahoma City were used as the input to the models. Four different forecasting models were examined, namely: (i) Persistence Model (PM), (ii) Modified Persistence Model (MPM), (iii) Autoregressive Moving Average (ARMA), and (iv) Weather Research and Forecasting (WRF). The constant rotational speed (constant–ω) controller was utilized in this study. The wind turbine performance measured in terms of the total amount of energy captured was examined and compared. An economic analysis was performed comparing the cost to implement a VAWT using the preferred forecasting model versus that expected in the ideal scenario when the wind speed was available in advance. The economic viability of the VAWT was quantified by comparing the

Levelized Cost Of Energy (LCOE) for the VAWT with the national electricity unit price. Detailed descriptions of the numerical models, analysis, and results of the second aim are reported in Chapter 3 of this dissertation.

The final aim of the research is to better understand the impact of different VAWT configurations on the amount of energy captured under gusty winds in an urban/suburban environment. Different VAWT designs (defined by airfoil shape, solidity, and height-to-diameter ratio) result in different performance specifications, characterized by their power performance coefficient versus tip speed ratio curve (C_p-TSR curve). It was hypothesized that, due to the large range of timescales inherent in gusty winds, the amount of enhanced energy captured by a VAWT during gusty wind conditions is relatively insensitive to the design configuration of the turbine. To test this hypotheses, the following scientific questions were addressed:

- How do differences in the C_p-TSR curves between different turbine designs affect the amount of energy extracted during gusty wind conditions?

- Is it possible to determine an optimal turbine configuration for a typical wind condition in an urban/suburban environment?

- What is the economic viability of each VAWT configuration examined in the study?

This hypotheses was tested by evaluating wind turbine performance over a range of VAWT configurations operated under identical gusty wind conditions characteristic of a real urban/suburban area. The ideal–TSR control strategy was utilized in this aim. Sonic anemometer data collected in 2009 at different sites in Oklahoma City were again used as the input to the numerical models. The performance of each wind turbine configuration was measured in terms of the total amount of energy captured. An economic analysis was also performed to evaluate the economic viability of each turbine configuration by comparing the LCOE of the VAWT with the national electricity unit price. Detailed descriptions of the numerical models, analysis, and results of the third aim are reported in Chapter 4 of this dissertation.

1.2 References

Ackermann, T. and L. Söder, 2002: An overview of wind energy-status 2002. *Renewable and Sustainable Energy Reviews*, **6 (1)**, 67–127.

Azau, S., 2010: A breath of fresh air the european wind energy association annual report 2009. Tech. Rep. ISSN 2032-9024, EWEA.

Bedon, G., M. R. Castelli, and E. Benini, 2013: Optimization of a darrieus vertical-axis wind turbine using blade element–momentum theory and evolutionary algorithm. *Renewable Energy*, **59**, 184–192.

Beri, H., Y. Yao, et al., 2011: Double multiple streamtube model and numerical analysis of vertical axis wind turbine. *Energy and Power Engineering*, **3 (03)**, 262.

Bertényi, T., C. Wickins, and S. McIntosh, 2010: Enhanced energy capture through gust-tracking in the urban wind environment. *48th AIAA Aerospace Sciences Meeting, Orlando, Florida, USA*.

Blackwell, B. F., R. E. Sheldahl, and L. V. Feltz, 1976: Wind tunnel performance data for the darrieus wind turbine with naca 0012 blades. Tech. rep., Sandia Labs., Albuquerque, N. Mex.(USA).

Box, G. E., G. M. Jenkins, and G. C. Reinsel, 2011: *Time series analysis: forecasting and control*, Vol. 734. John Wiley & Sons.

Brusca, S., R. Lanzafame, and M. Messina, 2014: Design of a vertical-axis wind turbine: how the aspect ratio affects the turbine?s performance. *International Journal of Energy and Environmental Engineering*, **5 (4)**, 333–340.

Cadenas, E. and W. Rivera, 2007: Wind speed forecasting in the south coast of oaxaca, mexico. *Renewable Energy*, **32 (12)**, 2116–2128.

Chong, W., K. Pan, S. Poh, A. Fazlizan, C. Oon, A. Badarudin, and N. Nik-Ghazali, 2013: Performance investigation of a power augmented vertical axis wind turbine for urban high-rise application. *Renewable Energy*, **51**, 388–397.

Clifford, K. T., 2011: Wrf model perofrmance for wind power forecasting in the coast ranges of central california. M.S. thesis, San Jose State University.

Danao, L. A., J. Edwards, O. Eboibi, and R. Howell, 2013: The performance of a vertical axis wind turbine in fluctuating wind–a numerical study. *Proceedings of the World Congress on Engineering*, Vol. 3, 3–5.

Deppe, A. J., W. A. Gallus Jr, and E. S. Takle, 2013: A wrf ensemble for improved wind speed forecasts at turbine height. *Weather and Forecasting*, **28 (1)**, 212–228.

EIA, 2017: Monthly energy review: Feburuary 2017. Tech. Rep. DOE/EIA-0035(2017/2), U.S. Energy Information Administration.

Fabbri, A., T. G. S. Román, J. R. Abbad, and V. H. M. Quezada, 2005: Assessment of the cost associated with wind generation prediction errors in a liberalized electricity market. *Power Systems, IEEE Transactions on*, **20 (3)**, 1440–1446.

Fiedler, A. and S. Tullis, 2009: Blade offset and pitch effects on a high solidity vertical axis wind turbine. *Wind Engineering*, **33 (3)**, 237–246.

Green-Blog, 2015, URL http://green-blog.org/media/images/2008/02/efficiencity.gif, Accessed: 2017-03-03.

Hara, Y., K. Hara, and T. Hayashi, 2012: Moment of inertia dependence of vertical axis wind turbines in pulsating winds. *International Journal of Rotating Machinery*, **2012**.

Islam, M., D. S.-K. Ting, and A. Fartaj, 2008: Aerodynamic models for darrieus-type straight-bladed vertical axis wind turbines. *Renewable and Sustainable Energy Reviews*, **12 (4)**, 1087–1109.

Kaldellis, J., 2002: Optimum autonomous wind–power system sizing for remote consumers, using long-term wind speed data. *Applied Energy*, **71 (3)**, 215–233.

Klemp, J., 2005: Advances in the wrf model for convection-resolving forecasting. *Advances in Geosciences*, **7**, 925–29.

Klipp, C., 2007: Wind direction dependence of atmospheric boundary layer turbulence parameters in the urban roughness sublayer. *Journal of Applied Meteorology and Climatology*, **46 (12)**, 2086–2097.

Kooiman, S. and S. Tullis, 2010: Response of a vertical axis wind turbine to time varying wind conditions found within the urban environment. *Wind Engineering*, **34 (4)**, 389–401.

Lei, M., L. Shiyan, J. Chuanwen, L. Hongling, and Z. Yan, 2009: A review on the forecasting of wind speed and generated power. *Renewable and Sustainable Energy Reviews*, **13 (4)**, 915–920.

Leung, D. Y. and Y. Yang, 2012: Wind energy development and its environmental impact: A review. *Renewable and Sustainable Energy Reviews*, **16 (1)**, 1031–1039.

Mahmoud, N., A. El-Haroun, E. Wahba, and M. Nasef, 2012: An experimental study on improvement of savonius rotor performance. *Alexandria Engineering Journal*, **51 (1)**, 19–25.

McIntosh, S., H. Babinsky, and T. Bertenyi, 2007: Optimizing the energy output of vertical axis wind turbines for fluctuating wind conditions. *45th AIAA Aerospace Sciences Meeting and Exhibit, Reno, Nevada*.

McIntosh, S., H. Babinsky, and T. Bertenyi, 2008: Unsteady power output of vertical axis wind turbines operating within a fluctuating free-stream. *46th AIAA Aerospace Sciences Meeting and Exhibit, Reno, Nevada*.

Michalakes, J., J. Dudhia, D. Gill, T. Henderson, J. Klemp, W. Skamarock, and W. Wang, 2005: The weather research and forecast model: software architecture and performance. *Proceedings of the 11th ECMWF Workshop on the Use of High Performance Computing In Meteorology*, 156–168.

Oliver, R., 2007: All about: Cities and energy consumption. URL `http://edition.cnn.com/2007/TECH/12/31/eco.cities/`, Accessed: 2014-08-24.

Paraschivoiu, I., 2002: *Wind turbine design: with emphasis on Darrieus concept*. Presses inter Polytechnique.

Paraschivoiu, I. and F. Delclaux, 1983: Double multiple streamtube model with recent improvements (for predicting aerodynamic loads and performance of darrieus vertical axis wind turbines). *Journal of Energy*, **7 (3)**, 250–255.

Paraschivoiu, I., F. Delclaux, P. Fraunie, and C. Beguier, 1983: Aerodynamic analysis of the darrieus rotor including secondary effects. *Journal of Energy*, **7 (5)**, 416–422.

Ramamurthy, P. and E. R. Pardyjak, 2011: Toward understanding the behavior of carbon dioxide and surface energy fluxes in the urbanized semi-arid salt lake valley, utah, usa. *Atmospheric Environment*, **45 (1)**, 73–84.

Roth, M., 2000: Review of atmospheric turbulence over cities. *Quarterly Journal of the Royal Meteorological Society*, **126 (564)**, 941–990.

Sanchez, I., 2006: Short-term prediction of wind energy production. *International Journal of Forecasting*, **22 (1)**, 43–56.

Schuerich, F. and R. E. Brown, 2011: Effect of dynamic stall on the aerodynamics of vertical-axis wind turbines. *AIAA Journal*, **49 (11)**, 2511–2521.

Shahzad, A., T. Asim, R. Mishra, and A. Paris, 2013: Performance of a vertical axis wind turbine under accelerating and decelerating flows. *Procedia CIRP*, **11**, 311–316.

Soman, S. S., H. Zareipour, O. Malik, and P. Mandal, 2010: A review of wind power and wind speed forecasting methods with different time horizons. *North American Power Symposium (NAPS), 2010*, IEEE, 1–8.

Stefan Gsnger, J. D.-P., 2015: 2015 small wind world report summary. Tech. Rep. March 2015 Report, WWEA.

Strickland, J. H., 1975: Darrieus turbine: a performance prediction model using multiple streamtubes. Tech. rep., Sandia Labs., Albuquerque, N. Mex.(USA).

Templin, R., 1974: Aerodynamic performance theory for the nrc vertical-axis wind turbine. *NASA STI/Recon Technical Report N*, **76**, 16 618.

Tirkey, A., Y. Sarthi, K. Patel, R. Sharma, and P. K. Sen, 2014: Study on the effect of blade profile, number of blade, reynolds number, aspect ratio on the performance of vertical axis wind turbine. *International Journal of Science, Engineering and Technology Research (IJSETR)*, **3 (12)**.

Watson, S., J. Halliday, and L. Landberg, 1992: Assessing the economic benefits of numerical weather prediction model wind forecasts to electricity generating utilities. *14th British Wind Energy Association Conference*, 291–297.

Weather Research and Forecasting (WRF), 2016: Weather research and forecasting model. URL `http://www.wrf-model.org/index.php`, Accessed: 2016-09-15.

CHAPTER 2

ENHANCED ENERGY CAPTURE BY A VERTICAL AXIS WIND TURBINE DURING GUSTY WINDS IN AN URBAN/SUBURBAN ENVIRONMENT

 Nguyen, L. and M. Metzger, 2015: Enhanced energy capture by a vertical axis wind turbine during gusty winds in an urban/suburban environment. *Journal of Renewable and Sustainable Energy,* 7 (5), 053118.

JOURNAL OF RENEWABLE AND SUSTAINABLE ENERGY **7**, 053118 (2015)

Enhanced energy capture by a vertical axis wind turbine during gusty winds in an urban/suburban environment

Lam Nguyen and Meredith Metzger
Department of Mechanical Engineering, University of Utah, Salt Lake City, Utah 84112, USA

(Received 11 May 2015; accepted 9 October 2015; published online 22 October 2015)

Wind resource maps of annual-averaged wind speeds, typically used in the siting of wind turbines and wind farms, can grossly underpredict the actual wind energy potential in areas with highly transient or gusty winds. The goal of the present study is to quantify the additional energy capable of being harvested by a small vertical axis wind turbine using control strategies that exploit the excess energy in wind gusts. A transient-response numerical model is utilized with input from actual wind data acquired by cup-vane and sonic anemometers located in both an urban and suburban area. The total energy captured by the turbine during the year 2013, along with its overall efficiency, was determined for two different control strategies: constant rotational speed (ω) controller and ideal tip speed ratio (TSR) controller. For the case of the constant ω controller, the turbine achieves maximum efficiency when it is operated at an optimal overspeed setting, ω_{opt}. Results indicate that ω_{opt} can be estimated from the turbulence intensity of the wind. For the case of the ideal TSR controller, turbine efficiency was observed a plateau to a maximum value when the nondimensional turbine response parameter ζ dropped below a critical value ζ_c. This is as expected since turbines with fast response times ($\zeta < \zeta_c$) are capable of instantaneously tracking fluctuations in the wind and thus effectively capturing the high energy content contained within each wind gust. The value of ζ_c exhibits a dependence on the characteristic gust time scale. Over the course of the year, the turbine in conjunction with the constant ω controller, operating at ω_{opt}, was capable of harvesting six times the energy of a naive controller operating a fixed ω based on the annual-averaged mean wind speed. The same turbine operating in conjunction with an ideal TSR controller, however, was successful in harvesting nearly thirteen times the energy of that with the naive controller. This may have significant implications on the viability of small turbines in relatively gusty urban/suburban areas, even when the annual-averaged wind speed is below a threshold typically considered practical for harvesting wind energy. [http://dx.doi.org/10.1063/1.4934585]

I. INTRODUCTION

Wind energy has been long recognized as a promising renewable energy resource because of its abundance and ubiquity. In the past few decades, considerable advancements have been made in wind turbine technology, which has lead to an increase in the number of wind turbines that have been deployed around the world.[17] Specifically, nameplate wind power capacity has increased to about 5 MW for large horizontal axis wind tubines.[5] Many countries, such as Germany, USA, Spain, Denmark, and recently China and Turkey, have made substantial efforts to develop their wind power industries.[1,20] The world wind power generation capacity has been growing rapidly with an average annual growth of about 30% over the last decade.[20] It is predicted that wind energy generation will satisfy 5% of the world's energy consumption needs by 2020.[20]

Most modern wind farms often feature large horizontal axis wind turbines (HAWTs) with megawatt capability because of their high power coefficients. This technology, however, has encountered several economical and social barriers due to the high fabrication cost, large size, and noise generation. Therefore, it is only possible to deploy megawatt-capacity HAWTs in remote sites, far from consumers. In order to reduce transmission loss and promote energy conservation, it is desirable to collocate renewable energy harvesting machines with consumer demand. Since urban areas consume two-thirds of the world's energy,[32] it is prudent to develop small-scale turbines that are suitable for harvesting wind energy specifically in the built environment and able to provide that energy in a decentralized fashion to local users. Small-scale wind turbines have some distinct benefits over large-scale units (especially for urban areas), including reduced capital investment on tower and transmission lines,[19] faster response times to fluctuating winds, and lower noise generation.[3]

The wind flow over houses/buildings is highly turbulent with rapid fluctuations in both magnitude and direction, making it challenging to extract wind energy in the urban area. Wind turbine design for the urban environment also encounters another difficulty because of the constraint on space. Although small HAWTs appear to be the first choice because of their high power coefficients and capacities, they suffer from several drawbacks, most predominantly being that their performance is highly dependent on the wind magnitude and direction. In other words, small HAWTs do not perform well in the turbulent winds inherent to urban environments. In addition, small HAWTs require a large footprint to accommodate their rotors, thus making them non-ideal wind turbine technology for the urban areas. In contrast, Vertical Axis Wind Turbines (VAWTs) offer a critical advantage for harvesting wind energy in urban environments, because of the ability to capture energy in any wind direction, thereby removing the need for a wind sensing and orientation mechanism. This versatility of VAWTs makes them ideal for installation in urban areas where wind conditions are inconsistent.

Wind conditions within the urban environment have been found to be more turbulent than that in rural areas, due to the increased surface roughness caused by the presence of buildings, houses, and trees.[3,18,21,29,35] Winds in the urban environment are characterized by gusts with large fluctuations in magnitude and direction that contain a large amount of energy.[18,21,29,35] Wind turbines designed for rural areas, however, have been shown to be ineffective in capturing the energy in a gusty wind.[23,24] Development of a turbine that could exploit this turbulent wind energy would yield a significantly increase in the total amount of energy captured. Berténi *et al.*[3] performed an experimental study of the potential excess energy contained in an unsteady wind (gust) compared to that of a steady wind.[3] A new parameter termed gust energy coefficient (GEC) was defined as the ratio of actual energy contained in the gusty wind integrated over a period of time to the steady energy based on the mean wind speed over the same time period. The results show an increase in the GEC of 22.7% as the turbulence intensity level of the wind increases from 0% to 26.8%. The authors also introduced the idea of a gust-tracking wind turbine capable of extracting the excess energy in the gusts.

The wind turbine's ability to respond to fluctuations in the wind speed depends on the aerodynamics of the blades, the inertia of the turbine, and the time lag of the controller. Computational fluid dynamics (CFD) simulations of VAWTs in unsteady winds have shed light on the former.[7,31,33] Specifically, Danao *et al.*[7] performed the CFD simulations of the performance of a VAWT under a sinusoidal wind with 12% fluctuating amplitude and 0.5 Hz fluctuation frequency. Their results showed a dependency on Reynolds number; namely, an increase in the wind speed has more effect on the tangential component of the lift than the drag, which helps to improve the overall performance of the turbine. Shahzad *et al.*[33] performed CFD simulations to analyze the performance behavior of a VAWT under an accelerating and decelerating incoming flow. Their results showed that the instantaneous torque and power output varied significantly when the incoming flow was accelerated/decelerated; however, the net effect on overall performance due to a cyclic combination of accelerated decelerated flow was not clear.

Recently, experiments and simulations were performed by Hara *et al.*[12] to study the effect of turbine inertia on the performance of a VAWT in a sinusoidally pulsating wind with amplitude ΔV and period T. They found that the VAWT studied was not affected by changing wind

direction, but that the overall performance was affected by variations in the wind speed. Similar results were also found in the studies performed by Kooiman and Tullis.[19] Hara *et al.*[12] found that there was a phase delay between the rotational speed and wind variation that owes to the effect originating from the moment of inertia. Additionally, Hara *et al.*[12] found that the energy efficiency of the wind turbine in a sinusoidal wind with constant ΔV remains nearly constant regardless of the moment of inertia of the turbine and period of oscillation T, but the energy efficiency decreases as the fluctuating amplitude ΔV increases. Further work is needed to determine whether this finding is universal and holds in the case of realistic winds having a wide range of amplitudes and frequencies.

The response time of the turbine has been shown to be important in terms of the amount of energy captured during unsteady wind conditions.[12,19,23,24] McIntosh *et al.*[23] found that the time scale associated with the unsteady wind was also important. They introduced a nondimensional quantity, named the turbine response parameter, defined as the ratio of the turbine response time to the gust period. As the turbine response parameter increases, the turbine is less able to track changes in wind speed, resulting in decreased energy capture. However, their study only analyzed a 300-s sample of unsteady wind. Also, using a single time scale to represent the unsteady wind may be problematic. McIntosh *et al.*[23] used a characteristic time scale based on the frequency corresponding to 99% of the total energy in the wind. It remains to be seen whether this is the most relevant time scale for a gusty wind. Higher frequency turbulent motions in the atmospheric surface layer do not contain significant energy. Therefore, a time scale based on the dominant frequency in the wind spectrum may be more appropriate.

The degree of unsteadiness of the wind can be quantified in terms of the turbulence intensity, I_v, defined as the standard deviation divided by the mean, and has been found to have a significant effect on the overall performance of the wind turbine.[3,19,30] Kooiman and Tullis[19] found that for low turbulence intensities ($I_v < 0.15$), turbine performance is insignificantly affected by wind fluctuations. However, as turbulence intensity increases ($I_v > 0.15$), the turbine performance coefficient decreases. This turbine power coefficient is defined as the ratio of the actual power captured by a wind turbine to the total available power in the unsteady wind. The degradation of turbine performance with increasing turbulence intensity of the wind has been shown in other studies as well.[3,25,30] Note, in the study of Kooiman and Tullis,[19] that the turbulence intensity was calculated using 10-s time interval. On the other hand, the averaging window typically used in atmospheric studies ranges from 10 min to an hour.[22,38] The short averaging period used by Kooiman and Tullis[19] denotes that their results underpredict the actual capability of wind turbines with response times longer than 10 s. It is also worth mentioning that the wind turbine used by Kooiman and Tullis[19] was operated at a constant rotational speed in each experiment. The rotational speed was not optimized for the given wind conditions. McIntosh *et al.*[23] suggested that in order to increase the energy captured during unsteady winds using a turbine operated at a constant rotational speed, an over-speed control technique should be applied. It remains to be determined how the optimal over-speed setting varies with turbulence intensity and whether enhanced energy capture is possible as the turbulence intensity increases.

This paper utilizes a numerical modeling approach to investigate the conditions under which enhanced energy capture is possible by a VAWT operating in gusty winds representative of an urban/suburban environment. The optimal operating point of the turbine is determined for two different control strategies: (i) constant rotational speed controller and (ii) ideal tip speed ratio (TSR) controller. The total energy captured by the VAWT for the two different control strategies is also compared. Finally, the effects of turbulent intensity, gust frequency, and turbine inertia on the overall performance of the turbine are explored.

II. NUMERICAL MODELS

Several numerical models were utilized in this research to investigate the possibility of enhancing the energy captured by a VAWT operating in gusty winds representative of an urban/suburban environment. The first model "Gust Energy Coefficient Model" (Section II A)

was developed to estimate the amount of excess energy available within the gust. This model provides a way to compensate for the underestimation of wind resource when the mean wind speed is used as a siting indicator. The second model "Gust Time Series Model" (Section II B) was developed to create piecewise continuous wind speed data in substitution of the instantaneous wind speed data that is rarely available publicly. This time series model was later used as an input to the transient response model. The "Turbine Model" (Section II C) simulated the aerodynamic performance of the wind turbine that is a necessary input in our transient model. The "Transient Response Model" (Section II D) was developed to understand the transient behavior of the turbine in order to accurately estimate the amount of energy that could be generated by the turbine in the urban environment. Finally, two types of controllers, including a constant rotational speed controller and an ideal tip-speed-ratio controller, were examined in the "Turbine Controller Model" (Section II E) to quantify the amount of additional energy capable of being harvested with different control schemes.

A. Gust energy coefficient model

Wind in the atmospheric surface layer contains a vast range of time scales spanning from seconds to months. Large fluctuations at the macrometeorological scale encompass diurnal to seasonal variations, while fluctuations at the micrometeorological scale are often on the order of seconds.[19,37] The term "gust" is used loosely in the present study to describe relatively large fluctuations in the wind speed on the micrometeorological scale. The available energy contained within a gust is quantified using the GEC, following the work of Berténi *et al.*[3] The GEC is defined as the ratio of actual energy in the instantaneous wind integrated over a time period of interest (E_G) to the energy assuming a steady wind over the same time period (E_S). One can calculate GEC as follows:

$$GEC = \frac{E_G}{E_S} = \frac{\frac{1}{2}\rho A \frac{1}{T}\int_0^T U^3 dt}{\frac{1}{2}\rho A \bar{U}^3}, \tag{1}$$

where T denotes the averaging time period, $U (= \bar{U} + u')$ represents the instantaneous wind speed, $\bar{U}$ is the mean wind speed over the averaging time period $0 \le t \le T$, and u' denotes the turbulent velocity. Note, $\overline{u'} = 0$ in this framework. Physically, GEC represents the amount of excess energy available to be captured, if a wind turbine could effectively respond to the instantaneous wind fluctuations. It is known that a significant amount of energy is contained within the frequency of the gust.[23] However, most wind sitings are based on the mean winds at a given location;[8,11] therefore, current siting techniques may significantly underestimate the actual wind potential at a given location. The GEC provides a mean to compensate for the underestimation of wind resources when the mean wind speed is used as a siting indicator. The expression for GEC in (1) can be written compactly as follows (see the Appendix):

$$GEC = 1 + 3I_T^2 + S_u I_T^3, \tag{2}$$

where I_T and S_u denote the turbulence intensity and skewness of the wind speed, respectively. Therefore, GEC is seen to depend solely on the second and third statistical moments of the wind signal. Note, for normally distributed wind fluctuations, $S_u = 0$, meaning that GEC increases quadratically with the turbulence intensity.

Figure 1 shows the gust energy coefficient as a function of turbulence intensity, comparing actual wind data to the prediction in Equation (2). Data were collected on June 14, 2005 from a sonic anemometer located at a height of 36 m above the ground in a suburban neighborhood in Utah's Salt Lake Valley. The area surrounding the test site was mostly residential in nature. Data from the sonic anemometer were sampled at 10 Hz. A detailed description of the site and

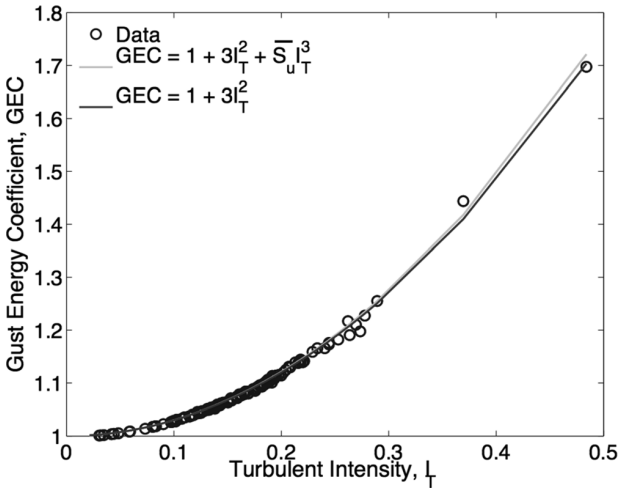

FIG. 1. Gust energy coefficient as function of turbulent intensity. Each point represents a 10-min average of sonic anemometer data collected on 14 June 2005.

instrumentation can be found by Ramamurthy and Pardyjak.[28] Each data point in Figure 1 represents a statistical average over a 10-min interval. In total, 24 h of data are shown in the figure. As can be seen, a wide range of turbulence intensity values ($0 < I_t < 0.5$) are obtained on this day. The results indicate that a significant amount of energy is contained within the gust as the turbulent intensity increases. There is a 6.7% increase in total available energy contained in the gust when the turbulence intensity measures 0.15. This increases to about 27% when the turbulence intensity reaches 0.3.

The solid lines in Figure 1 are based on Equation (2) for two cases: (i) $S_u = 0$, assuming data are normally distributed, and (ii) $S_u = \bar{S}_u$ where $\bar{S}_u$ corresponds to the average skewness over the entire 24 h time period. For the time period investigated, $\bar{S}_u = 0.1614$. There is almost no difference between the two predictions except at high I_T, which implies that skewness of the wind distribution has an insignificant effect on the GEC. This follows because the skewness of the turbulent wind at heights on the order of a few meters above ground level are expected to be small,[14] meaning that the GEC is only weakly dependent on S_u. Therefore, a good model for the excess energy contained in wind gusts predicts that the GEC increases quadratically with turbulence intensity in the form

$$GEC \approx 1 + 3\,I_T^2. \tag{3}$$

B. Gust time series model

An analysis of the transient response of a wind turbine under a gusty wind requires instantaneous wind speed data. Most of the publicly available data on wind speed, however, are typically derived from cup and vane anemometers and are often presented in the form of an average wind speed along with a maximum gust speed over a set time interval, which could vary from a few minutes to an hour or more. A gust time series model was created to convert discrete mean wind speed and gust data of this form into a piecewise continuous time series that preserves the low frequency, large-scale features of the actual instantaneous signal. The gust time series model was used as an input to our transient wind turbine model (presented in Section II D), in order to study the total energy captured by a wind turbine in the presence of real gusty wind over the course of a full year. Because the gust time series model serves as an integral part of the present study, details of the model are described below.

Figure 2 illustrates the gust time series model compared to a sample of sonic anemometry data. In the figure, M_1 and G_1 represent the measured mean speed and maximum gust speed over

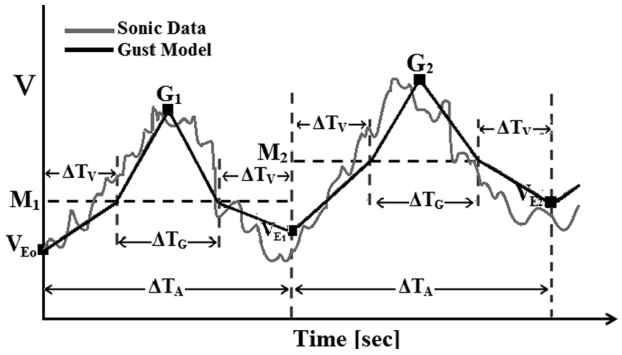

FIG. 2. Schematic of the gust model that produces a piecewise continuous velocity time series. M and G represent the measured mean wind velocity and wind gust, respectively, over each averaging interval delineated by the vertical dashed lines.

the first averaging block, delineated by the vertical dashed lines and labeled as T_A. Similarly, M_2 and G_2 represent the measured mean speed and the corresponding wind gust for the second averaging block. Note the M_i and G_i values for each averaging block constitute the available data. The time series model based on M_i, G_i, and ΔT_A utilizes the piecewise linear functions. To construct the piecewise linear functions, each averaging block is divided into three separate subintervals, two of which have the same period, as shown in Figure 2. The center subinterval has a duration ΔT_{G_i}, which represents the period of time that the wind velocity is above its mean value M_i. Note the gust value G_i is assumed to occur in the center subinterval. The two other subintervals have a period ΔT_{V_i}, which represents the time when the wind velocity is below the mean value M_i. The subintervals are related by the fact that $2\,\Delta T_{V_i} + \Delta T_{G_i} = \Delta T_A$. The value of the wind velocity at the end of each interval is denoted as V_{E_i}; and the value of the wind velocity at the beginning of the time series is denoted by V_{E_0}. To represent the randomness of the actual wind signal, the values of V_{E_i} for $i = 0, 1, 2, \ldots, N$ are assigned using a random number generator that selects a value for V_{E_i} within a predefined range based on a fraction of the mean value M_i. Typically a range of $0.45 \leq V_{E_i}/M_i \leq 0.95$ was used, although a sensitivity analysis was performed (and is described at the end of the section) to quantify the effect of this range on the model output. Once M_i, G_i, and V_{E_i} are known, one can solve for ΔT_{G_i} of the ith interval by equating the area of the triangle above the mean to the area of the two triangles below the mean to obtain

$$\Delta T_{G_i} = \frac{T_A(2\,M_i - V_{E_{i-1}} - V_{E_i})}{2\,G_i - V_{E_{i-1}} - V_{E_i}}. \tag{4}$$

This procedure ensures that the piecewise model time series maintains the true mean velocity of M_i in each block.

The gust time series model described above was validated using the same sonic anemometry data as that in Section II A. In order to create the necessary input data for the model, the sonic anemometry wind signal was first divided into 5-min blocks (no overlap between blocks). The mean and maximum wind speed in each block was then used to create the M_i and G_i arrays for the model. In this case, 1 h of sonic anemometry data is presented, which yields 12 discrete blocks, i.e., $i = 0, 1, \ldots, 12$. A piecewise continuous model of the wind velocity time series was then constructed from the M_i and G_i data using the procedure described in the preceding paragraph. The results are shown in Figure 3 compared with the original 1-h segment of instantaneous sonic anemometry data. As illustrated, the gust time series model is not able to reproduce the small scale, high frequency variations in the sonic data. In addition, the model is not always in phase with the actual wind gusts. Overall, the gust time series model captures the trends of the sonic data and, more importantly, shows a good representation of the large scale, low frequency features in the sonic wind data.

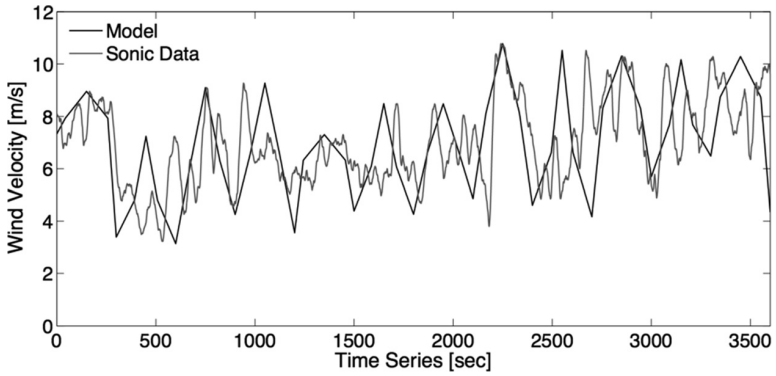

FIG. 3. Comparison of the gust time series model with a 1-h segment of instantaneous sonic anemometry data collected from a suburban neighborhood in Utah's Salt Lake Valley on 14th June 2005.

Despite the observed discrepancies with the instantaneous sonic data, the gust time series model performs surprisingly well in terms of predicting the total available energy in the wind. For the 1 h segment of data shown in Figure 3, the total available energy, i.e., the numerator of (1), assuming an area of 2.56 m^2 and a constant fluid density of 1.12 kg/m^3 is 2153 W for the instantaneous sonic data and 2120 W for the gust time series model. This translates into a 1.56% difference in the total available energy between the actual wind and the model time series. Since the total available energy is the quantity of primary interest in the present study, the gust time series model is deemed acceptable.

Since the gust time series model uses a random number generator to assign values of the wind velocity at the end of each interval, V_{E_i}, a sensitivity analysis was performed to quantify the variation in the model output (total available energy) over 100 different realizations. In addition, the model selects the values for V_{E_i} within an allowable range that varies with each block, $(V_{E_i})_{\min} \leq V_{E_i} \leq (V_{E_i})_{\max}$, where $(V_{E_i})_{\min}$ and $(V_{E_i})_{\max}$ are prescribed based on a set fraction of the mean wind velocity in that block M_i, i.e., $(V_{E_i})_{\min}/M_i = P_{\min}$ and $(V_{E_i})_{\max}/M_i = P_{\max}$. In order to initiate the model, the user defined values for $P_{\min}$ and $P_{\max}$ which remain constant for all blocks. Different combinations were selected in the range $0.45 \leq P_{\min} \leq 0.6$ and $0.85 \leq P_{\max} \leq 0.95$. The results indicate that the difference between the total available energy calculated by the model compared to the true value remains less than 4% for all of the test cases. The gust time series model will be used in subsequent model in conjunction with cup and vane anemometry data to investigate the ability of a wind turbine to capture energy from gusty winds over long periods of time.

C. Turbine model

Various numerical models have been developed to predict the power performance of a VAWT, a survey of which can be found by Paraschivoiu and Delclaux[27] and Islam *et al.*[15] For example, Schuerich and Brown[31] developed a CFD model to predict the aerodynamic performance of a VAWT based on discretizing the vorticity transport formulation of the Navier-Stokes equations. While the CFD models can provide detailed information about the flow field, a major drawback is the computational expense. In the present study, CFD models would have been prohibitive. Therefore, a simpler modeling approach was preferred, which allowed the transient response of a VAWT to be studied over the course of a full year using actual urban/suburban wind data as an input. This would not be a straightforward task in a CFD framework. Instead, the present study utilizes the Blade Element Momentum (BEM) theory as the backbone of the turbine performance model. BEM is a common feature of many existing numerical models of VAWTs, including the single streamtube model,[4] the double multiple streamtubes model,[2,15] and the 2D vortex model.[24] Transient response can then be obtained using a 4th order Runge-

Kutta time integration of the pseudo-steady forces on the VAWT calculated from the BEM, following similar strategies of McIntosh *et al.*[23] and Hara *et al.*[12]

1. BEM theory

BEM theory utilizes the actuator disc method[10] to determine the momentum deficit downstream of the VAWT, in combination with empirical lift and drag coefficients for the blades in order to calculate the power performance of the turbine. The actuator disc method is based on a control volume analysis, in which the control surface is represented by a streamtube, as shown in Figure 4. The rotating wind turbine is treated as a single actuator disc that creates a jump discontinuity in pressure at the location of the disc. In this model, the actuator disc represents a line in space; and as such, the induced velocity is assumed to be constant across the disc. In addition, the flow is assumed to be homogeneous, incompressible, and steady; the thrust is assumed to be uniform over the disc; and the wake is assumed to be non-rotational. Note the latter assumption is valid in the case of a VAWT, since the rotation vector is aligned along the axis of the turbine which remains perpendicular (or nearly perpendicular) to the mean flow direction. Therefore, the increase in angular momentum occurs in a direction transverse to that of the linear momentum, which means it should not affect the velocity V through the streamtube as it does in the case of a horizontal axis wind turbine. In addition, the static pressure far upstream and downstream of the disc is assumed to be equal to the ambient static pressure. Applying conservation of linear momentum to the defined control volume, the thrust force T acting on the turbine can be expressed as

$$T = [4a(1-a)]\left(\frac{1}{2}\rho A V_1^2\right), \tag{5}$$

where V_1 represents the upstream wind speed approaching the turbine and a denotes the axial induction factor, defined as the fractional velocity deficit due to the presence of the turbine,

$$a = \frac{V_1 - V_2}{V_1}. \tag{6}$$

Details of the derivation can be found by Paraschivoiu.[26]

The forces acting on the blades of the turbine can be calculated using empirical lift and drag coefficient data (C_L and C_D, respectively) appropriate for the airfoil shape. In order to

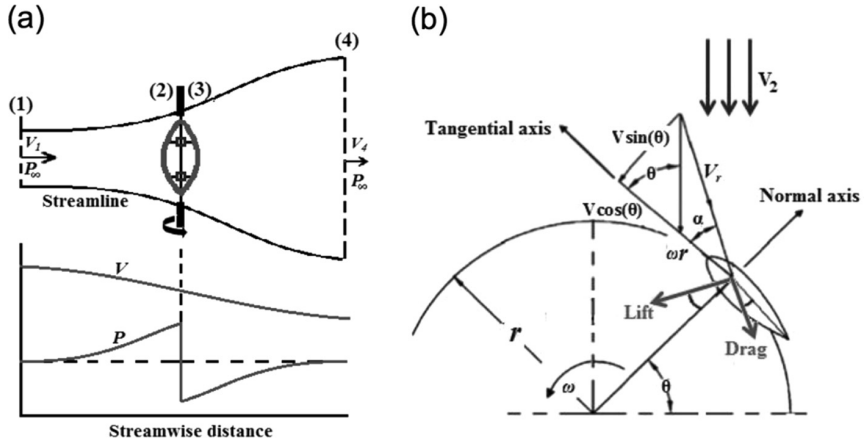

FIG. 4. (a) Schematic of the actuator disk model of a VAWT, where V and P denote the wind velocity and pressure, respectively. (b) Schematic of the velocity and force components acting on a segment of the airfoil blade. Adapted from Figure 2 of Beri *et al.*[2]

accomplish this, the blades are discretized into infinitesimally thin slices as shown in Figure 4(b). The differential lift and drag forces on each infinitesimal slice are calculated at the corresponding angle of attack α based on a look-up table containing C_L and C_D data as a function of α and Reynolds number. Note that C_L and C_D are defined using the velocity V_2 at the location of the actuator disc. From Figure 4(b), it is clear that α depends on the relative velocity V_r, which is a vector sum of the disc velocity V_2 and the induced velocity due to the rotation of the turbine, $V_i\,(=r\,\omega)$ where r denotes the local turbine radius (distance from the axis of rotation of the turbine to the quarter chord of the blade element) and ω represents the rotational speed of the turbine. For the case of an eggbeater-shaped Darrieus VAWT as used in the present study, the angle of attack α is calculated for a given azimuth angle, θ, as follows:[36]

$$\alpha = \tanh\left(\frac{\sin\theta\,\cos\delta}{\frac{r\,\omega}{V}+\cos\theta}\right). \tag{7}$$

The local blade slope angle δ accounts for the changes in the local radius r with height, and is necessary for turbines without straight blades Templin.[36]

The differential lift and drag forces are then decomposed into their respective normal and tangential components

$$dF_n = \frac{1}{2}\,Nc\rho V_r[C_L\,\cos\alpha + C_D\,\sin\alpha]\,dh, \tag{8}$$

$$dF_t = \frac{1}{2}\,Nc\rho V_r[C_L\,\sin\alpha - C_D\,\cos\alpha]\,dh, \tag{9}$$

where N is the number of blades, c denotes the chord length, and dh represents the differential height of the blade element. The total drag force D acting on the turbine, as a result of the momentum deficit across the turbine, can then be obtained by taking the component of dF_n and dF_t aligned with the disc wind velocity V_2 and integrating with respect to both h over the entire height of the turbine H, and θ over one full revolution of the rotor,

$$D = \frac{1}{2\pi}\int_{\frac{-H}{2}}^{\frac{H}{2}}\int_0^{2\pi}\left[(\sin\theta)\,dF_n - \left(\frac{\cos\theta}{\cos\delta}\right)dF_t\right]d\theta\,dh. \tag{10}$$

Note that by equating D from (10) with T from the actuator disc method (5), one can solve for the unknown value of the axial induction factor a, which can then be used to specify the value of V_2. Once V_2 is known, the resultant torque Q, output power P, and power coefficient C_P of the VAWT can be evaluated as

$$Q = \frac{1}{2\pi}\int_{\frac{-H}{2}}^{\frac{H}{2}}\int_0^{2\pi}\left[r(h)\left(\frac{1}{\cos\delta}\right)dF_t\right]d\theta\,dh, \tag{11}$$

$$P = Q\,\omega, \tag{12}$$

$$C_p = \frac{P}{\frac{1}{2}\rho A V_1^3}, \tag{13}$$

where $A = \frac{8}{3}R^2$ denotes the frontal area of the turbine for an eggbeater-type turbine. Here, R denotes the maximum radius of the turbine.

2. Turbine model validation

The case study used to validate the BEM numerical model is that of a Darrieus VAWT with 3 blades, a maximum radius of $R = 0.98$ m, and a height of $H = 2$ m. The three turbine

blades are based on the NACA 0012 airfoil shape with a 5.88 cm chord length and 0° pitch angle. Figure 5 shows the power coefficient (C_p) versus tip speed ratio (TSR $= R\omega/V$) for the present BEM numerical model compared to experimental results, from both laboratory and field data.[4] The wind turbine was tested in the 4.6 m × 6.1 m Vought system division low speed wind tunnel. A detailed description of the experimental setup can be found by Blackwell *et al.*[4] Lift and drag coefficient data are incorporated from two different sources, Jacobs and Sherman[16] for angle of attack less than 28° and Sheldahl and Klimas[34] for angle of attack greater than 28°. In all cases, the geometry and configuration of the VAWT are identical; however, the Reynolds number could not be matched exactly. For purposes of the validation study, the numerical model utilized a Reynolds number of $Re = 150\,000$ (400 rpm), consistent with that of the field experiment, while the wind tunnel experiment was run at $Re = 154\,000$. It is noted that the wind turbine was operated at 460 rpm in the field experiment and 400 rpm for the wind tunnel experiment. As apparent from Figure 5, results from the wind tunnel and field experiments do not completely align, despite the fact that Re is very close and the geometries of the turbines are identical. Except for a narrow range of tip speed ratios near TSR = 4.25, the wind tunnel C_p values consistently under predict those from the field experiment. Blackwell *et al.*[4] suggested that differences in the measured performance of a turbine tested in a wind tunnel versus in the field could be a result of wind blockage effects or it could be a real (but unexplained) difference.

Figure 5 also shows that the numerical model compares favorably with the results from the field experiment for tip speed ratios greater than the peak (TSR > 5), though there are noticeable deviations to the left of the peak, for TSR < 5. In the lower tip speed ratio range ($2 \leq$ TSR ≤ 4), the numerical model underpredicts the C_p values from the field by about 9%–18%, and tends to follow the results from the wind tunnel experiment. The numerical model correctly captures the overall shape of the power performance curve, and is able to predict the peak value of C_p to within 3.0% of the field data, as well as predict the optimum TSR, defined as the tip speed ratio yielding the peak C_p. Therefore, the numerical model is deemed satisfactory for purposes of the present study.

D. Transient response

Understanding the transient response of a wind turbine under gusty wind conditions is necessary in order to obtain an accurate estimate of the amount of energy that can be generated by the turbine in urban environments. Although VAWTs are unaffected by wind direction,[19] variations in wind speed do significantly impact the overall performance of the wind turbine, owing

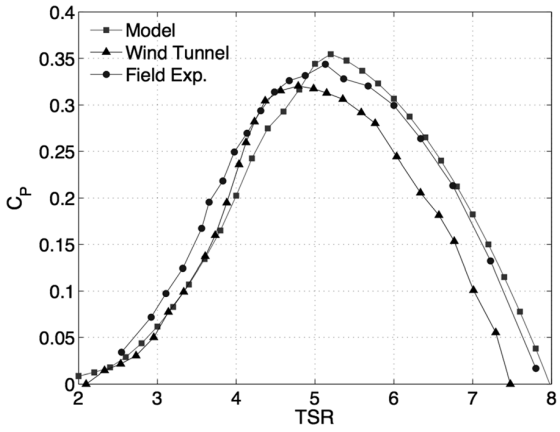

FIG. 5. Power coefficient performance curve vs. tip speed ratio comparing the present numerical model with experimental data. In all cases, the same geometry VAWT was used. The Reynolds number for the numerical model and field experiments was $Re = 150\,000$, while that for the wind tunnel experiments was $Re = 154\,000$.

to the moment of inertia of the turbine, the applied loading torque, the temporal response of the controller, and the aerodynamics of the turbine blades.[12,19] The transient response of a wind turbine to an unsteady wind speed can be modeled as

$$I\frac{d\omega}{dt} = Q - T_L, \tag{14}$$

where I is the moment of inertia of the wind turbine, Q is the aerodynamic torque of the turbine, T_L is the applied loading torque from the generator, and ω is the rotational speed of the turbine. In the transient model, the aerodynamic torque Q depends on the tip speed ratio and incoming wind speed according to (11).

Figure 6 illustrates graphically how changes in the incoming velocity affect the power coefficient C_p, for the case where the rotational speed ω of the turbine remains constant. In the example considered, the incoming velocity increases in a piecewise linear fashion from two constant states, labeled as operating point 1 (OP 1) and operating point 2 (OP 2) as shown. Because ω remains constant in this example, the tip speed ratio varies inversely proportional with V. At the same time, the turbine power coefficient C_P moves along the trajectory shown in the plot. Note that this model utilizes lift and drag coefficient data valid for steady flow. Therefore, transient behavior in this framework is modeled as the infinitesimal change between two pseudo-steady states. A more appropriate model to predict the aerodynamics performance of the VAWT should include dynamic stall effects, as the cyclic motion of the blades induces large variation in the angle of attack on the wind turbine blades.[31] However, this increases the complexity of the model, and requires unsteady lift and drag coefficient that is difficult to obtain. Therefore, as a first step in understanding the amount of additional energy that could be harvested by a VAWT during gusty winds, the present study opts for a more simplistic modeling framework.

E. Turbine controller

The ability of the turbine to respond to fluctuations in the wind speed depends on the response characteristics of the system, an important aspect of which is the controller. Different control methods can be used to optimize or limit the amount of energy captured by the wind turbine. The present study only considers electrical controllers that adjust the synchronous speed of the generator, rather than mechanical controllers such as pitch and yaw adjustment, which cannot be used as control strategies on the VAWTs. Two types of controllers are

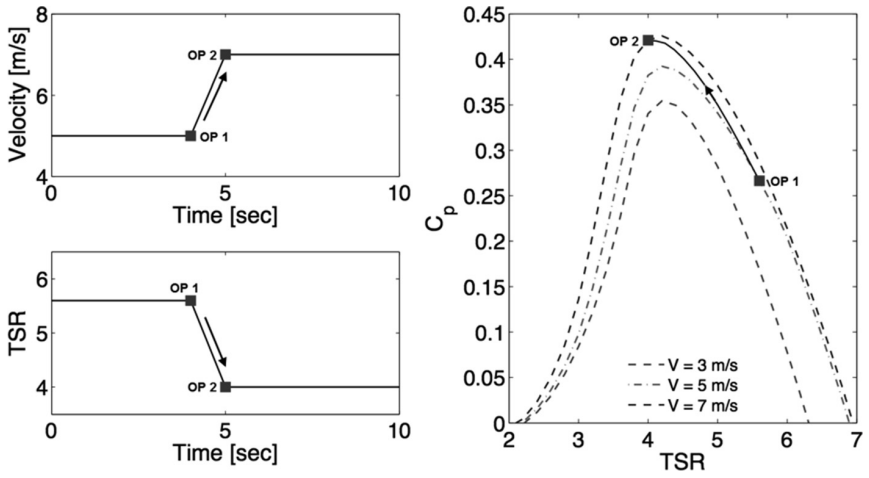

FIG. 6. Illustration of how the power coefficient C_p varies with a piecewise linear increase wind velocity.

examined: (i) constant rotational speed, or *constant-ω* and (ii) ideal tip speed ratio, or *ideal-TSR*. The amount of total energy extracted by a VAWT in an urban environment using each type of controller is quantified.

1. Constant rotational speed controller

The constant-ω controller drives the turbine rotor at a fixed speed regardless of variations in the incoming wind speed. Typically in this design, the generator is directly coupled to the power grid, which causes the generator speed to lock to the frequency of the power line. The actual speed of the turbine rotor is then determined by the gear ratio of the drive train connecting the turbine and generator as illustrated in Figure 7. For purposes of the present study, it is assumed that the gear ratio can be adjusted to achieve any desired ω. Once set, the turbine is forced to spin at the prescribed ω, unless the gear ratio is readjusted. In this manner, the constant ω controller is considered to be the most practical and simplest type of wind turbine controller.

With a constant-ω controller, the TSR of the turbine is inversely proportional to the incoming wind speed. Therefore, variations in the wind speed cause the wind turbine to deviate from its most efficient operating point. The current operating point of the turbine (on a C_p versus TSR plot) at any given time, and the amount of energy being captured, can be determined by setting the angular acceleration term in (14) to zero, i.e., $d\omega/dt = 0$. Since the inertia of the turbine remains constant in this type of control strategy, the applied torque (T_L) is equal to the current aerodynamic torque (Q). The latter is calculated based on the BEM method as described in Section II C 1 using the real-time wind speed as input. Once $T_L(t)$ is calculated as a function of time, the total energy captured by the turbine is simply the power integrated over the time period of interest, $E = \int \omega \cdot T_L(t)\, dt$. Interestingly, an *optimal* ω exists for each time period that yields the maximum amount of energy captured using a constant speed controller. This idea is explored further in Section III A.

2. Ideal tip speed ratio controller

The ideal-TSR controller provides active control of the turbine, allowing the turbine to respond instantaneously to wind gusts thereby extracting the maximum amount of energy available from the wind. This type of controller instantaneously adjusts ω in response to variations of the incoming wind speed to ensure continuous operation at the ideal TSR setting of the turbine. In practice, variable speed operation is achieved by power electronics that continuously switch the connection between the generator and grid to change the synchronous speed of the generator independently of the frequency of the grid. The digital control signal is supplied by a microprocessor that has been programmed with the response characteristics of the specific turbine. Alternatively, one might be able to achieve the same effect using a continuous variable transmission system.[6,13]

The ideal-TSR control method regulates the rotational speed of the turbine to maintain an ideal TSR setting that yields the maximum C_p at every given moment in time. In the present study, the electronics are modeled using a proportional feedback control strategy, as illustrated in Figure 8, where K_p represents the proportional gain constant. A realistic controller is unable to instantaneously track fluctuations in the wind speed, due to the gain constant (K_p) of the controller and the inertia (I) of the turbine which combine to produce a time lag in the response. The following methodology was used to determine the total energy captured over any given

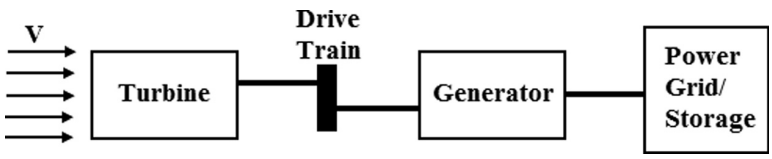

FIG. 7. Block diagram of constant rotational speed controller.

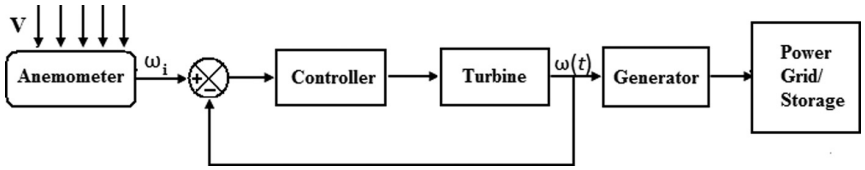

FIG. 8. Block diagram of ideal tip speed ratio controller.

time period. First, the dynamics of the system (controller and turbine) is written in the Laplace domain by following equation:

$$\frac{\omega(t)}{\omega_i} = \frac{K_p}{Is + K_p}, \tag{15}$$

where $\omega(t)$ is time varying rotational speed of the turbine and ω_i is the ideal rotational speed of the turbine. Using real-time wind speed data as input, the ideal TSR, ideal rotational speed (ω_i), and maximum C_p (as well as maximum aerodynamic torque Q) are determined as a function of time from the BEM method described in Section II C 1. The time-varying rotational speed of the turbine $\omega(t)$ is calculated from the ideal rotational speed and substituted into Equation (15). The loading torque $T_L(t)$ is subsequently calculated by solving Equation (14), and multiplied by $\omega(t)$ to obtain power, which is then integrated over the time period of interest to yield the total energy captured.

III. RESULTS

The transient numerical model is applied to an example VAWT in order to examine the time response of the turbine to gusty winds characteristic of that in a suburban/urban environment. The total energy captured over the duration of a full year in operation is quantified for two different types of controllers (constant-speed and ideal-TSR). The wind turbine configuration used to generate the results consists of an eggbeater Darrieus-type turbine having three blades based on the NACA 0015 airfoil shape with a chord length of 9 cm. The solidity of the wind turbine is 0.3; the height measures 2 m; and the maximum radius measures 1 m. The wind turbine is subjected to two sets of actual wind speed data: (i) sonic anemometry data collected from a suburban neighborhood in Utah's Salt Lake Valley from 14 to 16 June, 2005 and (ii) cup and vane anemometry data collected during 2013 from a MesoWest wind monitor located on the roof of the William Browning Building (WBB) on the University of Utah campus. The sonic data were sampled at 10 Hz and subsequently block averaged into 10-min intervals for purposes of the present analysis. This selection of time interval is typically used as the standard in wind engineering.[22,38] The cup and vane data are recorded as 5-min averages along with the corresponding 5-min gust value. These data were subsequently used in the gust model presented in Section II B to generate a piecewise continuous time series of wind speed, which was then used as input to the transient turbine model. In order to effectively quantify the wind turbine performance in gusty conditions, the Turbine Energy Coefficient parameter (C_E) is defined as the ratio of the total energy captured by the wind turbine over a time period of interest to the total energy available within the gusty wind,

$$C_E = \frac{\int_0^T P(t)\,dt}{\int_0^T \frac{1}{2}\rho A V^3\,dt}. \tag{16}$$

As such, C_E can be thought of as the true efficiency of the turbine.

A. Constant rotational speed controller

The main question when employing a constant-ω controller is what rotational speed should be used. In the steady-state conditions, the obvious choice is to operate the turbine at a fixed

speed corresponding to the peak C_p value. For example, considering the turbine performance results in Figure 6 for a steady-state wind speed of $\bar{V} = 5$ m/s, the best performance would be achieved with an optimal TSR of 4.2 corresponding to a peak value of $C_p = 0.39$. This translates into an optimal steady-state rotational speed of 200 rpm. The optimal steady-state ω increases as the mean wind speed increases. However, steady-state conditions rarely exist in reality, especially in the suburban/urban environment. It was shown in Figure 1 that the amount of available energy in a gusty wind relative to that of a steady-state wind with the same mean value increases quadratically with the turbulence intensity. McIntosh *et al.*[23] found that in order to capture the additional energy in a gusty wind, the operating speed of the turbine needs to be set to a value greater than the steady-state rotational speed. This optimal rotational speed for unsteady winds is referred to as an *optimal overspeed* setting (ω_{opt}). The value of ω_{opt} depends both on the gust characteristics of the incoming wind as well as the performance characteristics of the turbine, and must be calculated specifically for the time period of interest in order to realize the highest efficiency. In the present study, a numerical optimization routine based on the Golden-Section search algorithm was used to find ω_{opt} for each time period of interest. Based on ω_{opt}, one can calculate the optimal overspeed ratio as $\text{TSR}_{\text{opt}} = \omega_{\text{opt}} R/\bar{V}$, where $\bar{V}$ denotes the mean wind speed over the time period of interest. When operated at TSR_{opt}, the wind turbine is capable of more efficiently capturing the large amounts of energy contained within the gusts.

Figure 9 illustrates the relationship between the turbulence intensity level of the incoming wind (I_T) and the optimal overspeed ratio (TSR_{opt}) calculated based on the same data. The black diamonds represent I_T and TSR_{opt} determined over discrete 10-min time intervals from the sonic anemometry data, while the circles represent I_T and TSR_{opt} determined over discrete 24-h time intervals from the MesoWest wind monitor data. More scatter is observed at higher turbulence intensity because of the longer time intervals used. The solid line denotes a quadratic curve fit to the combined sonic and wind monitor data, and appears to follow faithfully represent the general trend of the data. The $\star$ in Figure 9 was calculated using a time interval spanning the full year of 2013 wind monitor data, and falls close to the curve fit line (note that the $\star$ was not included in the curve fit analysis). This means that a turbine located at the measurement site, with the same physical configuration as that used in the present study, should have operated at $\text{TSR}_{\text{opt}} = 13.3$ in order to extract the most energy possible during 2013 using a constant-ω controller. Since the average annual velocity at the measurement site during 2013

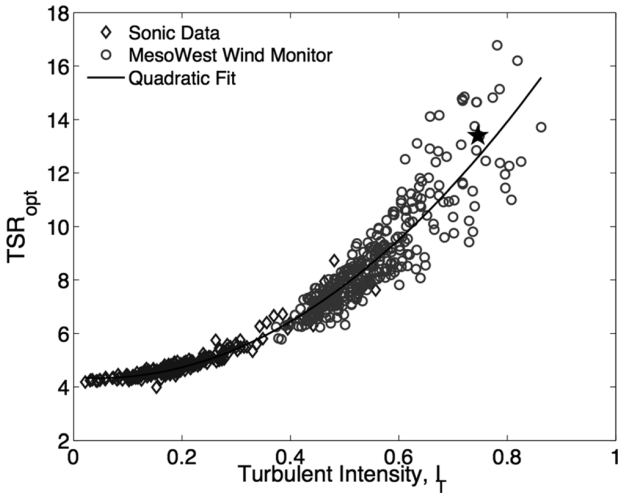

FIG. 9. Influence of turbulence intensity on the optimal overspeed ratio for a constant speed controller. Each point of sonic data represents a 10-min time interval, while each point of the MesoWest wind monitor data represents a 24-h time interval. The star ($\star$) was obtained using a time interval spanning the entire year of 2013 MesoWest wind monitor data. The curve fit is based on all of the data excluding the $\star$.

was 2.7 m/s, an optimal tip speed ratio of 13.3 translates into an optimal fixed speed of $\omega_{opt} = 334$ rpm. This high operating rotational speed allows the turbine to capture the energy contained within the wind gust more efficiently.

The influences of wind velocity, turbulent intensity, and gust frequency on the energy coefficient (C_E) of the turbine for a constant-ω controller are shown in Figure 10. The data in Figure 10(a) indicate that with a constant speed controller, the performance of the turbine degrades as the turbulence intensity of the wind increases. This is as expected since gusty winds with a high level of turbulence intensity contain more available energy than those with a lower turbulence intensity (this effectively makes the denominator of C_E much larger for gusty winds with high I_T). With a constant speed controller, however, the turbine is not able to respond to the variations in wind speed, and therefore, is inefficient in capturing the increase in the available energy in the gusts despite being operated at its TSR_{opt}. Figure 10(a) also indicates that the magnitude of the mean wind speed has a significant effect on the overall performance of the turbine. At the same level of turbulence intensity, the turbine is able to realize better performance in cases with higher mean wind speed. This is due to the effect of the Reynolds number on the aerodynamics of the turbine blades. Specifically, the lift coefficient of the airfoil increases with the increasing Reynolds number, which allows the turbine blades to generate more aerodynamic torque as the mean wind speed increases, thereby increasing turbine performance. Reynolds number effect on the overall performance of wind turbines has also been observed in the study by Kooiman and Tullis.[19]

The relationship between the gust frequency and energy coefficient is illustrated in Figure 10(b). The characteristic gust frequency used in this analysis is the most dominant frequency, as obtained from a Fast Fourier Transform of each 10-min interval. The lowest frequency in the transform corresponds to the fundamental frequency, i.e. $(600\,\text{s})^{-1}$ or 1.67×10^{-3} Hz. The second harmonic in the transform corresponds to 3.33×10^{-3} Hz, and so on. This explains why the data are organized into discrete frequency bands. For a given mean wind speed, no clear relationship between the gust frequency and the energy coefficient is observed. As the mean wind speed increases, C_E increases independent of the gust frequency due to Reynolds number effects as discussed earlier. The present results suggest that the turbulence intensity and mean wind speed are the primary factors affecting turbine performance when using a constant-ω controller, whereas the frequency content of the gusty wind is relatively insignificant.

B. Ideal tip speed ratio controller

In the ideal tip speed ratio controller, inertial effects play an important role on the response behavior of the turbine. In order to obtain a realistic value of the moment of inertia of the turbine, a Computer-Aided Design (CAD) model of the VAWT was created using Solidworks 3D 2014. The blades were assumed to be made of fiberglass; and the turbine hub and support structure were assumed to be made of Aluminum 2024. Based on the CAD model, the wind turbine

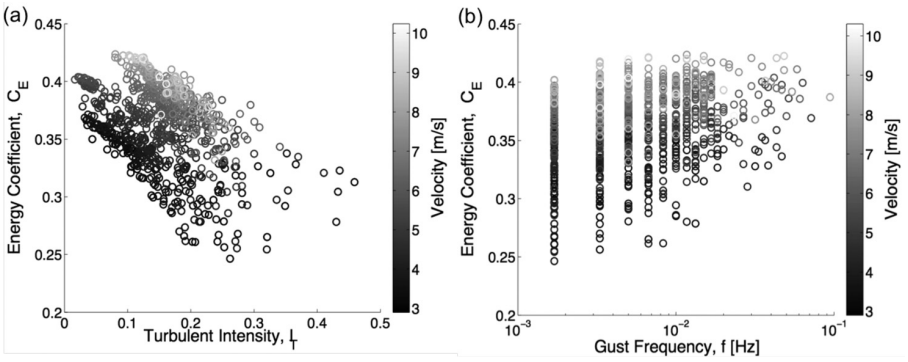

FIG. 10. Wind turbine performance using a constant speed controller. Effect of (a) turbulence intensity and (b) gust frequency on the turbine energy coefficient.

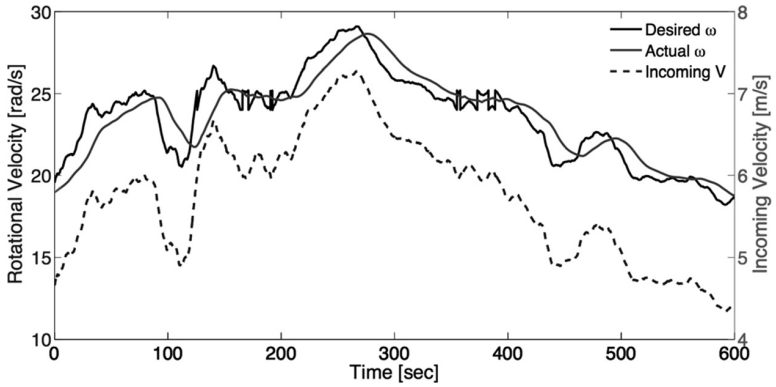

FIG. 11. Sample 10-min interval of sonic data illustrating the time lag between the desired and actual rotational speeds of the turbine. The time lag for this interval was determined to be about 9.3 s, based on an analysis of the cross-correlation between the desired and actual speeds.

mass moment of inertia is determined to be about 10 kg m^2. The actual operating speed of the turbine is allowed to vary in time according to the governing equation provided in Section II E 2. Due to the effect of the gain constant in the feedback controller and the turbine inertia, a time lag exists between the wind speed and the turbine rotational speed. This time lag defines the response time T_r of the turbine. Figure 11 shows a sample 10-min time interval from the sonic data indicating an approximate time lag of 9.3 s ($T_r = 9.3$ s) between the desired rotational speed and the actual rotational speed. Note that a gain constant of $K_p = 1$ was used. The time lag was determined based on the cross correlation between the ideal (desired) and actual rotational speeds. Naturally, T_r depends on both the mass moment of inertia of the turbine as well as on the value of K_p used. The effect of T_r on turbine performance is explored below.

The present analysis follows the work of McIntosh *et al.*,[23] which defined the nondimensional turbine response parameter (ζ) as the ratio of the turbine response time T_r to the characteristic gust time scale T_g, i.e., $\zeta = T_r/T_g$. McIntosh *et al.*[23] further defined the gust time scale as the inverse of the characteristic gust frequency (f_c), taken to be the frequency containing 99% of the power in the wind. Note that an increase in ζ means the turbine is less responsive to wind gusts (in fact, for the constant-ω controller, $\zeta \to \infty$). Ideally, to capture as much energy in the gusts as possible, one desires a low ζ value, i.e., $\zeta \ll 1$. Figure 12 shows the effect of the turbine response parameter on turbine performance for the case of the ideal tip speed ratio controller. In Figure 12(a), the data are parameterized based on the mean wind speed; while in Figure 12(b), data are parameterized by turbulence intensity. Each point in the figures represents a discrete 10-min time interval from the sonic data. Importantly, in order to

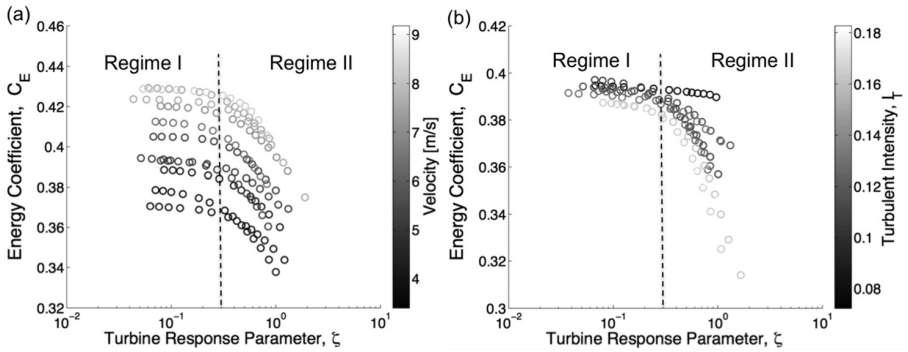

FIG. 12. Effect of turbine response parameter on performance using an ideal tip speed ratio controller. (a) Parameterization by mean wind speed for a narrow band of turbulence intensity in the range $0.1 < I_T < 0.12$. (b) Parameterization by turbulence intensity for a narrow band of wind speed in the range $3.9 < \bar{V} < 4.1$ m/s.

isolate the effects of mean wind speed, the data in Figure 12(a) are restricted to a narrow turbulence intensity band of $0.1 < I_T < 0.12$. Similarly, to isolate the effects of turbulence intensity, the data in Figure 12(b) are restricted to a narrow wind speed band of $3.9 < \bar{V} < 4.1$ m/s. The increase of C_E with mean wind speed noticed in Figure 12(a) is again attributed to Reynolds number effects.

The data suggest two general regimes: (i) constant performance, i.e., C_E independent of ζ for low values of ζ and (ii) degrading performance, i.e., C_E decreasing with ζ for high values of ζ. The transition point appears to be independent of mean wind speed and occurs near a critical value of $\zeta_c \approx 0.3$, as denoted by the vertical dashed line in Figure 12(a). The present results support that of McIntosh *et al.*;[23] however in the study by McIntosh *et al.*,[23] C_E decreases more dramatically and near linearly compared to C_E in the present study.

Figure 12(b) illustrates the impact of turbulence intensity on the turbine energy coefficient. For slower responding turbines ($\zeta > \zeta_c$), high levels of turbulence intensity cause a degradation in performance, in agreement with the results for the constant-ω controller. For turbines with a fast response time ($\zeta \leq \zeta_c$), turbulence intensity has less effect on performance. Though the data clearly suggest that C_E increases slightly with decreasing I_T. Therefore, maximum efficiency is achieved with the ideal tip speed ratio controller during winds with mild turbulence intensity levels (less than 10%) when the response parameter of the turbine is less than the critical value (i.e., $\zeta \leq \zeta_c$). These results are significant for design purposes and can help to set an upper bound on the maximum efficiency achievable with a given turbine configuration. Knowledge of ζ_c for a given turbine located at a particular site can be used to set target specifications on the turbine mass moment of inertia and the gain constant of the controller in order to achieve the best performance possible in gusty winds.

The effect of the characteristic gust time scale on turbine energy coefficient is illustrated in Figure 13. The data in this plot are restricted to a narrow band of mean wind speed ($7.1 < \bar{V} < 7.3$ m/s) and a narrow band turbulence intensity ($0.13 < I_T < 0.15$), in order to isolate the effect of T_g. For fast-response turbines (low value of ζ), data collapse into a single plateau region indicating that the characteristic gust time scale has no impact on the turbine energy coefficient for fast-response turbines. This is as expected, highly responsive turbines are able to faithfully track even small fluctuations in the wind, and efficiently capture a significant amount of the energy available in all gusts. The data, however, peel away from the plateau region at ζ values that appear to depend on T_g. For example, winds with a lower T_g have a longer plateau region (i.e., higher ζ_c). Recall that ζ_c identifies the point at which the plateau region ends and performance degrades. The data in Figure 13 suggest that ζ_c decreases with increasing T_g. Therefore, using the current definition of T_g, a universal ζ_c cannot be identified from the present

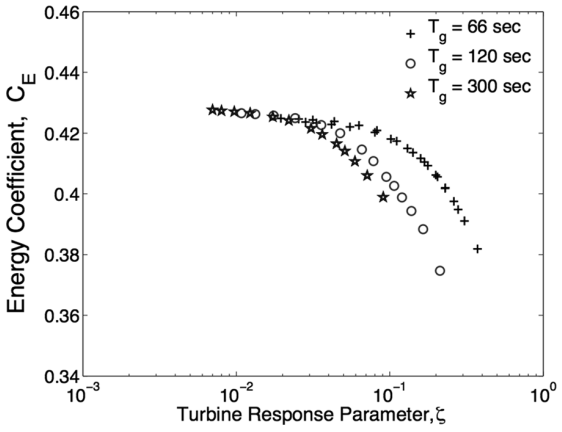

FIG. 13. Efficiency as a function of the turbine response parameter for three cases with different characteristic gust time scales, T_g. In each case, the mean wind speed and turbulence intensity are restricted to a narrow range of 7.1 m/s $< \bar{V} <$ 7.3 m/s and $0.13 < I_T < 0.15$, respectively, in order to isolate the effect of the gust time scale.

data. In the present study, T_g is defined as the inverse frequency containing 99% of the total energy in the wind. Other ways of defining the characteristic gust time scale may lead to universal behavior, and is left as a task for future work.

C. Controller comparison

Although turbine efficiency (referred to herein as the Turbine Energy Coefficient, C_E) is an important quantity for characterizing the performance of a turbine, ultimately one would like to know the total amount of energy captured by the turbine during a time period of interest. This was done using the full year of 2013 MesoWest wind monitor data for the two types of controllers: ideal-TSR and constant-ω. For the ideal-TSR controller, the turbine moment of inertia and proportional gain constant are set to 10 kg m^2 and 1, respectively. For the constant-ω controller, three test cases were performed. In test case 1, the turbine is operated at a steady-state ω based on the annual-averaged mean wind speed and the TSR value corresponding to the peak in the steady-state C_p curve. This is referred to as the "naive" constant-ω controller because it does not take advantage of the increased energy available in the wind gusts, but only utilizes information about the annual-averaged mean wind speed, which was 2.7 m/s at the measurement site for 2013. In test case 2, the turbine is operated at its optimal overspeed, where ω_{opt} is calculated from the full year of data (this test case corresponds to the $\star$ in Figure 9). In test case 3, the optimal overspeed setting is adjusted on a daily basis over the course of the year. This may or may not be feasible in practice, but is presented here to demonstrate the potential performance gains if one could adapt to variations in the daily averaged turbulence intensity. The rotational speed of the turbine used in test case 1 and 2 are 106 rpm and 334 rpm, respectively. The high rotational speed of 334 rpm for test case 2 allows the turbine to take advantage of the increased energy in the wind gusts, which are characterized by a high turbulence intensity ($I_T \sim 0.75$) when averaged over the entire year, as shown in Figure 9. In test case 3, the rotational speed varies from 45 rpm to 480 rpm as the optimal overspeed setting is adjusted daily.

Figure 14 shows the results from the comparison. More than an order of magnitude difference exists between the amounts of energy extracted by the turbine using the ideal-TSR controller versus that of the naive constant-ω controller. By simply operating at an appropriate overspeed setting based on actual wind gust information at the site, one is able to capture six times the energy of the naive controller. Operating at an optimal overspeed allows the turbine to harvest the energy contained within the gust more efficiently. Having the capability of adjusting the optimal overspeed setting on a daily basis, rather than using a fixed overspeed for the entire year, allows the turbine to capture an additional 27% more energy. As expected, the

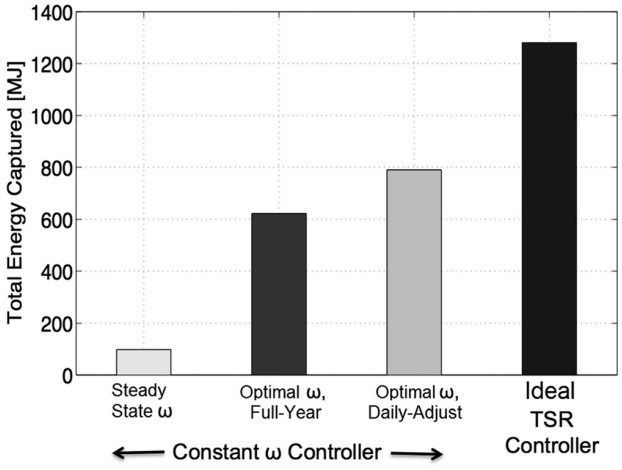

FIG. 14. Total energy captured by the turbine during the year 2013 using the constant speed and ideal tip speed ratio controllers.

ideal-TSR controller provides superior performance, since the turbine is capable responding instantaneously to individual wind gusts. In 2013, the amount of energy captured by the ideal-TSR controller is nearly thirteen times greater than the naive controller. This ideal-TSR controller allows the turbine to capture an additional 106% and 62% more energy compared to the turbine controllers used in test cases 2 and 3, respectively. The data indicate that a small turbine located at this site could harness as much as 1300 MJ (360 kWh) of energy for the year of 2013 despite the low annual average wind speed, compared to about 100 MJ predicted by siting based on the annual-averaged wind speed.

IV. CONCLUSION

The present study focuses on the performance characteristics of a VAWT in response to gusty winds. A numerical modeling approach is developed to study the efficiency and total energy captured by a VAWT using two different types of system controllers: (i) constant rotational speed controller and (ii) ideal TSR controller. One of the main features of the study is the use of a full year of data in the performance analysis. Another important feature of the study relates to exploring the effect of turbulence intensity on the turbine performance.

The numerical modeling approach utilizes the actual wind time series as input data to the semi-empirical BEM in order to calculate aerodynamic torque and rotational speed as a function of time. Wind speed data were obtained from a sonic anemometer and cup and vane anemometer located at two sites in Utah's Salt Lake Valley characterized as suburban and urban, respectively. The sonic anemometer recorded the three components of the velocity vector at a sampling frequency of 10 Hz; while the cup and vane anemometer recorded the mean and maximum horizontal wind speed during consecutive 5-min intervals. In order to be compatible with the numerical framework, the discrete 5-min averaged cup and vane anemometer data were converted into a piecewise continuous time series using a gust model that successfully reproduced the large scale features of the wind signal. Validation with the sonic anemometry data showed that the gust model, while unable to track all of the instantaneous features of the wind signal, is capable of predicting the correct available energy to within 4%, which is considered acceptable for purposes of the present study.

Wind data from the combined sites demonstrate that the amount of available energy in a gusty wind, relative to that of the mean wind, increases quadratically with turbulence intensity. This provides motivation for striving to harness the energy contained in wind gusts and provides an upper bound on the amount of energy available to be harvested. For both types of system controllers, the efficiency of the turbine was found to be strongly dependent on turbulence intensity as well as the mean wind speed. The latter is due to Reynolds number effects on the aerodynamics of the flow over the turbine blades, i.e., higher chord Reynolds numbers lead to the generation of more aerodynamic torque by the airfoil blades. The effect of gust frequency on turbine efficiency was observed to be insignificant.

For the case of the ideal TSR controller, turbine efficiency was observed to plateau to a maximum value when the nondimensional turbine response parameter ζ dropped below a critical value ζ_c. In this regime ($\zeta < \zeta_c$), the turbine responds quickly to fluctuations in the wind. As the turbine response parameter increases above the critical value ($\zeta > \zeta_c$), the turbine is no longer able to closely track the gusts, and efficiency drops. Unfortunately, the value of ζ_c was found to be nonuniversal. Results indicate that ζ_c decreases as the characteristic gust time scale increases. In the present study, the characteristic gust time scale is defined as the inverse of the frequency containing 99% of the energy in the wind. An alternative definition for the characteristic gust time scale may lead to a universal value of ζ_c, though this has yet to be determined and is suggested as future work. This has important practical ramifications, because a universal ζ_c value would allow engineers to calculate a target value for the turbine response time T_r that would guarantee operation in the high efficiency regime. Based on the target specification for T_r, the mass moment of inertia of the turbine and proportional gain constant of the controller can then be sized appropriately for a given site.

For the case of the constant-speed controller, it was shown that the turbine should be operated at an overspeed setting ω_{opt} based on the turbulence intensity of the incoming wind in order to capture as much energy as possible. Using an optimal overspeed setting allowed six times the energy to be captured during the year 2013, compared to the energy captured using a fixed speed based naively on the annual average wind speed for 2013. An additional 27% more energy could be captured if the optimal overspeed setting was adjusted on a daily basis. The amount of energy captured by the ideal-TSR controller for the year 2013 was nearly thirteen times greater than that of the naive constant speed controller, and nearly double the energy captured using the daily adjusted optimal overspeed controller. This is significant because the concept of an ideal-TSR controller may provide the difference necessary in order to make wind technology viable in some urban areas, whereas a turbine operating with a constant-ω controller would not be capable of providing enough energy to make the investment worthwhile. This would be especially true in areas where the annual-average wind speed may be low, but large wind gusts are common.

Note that the present implementation of the numerical model employs static airfoil data. It is well known that the lift and drag forces acting on an airfoil undergo hysteresis in unsteady wind conditions. Dynamic stall data exist for a few airfoil shapes.[9,31] The study by Schuerich and Brown[31] indicates improved simulation results of VAWT performance with numerical models that incorporate the effect of dynamic stall. This has found to be especially true for helical turbines, and to a lesser extent, Darrieus turbines.[31] Including dynamic stall data in the present modeling scheme is not expected to change the overarching conclusions of this work, but may provide a more accurate evaluation of the percent increase in performance using an optimal overspeed setting versus the ideal TSR controller. Future experimental measurements of actual turbine performance during gusty wind conditions are also warranted to confirm the numerical results.

ACKNOWLEDGMENTS

The authors gratefully acknowledge the help of Prathap Ramamurthy and Eric Pardyjak for providing the sonic anemometry data. L.N. was funded by a Graduate Research Fellowship from the University of Utah during a portion of this work.

APPENDIX: GUST ENERGY COEFFICIENT MODEL CALCULATION

Expanding the numerator of (1) leads to the following expression:

$$\begin{aligned} GEC &= \frac{\frac{1}{T}\int_0^T (\bar{U}+u')^3 dt}{\bar{U}^3}, \\ &= \frac{\frac{1}{T}\int_0^T \left(\bar{U}^3 + 3\bar{U}^2 u' + 3\bar{U}u'^2 + u'^3\right) dt}{\bar{U}^3}, \\ &= \frac{\frac{1}{T}\int_0^T \bar{U}^3 dt + 3\bar{U}^2 \frac{1}{T}\int_0^T u' dt + 3\bar{U}\frac{1}{T}\int_0^T u'^2 dt + \frac{1}{T}\int_0^T u'^3 dt}{\bar{U}^3}. \end{aligned} \tag{A1}$$

Note that the first term in (A1) reduces to unity, since the time average of the mean wind speed is simply the mean wind speed, i.e., $\bar{U}$ remains independent of time over the time interval $0 \le t \le T$. Additionally, the second term in (A1) cancels, since the time average of the turbulent wind, by definition, is zero, i.e., $\overline{u'} = 0$. Finally, the definitions of turbulence intensity (I_T) and skewness (S_u) are introduced,

$$I_T = \frac{\sigma_u}{\bar{U}} = \frac{\left(\frac{1}{T}\int_0^T u'^2 dt\right)^{\frac{1}{2}}}{\bar{U}}, \tag{A2}$$

$$S_u = \frac{\frac{1}{T}\int_0^T u'^3 dt}{\sigma_u^3}, \tag{A3}$$

where σ_u denotes the standard deviation of the wind speed. Substituting these definitions into (A1) yields the final expression

$$GEC = 1 + 3\,I_T^2 + S_u\,I_T^3. \tag{A4}$$

[1]T. Ackermann and L. Söder, "An overview of wind energy-status 2002," Renewable Sustainable Energy Rev. **6**(1), 67–127 (2002).
[2]H. Beri and Y. Yao *et al*., "Double multiple streamtube model and numerical analysis of vertical axis wind turbine," Energy Power Eng. **3**(3), 262 (2011).
[3]T. Bertényi, C. Wickins, and S. McIntosh, "Enhanced energy capture through gust-tracking in the urban wind environment," AIAA Paper No. 1376, 2010.
[4]B. F. Blackwell, R. E. Sheldahl, and L. V. Feltz, "Wind tunnel performance data for the darrieus wind turbine with NACA 0012 blades," Technical Report No. SAND76-0130, Sandia Laboratories, Albuquerque, New Mexico, 1976.
[5]W. Chong, K. Pan, S. Poh, A. Fazlizan, C. Oon, A. Badarudin, and N. Nik-Ghazali, "Performance investigation of a power augmented vertical axis wind turbine for urban high-rise application," Renewable Energy **51**, 388–397 (2013).
[6]J. Cotrell, "Assessing the potential of a mechanical continuously variable transmission for wind turbines," Technical Report No. NREL/CP-500-38212, National Renewable Energy Laboratory (NREL), Golden, CO, 2005.
[7]L. A. Danao, J. Edwards, O. Eboibi, and R. Howell, "The performance of a vertical axis wind turbine in fluctuating wind—a numerical study," in *Proceedings of the World Congress on Engineering* (2013), Vol. 3, pp. 3–5.
[8]M. J. Dvorak, C. L. Archer, and M. Z. Jacobson, "California offshore wind energy potential," Renewable Energy **35**(6), 1244–1254 (2010).
[9]S. T. Gangwani, "Synthesized airfoil data method for prediction of dynamic stall and unsteady airloads," Technical Report No. NASA-CR-3672, 1983.
[10]H. Glauert, "Airplane propellers," in *Aerodynamic Theory* (Springer, 1935), pp. 169–360.
[11]S. Han, L. Gao, Y. Liu, and W. Yang, "Post evaluation of wind resource assessment and micro-siting," J. Power Energy Eng. **2**(4), 288 (2014).
[12]Y. Hara, K. Hara, and T. Hayashi, "Moment of inertia dependence of vertical axis wind turbines in pulsating winds," Int. J. Rotating Mach. **2012**, 910940.
[13]N. Haro, "Active drive train control to improve energy capture of wind turbines," M.S. thesis, Boise State University, 2007.
[14]Y. He, A. H. Monahan, and N. A. McFarlane, "Diurnal variations of land surface wind speed probability distributions under clear-sky and low-cloud conditions," Geophys. Res. Lett. **40**(12), 3308–3314, doi:10.1002/grl.50575 (2013).
[15]M. Islam, D. S.-K. Ting, and A. Fartaj, "Aerodynamic models for Darrieus-type straight-bladed vertical axis wind turbines," Renewable Sustainable Energy Rev. **12**(4), 1087–1109 (2008).
[16]E. N. Jacobs and A. Sherman, "Airfoil section characteristics as affected by variations of the Reynolds number," NACA, Report No. 586, 1937.
[17]J. Kaldellis, "Optimum autonomous wind–power system sizing for remote consumers, using long-term wind speed data," Appl. Energy **71**(3), 215–233 (2002).
[18]C. Klipp, "Wind direction dependence of atmospheric boundary layer turbulence parameters in the urban roughness sublayer," J. Appl. Meteorol. Climatol. **46**(12), 2086–2097 (2007).
[19]S. Kooiman and S. Tullis, "Response of a vertical axis wind turbine to time varying wind conditions found within the urban environment," Wind Eng. **34**(4), 389–401 (2010).
[20]D. Y. Leung and Y. Yang, "Wind energy development and its environmental impact: A review," Renewable Sustainable Energy Rev. **16**(1), 1031–1039 (2012).
[21]W. D. Lubitz, "Impact of ambient turbulence on performance of a small wind turbine," Renewable Energy **61**, 69–73 (2014).
[22]J. Manwell, J. Gowan, and A. Rogers, *Wind Energy Explained: Theory, Design, and Application* (Wiley, 2002).
[23]S. McIntosh, H. Babinsky, and T. Bertenyi, "Optimizing the energy output of vertical axis wind turbines for fluctuating wind conditions," AIAA Paper No. 1368, 2007.
[24]S. McIntosh, H. Babinsky, and T. Bertenyi, "Unsteady power output of vertical axis wind turbines operating within a fluctuating free-stream," AIAA Paper No. 1324, 2008.
[25]S. C. McIntosh and H. Babinsky, "Aerodynamic modeling of swept-bladed vertical axis wind turbines," J. Propul. Power **29**(1), 227–237 (2013).
[26]I. Paraschivoiu, *Wind Turbine Design: With Emphasis on Darrieus Concept* (Presses Internationales Polytechnique, 2002).
[27]I. Paraschivoiu and F. Delclaux, "Double multiple streamtube model with recent improvements (for predicting aerodynamic loads and performance of Darrieus vertical axis wind turbines)," J. Energy **7**(3), 250–255 (1983).
[28]P. Ramamurthy and E. R. Pardyjak, "Toward understanding the behavior of carbon dioxide and surface energy fluxes in the urbanized semi-arid salt lake valley, Utah, USA," Atmos. Environ. **45**(1), 73–84 (2011).

[29]M. Roth, "Review of atmospheric turbulence over cities," Q. J. R. Meteorol. Soc. **126**(564), 941–990 (2000).
[30]F. Scheurich and R. E. Brown, "Modelling the aerodynamics of vertical-axis wind turbines in unsteady wind conditions," Wind Energy **16**(1), 91–107 (2013).
[31]F. Schuerich and R. E. Brown, "Effect of dynamic stall on the aerodynamics of vertical-axis wind turbines," AIAA J. **49**(11), 2511–2521 (2011).
[32]K. C. Seto and S. Dhakal, "Chapter 12: Human settlements, infrastructure, and spatial planning," Technical Report No. IPCC WCIII AR5, International Panel on Climate Change 5th Assessment Report, 2014.
[33]A. Shahzad, T. Asim, R. Mishra, and A. Paris, "Performance of a vertical axis wind turbine under accelerating and decelerating flows," Procedia CIRP **11**, 311–316 (2013).
[34]R. E. Sheldahl and P. C. Klimas, "Aerodynamic characteristics of seven symmetrical airfoil sections through 180-degree angle of attack for use in aerodynamic analysis of vertical axis wind turbines," Technical Report No. SAND80-2114, Sandia National Laboratories, Albuquerque, NM, 1981.
[35]K. Sunderland, T. Woolmington, J. Blackledge, and M. Conlon, "Small wind turbines in turbulent (urban) environments: A consideration of normal and weibull distributions for power prediction," J. Wind Eng. Ind. Aerodyn. **121**, 70–81 (2013).
[36]R. Templin, "Aerodynamic performance theory for the NRC vertical-axis wind turbine," NASA STI/Recon Technical Report No. 76, 1974.
[37]I. Van der Hoven, "Power spectrum of horizontal wind speed in the frequency range from 0.0007 to 900 cycles per hour," J. Meteorol. **14**(2), 160–164 (1957).
[38]J. Wyngaard, "Atmospheric turbulence," Annu. Rev. Fluid Mech. **24**(1), 205–234 (1992).

CHAPTER 3

COMPARISON OF FORECASTING METHODS FOR VERTICAL AXIS WIND TURBINE APPLICATIONS IN AN URBAN/SUBURBAN AREA

JOURNAL OF RENEWABLE AND SUSTAINABLE ENERGY **9**, 023302 (2017)

Comparison of forecasting methods for vertical axis wind turbine applications in an urban/suburban area

Lam Nguyen and Meredith Metzger
Department of Mechanical Engineering, University of Utah, Salt Lake City, Utah 84112, USA

(Received 3 December 2016; accepted 24 February 2017; published online 9 March 2017)

Wind forecasting plays an important role in the economic benefit and system reliability of wind turbine power generation. The goal of the present study is to investigate different forecasting methods that can be used to improve the amount of energy captured by a small-scale vertical axis wind turbine (VAWT) operating in a gusty wind environment typical of an urban/suburban area. Four forecasting methods are studied in the present research: Persistence Method, Modified Persistence Method, Autoregressive Moving Average (ARMA) model, and Weather Research and Forecasting (WRF) model. The forecasting models are used to predict the wind conditions and optimal rotational speed of VAWTs located in Oklahoma City for data collected in 2009. In all cases, a constant rotational speed controller was used with a forecasting horizon of 1 day. The results indicate that a 5% increase in accuracy of the wind forecast could increase the total amount of energy captured by the VAWT by as much as 13%. The results also indicate that the use of a tuned speed adjustment factor (AF) in the modified persistence method improves the overall performance of the VAWT by as much as 6% compared to the persistence method. The value of AF was found to be site-independent and linearly proportional to the annual average wind speed. For the ARMA model, there exists an optimal amount of training data and forecasting horizon that results in minimal error when the forecasting data are compared to the actual data. For each of the sites investigated, the modified persistence method appears to slightly outperform the persistence, ARMA, and WRF models. In all cases, the forecasting models allow the VAWT to capture approximately 78%–85% of the optimal amount of energy that could be generated assuming the actual wind data were known in advance. The economic viability of the VAWT is also examined by comparing the Levelized Cost of Energy (LCOE) for the VAWT with the national electricity unit price. The LCOE of the system is competitive with the national electricity unit price at the sites where the annual average wind speed is 4.3 m/s or greater. *Published by AIP Publishing.* [http://dx.doi.org/10.1063/1.4978304]

I. INTRODUCTION

The deployment of wind turbine technology around the world has increased considerably in the past few decades.[17,29,37] Wind power output from a wind turbine is dependent on wind conditions that vary with time depending on regional weather patterns and type of landscape.[40] This, in turn, affects the operation of the utility system, such as regulation/loading following, schedule planning or unit commitment.[18] An accurate wind forecasting method provides one way to overcome many of these problems. For example, accurate wind speed prediction provides valuable information for the wind turbine controller and allows for the wind turbine to be well adjusted to increase wind power generation and reduce reverse capacity.[4] In addition, the accurate forecast of wind speed and power is extremely helpful in optimizing the wind turbine operation with a significant penetration level from the wind that allows for minimal operating cost and maximal system reliability.[25,37,40] In a study performed by Fabbri *et al.*,[14] it is

suggested that the error prediction cost would be as much as 10% of the total income from selling wind energy. Considerable research over the last two decades has been conducted on forecasting wind conditions for wind turbine applications.[24,31,37,38,43] Theoretically, there should be no difference in the forecasting methods used for applications involving horizontal axis wind turbines (HAWTs) versus vertical axis wind turbines (VAWTs); however, the majority of the prior research has focused on applications of large HAWTs. It remains to be determined how wind forecasting could help in improving the power performance of small VAWT applications. It is hypothesized in the present study that accurate wind forecasting accompanied by daily adjustment of the rotational speed of the turbine could enhance VAWT performance compared to operation at a fixed rotational speed based on the annual average wind speed.

Several wind forecasting techniques have been developed and reported over the years, with most falling into two main categories: a statistical approach and a physical approach. The statistical approach is based on a training procedure that uses the difference between the actual data and the predicted data in order to determine the coefficients in a mathematical model. This approach is relatively inexpensive and provides fairly accurate results for short-term forecasting.[21,40] The physical approach uses a parameterization based on the physical description of the atmosphere, such as terrain, pressure, and temperature to estimate the future wind condition.[5,40] Models developed using this approach are often rendered on a supercomputer and are computationally expensive but can provide accurate long-term forecasts.[40] Besides the two main approaches mentioned, other methods have been developed recently for the application of wind prediction, including the deterministic method and artificial neural networks (ANNs). In a study performed by Drisya *et al.*,[9] a new deterministic forecasting method was developed to forecast short term prediction of the wind speed at locations where the wind speed dynamic was relatively chaotic. The results show that the model accurately forecasts the wind speed up to a 3-h forecasting horizon. In addition, with the development of artificial intelligence recently, a new artificial neural network method has been developed to forecast wind speed and power for wind turbine applications.[4,5,38] The ANN model consists of a number of layers composed of artificial neurons. The learning algorithm governing the connection between neurons in the network is obtained through a training process. The weight applied to each artificial neuron is continually adjusted through the training process to improve the forecasting accuracy and generalize abilities.[4,38] The ANN can forecast wind speed over a range of forecast horizons from hours to years depending on the application.[4,38] The present study only examines models of the first two types mentioned: (i) statistical approach and (ii) physical approach.

The simplest method in the statistical approach is the Persistence Model (PM), which assumes that the future value is the same as the current one.[40,47] PM is fairly accurate for short-term wind speed forecasting, such as less than 10 min.[47] However, in cases with highly variable winds, the accuracy of PM degrades rapidly when the time scale of forecasting increases. PM is not only the simplest statistical type model but also the most economical to use in wind speed and power forecasting.[5] Electric utility and real-time grid operation use PM for ultra short-term forecasting from a few minutes to less than an hour.[5] Even though PM may not be the best forecasting model for wind speed and available power, it is commonly used as a reference for evaluating the performance of more sophisticated forecasting methods.[5,40,47] A new forecasting method is considered to be "advanced" and worth implementation, if it outperforms PM. In a study conducted by Milligan *et al.*[24] investigating different forecasting methods for a wind farm, PM was used as a reference for evaluating the performance of an Autoregressive Moving Average (ARMA) model. Calculation of the root mean square error suggested that for the first 2 h, PM forecasted nearly as accurately as the developed ARMA model.

Among many other forecasting models, ARMA is the most popular in the time-series based approach to predict the future value of wind speed and power.[5,40] Some variations from this model include the Autoregressive Integrated Moving Average (ARIMA), Seasonal Autoregressive Integrated Moving Average (SARIMA), and fractional Autoregressive Integrated Moving Average (f-ARIMA). The use of these models varies depending on the purpose of the application and forecasting time horizon, ranging from second/minute to week/month.[13,18,40,47] For example, Cadenas and Rivera[4] compared two different techniques for wind forecasting in the South Coast of the state

of Oaxaca, Mexico, in 2007. The study was performed using SARIMA and Artificial Neural Network (ANN) methods applied to a time series based on 7 years of wind speed measurements. The final results suggest that the SARIMA model provides better sensitivity to the prediction of wind speed than the ANN model. It is worth mentioning that the model forecasted the monthly averaged wind speed, which represents a very long-term forecasting horizon. This long forecasting horizon produces useful information for long-term planning and development, such as resource allocation, economics viability, or maintenance planning. However, it yields little or no information on the short-term variation of the wind speed (such as minute to day), which is particularly important for wind turbine operation and decision making, such as generator on/off decision, reverse requirement, or regulation action.[5]

Much of the research on wind speed forecasting with application to wind turbines focuses on short-term forecasting.[13,18,35,43] A variety of ARMA models have been developed and studied over the years with differing results. Each model has its own advantages and limitations that are imposed by the model parameters. For example, Erdem and Shi[13] examined four different ARMA-based approaches for short-term forecasting wind speed and direction: component ARMA model, traditional/linked ARMA model, vector autoregressive (VAR) model, and restricted VAR model. The models were used to forecast the hourly wind speed and direction for two different wind observation sites in North Dakota in 2011. The results suggested that the component ARMA model was better in predicting the wind direction than the traditional/linked ARMA model, whereas the opposite was observed for wind speed forecasting. Similarly, Torres *et al.*[43] used the ARMA model to predict the hourly averaged wind speed for 10 h advanced and compared it with the persistence model. The time series data were transformed and standardized before incorporating into the ARMA model. The results indicate that acceptable accuracy (root mean square error less than 1.5 m/s) may only be achieved for short-term forecasting. The results also indicate that the persistence model outperforms the AMRA model for the first hour, while the opposite was observed for 10 h advanced. Note that most of the research to date using the ARMA-based approaches for wind turbine applications has focused on forecasting the wind speed, rather than forecasting the appropriate turbine settings to maximize wind power/energy captured.[13,31,43] In addition, the research on wind forecasting has been mainly used for large horizontal axis wind turbine applications.[18,44] The authors are not aware of any literature describing wind forecasting applied to small vertical axis wind turbines, especially with regard to applications in gusty wind environments.

One of the challenges with ARMA-based models is optimizing the amount of training data required and determining the optimal forecasting horizon.[24] Often in the literature, the training period and forecasting horizon used for an ARMA model are not well justified or simply selected randomly.[13,18,22,43] For example, in a study performed by Kavasseri and Seetharaman,[18] the f-ARIMA model was used to forecast the day-ahead wind speed and power. Four weeks of wind speed data were used in the training process of the model, and the wind speed and power were forecasted for an interval of 24 h and 48 h. The results indicate that the f-ARIMA model improved forecasting accuracy by 42% compared with the persistence model. However, the research did not mention how the training data or forecasting horizon were selected, as these could potentially affect the forecasting accuracy. Similarly, the study performed by Milligan *et al.*[24] compared the forecasting accuracy of the ARMA model to the persistence model. The study forecasted hourly averaged wind speed for 6 h advanced. The model was trained using a range of training periods; however, the results from only two training periods (of 2 weeks and 3 weeks) were presented. It is worth noting that the optimization method used to select the training period was not clearly stated or presented. The results also suggest that the ARMA model is site dependent, i.e., there exists one optimal ARMA model for each site.

Recently, the Weather Research and Forecasting (WRF) model has been used to forecast wind speed and wind power for wind turbine applications.[7,8] The WRF model is an efficient and flexible simulation program, with grid resolutions from 1 to 10 km, which has been designed for a wide range of weather forecast and research applications.[19,23] The WRF model is maintained and supported for broad community use with over 30 000 users in over 150 countries.[45] Clifford[7] used the WRF model to forecast the near-surface wind speed and available

wind power in the Altamont Pass wind farm near Livermore, California. The results indicate that the WRF-modeled wind speeds were close to those observed.

One important aspect that needs to be considered when deploying wind technology is economic analysis. The studies on the economic analysis of wind energy that have been conducted over the years mainly focus on wind farms containing large horizontal axis turbines.[15,27,36] There is a lack of research on the economic analysis of small scale wind turbines, as would be used in urban areas. The unit cost of electricity from a wind turbine is affected by many factors that can be grouped into two main categories: (1) capital cost and (2) operating and maintenance cost.[15,27] The capital cost often consists of the system/module cost, balance of system (BOS) cost, and financial cost.[15,27] The wind turbine system cost consists of the cost associated with the turbine blades, rotor, and generator. BOS cost consists of the equipment required to successfully generate power and provide electricity for usage. For wind turbine applications, BOS often consists of an inverter, electrical controller, battery storage, wiring, installation, etc.[15,27] For large horizontal axis wind turbines, the turbine, BOS, and financial costs account for approximately 68%, 23%, and 9% of the total capital cost, respectively.[27] It is expected that these percentages will change significantly for small scale wind turbines. For example, BOS cost comprises about 55%–60% of the total capital cost of a small residential photovoltaic system.[15] The operating and maintenance cost of large horizontal axis wind turbines typically ranges between \$0.01/kWh and \$0.025/kWh,[15] depending on the location.

One of the most common methods used in economic analysis of renewable energy, including wind, solar, biomass, etc., is the Levelized Cost of Energy (LCOE).[1,15,27,36] The LCOE represents the price at which energy must be sold in order to reach the break-even point in the investment over the lifetime of the technology. For large horizontal axis wind turbines, the LCOE ranges between \$0.06/kWh and \$0.14/kWh for on-shore wind turbines and \$0.13/kWh and \$0.19/kWh for off-shore wind turbines.[15] Ayodele *et al.*[1] performed an economic analysis of a small-scale wind turbine for power generation in Johannesburg, South Africa, using the LCOE method. The analysis investigated a wide range of wind turbines from 1 kW to 60 kW rated power. The results suggested that the LCOE varies depending on the size of the turbine. The most cost effective turbine in the study exhibited a LCOE value ranging from \$0.25 to \$0.33/kWh. It is worth mentioning that this LCOE value could change significantly for similar sized wind turbines in the U.S. when factoring in the production tax credit (PTC) and Investment tax credit (ITC). The PTC and ITC are recent programs approved by the U.S. Government to support new development of renewable energy technology. The ITC allows consumers to claim back 30% of the total investment, while the PTC allows consumers to claim back \$0.023/kWh of the energy production for wind energy.[3]

The present study utilizes a numerical modeling approach to investigate different forecasting methods that can be used to improve the total energy captured by a vertical axis wind turbine (VAWT) operating under gusty wind conditions representative of a typical urban/suburban area. The study is split into two parts. First, the resultant total energy captured by the turbine over a one-year time frame is measured to identify which forecasting method should be implemented. Second, an economic analysis is performed comparing the cost to implement a VAWT using the preferred forecasting method versus that expected in the ideal scenario where the actual wind conditions are known in advance. The results are used to evaluate the economical benefit of the system and to formulate a recommendation on which condition/location the small VAWT should be deployed.

II. WIND TURBINE CONFIGURATION

The wind turbine configuration used in the present study consists of an eggbeater Darrieus-type turbine having three blades based on the NACA 0015 airfoil shape with a chord length of 9 cm. The solidity of the turbine is 0.3. The turbine has a height of 2 m and a maximum radius of 1 m. This turbine was chosen because (i) data exist to validate the numerical models and (ii) the size is believed to be appropriate for application in an urban/suburban area, such as on the rooftop of a residential home or commercial building. In the present study, the turbine

performance model is subjected to actual wind speed time series as measured at fifteen different sites in Oklahoma City, USA, in 2009 (see Table I and Figure 1). Data were acquired from sonic anemometers mounted directly to traffic signals at a height of 9 m. Data were quality assured in near real time at an interval of 1 min. A detailed description of the experiments can be found in the study by Basara *et al.*[2]

A constant rotational speed (or constant-ω) controller is examined in this study. The constant-ω controller drives the turbine rotor at a fixed rotational speed regardless of variations in the incoming wind speed. A detailed description and analysis of the controller can be found in a preceding paper by Nguyen and Metzger.[29] The constant-ω controller represents the traditional type of control strategy and the simplest one to employ in practice. However, because performance is a strong function of tip speed ratio (TSR), any variations in wind speed can have a negative impact on energy captured in the case of a constant-ω controller. The work presented herein focuses on the application of wind and performance forecasting in order to enhance the total amount of energy captured.

One of the main considerations when employing a constant-ω controller is the rotational speed at which the turbine should be operated in order to maximize the amount of energy captured. In the study performed by Nguyen and Metzger,[29] an empirical relation was found between the turbulence intensity (I_T) of the wind and the optimal tip speed ratio (TSR_{opt}) of the wind turbine for the case of a constant-ω controller. Turbulence intensity is defined as the standard deviation of the wind speed divided by the mean wind speed over the time period of interest ($I_T = \sigma_V/\bar{V}$). The relationship between I_T and TSR_{opt} is illustrated in Figure 2 using both our previous data from Salt Lake City in 2013[29] and the data from Oklahoma City in 2009. Each point in the figure represents a calculation over either a discrete 10-min time interval or a 24-h time interval depending on the site. The turbulence intensity was calculated directly from the measured wind data, and the optimal TSR was calculated over each interval using the numerical methods of Nguyen and Metzger.[29] For the case of steady winds ($I_T = 0$), the optimal TSR is 4, corresponding to the peak in the power coefficient C_p versus TSR curve; see Figure 5 in Nguyen and Metzger.[29] However, as the turbulence intensity increases (i.e., winds becoming more gusty), results indicate that the turbine should be driven at an overspeed, in order to capture as much energy as possible. The composite data were curve fit to obtain the following site-independent empirical relation:

TABLE I. Location of sites in Oklahoma City where wind data were acquired. The annual average wind speed and annual average turbulence intensity were computed for year 2009.

Site name	Street address	Annual average wind speed (m/s)	Annual average turbulence intensity
KSW 101	W Reno Ave. and S Cemetery Rd.	4.95	0.363
KSW 102	SW 5th St. and S MacArthur Blvd.	3.98	0.423
KSW 108	Amelia Earhart Ln and Terminal Dr	4.97	0.349
KSW 109	SE 66th St. and S Shields Blvd.	3.79	0.412
KSW 110	SW 74th St. and State Highway 152	3.94	0.383
KSW 111	J Lee Keels Blvd. and S May Ave.	4.32	0.401
KCB 101	NE 5th St. and N Oklahoma Ave.	3.18	0.404
KCB 110	E Reno Ave. and S Lincoln Blvd.	3.84	0.392
KNE 104	NE 10th St. and N Phillips Ave.	3.75	0.353
KNE 202	NE 18th St. and N Lincoln Blvd.	3.08	0.396
KSE 101	SE 29th St. and S Eastern Ave.	3.75	0.399
KSE 102	Embers Dr and S Sooner Rd.	3.85	0.411
KNW 103	Britton Rd. and N May Ave.	3.84	0.387
KNW 104	River Bend Blvd. and N Council Rd.	4.69	0.372
KNW 107	NW 30th St. and N May Ave.	3.47	0.422

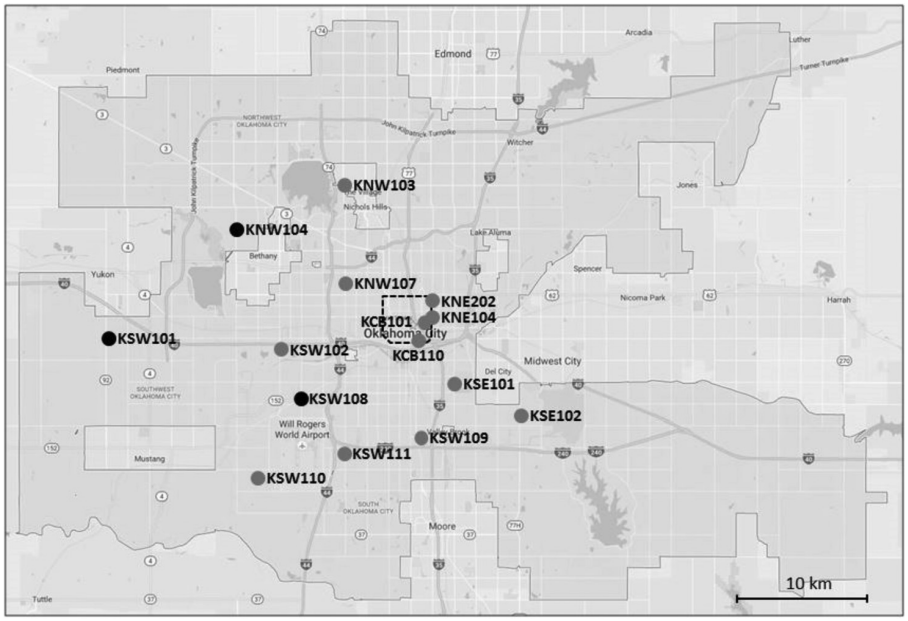

FIG. 1. Location of sites in Oklahoma City where wind data were acquired.

$$TSR_{opt} = 14.93I_T^2 - 0.54I_T + 4.27. \tag{1}$$

This relation is important because, if one can predict the turbulence intensity of the wind, then the optimal overspeed can be set according to (1).

In the present study, the constant-ω controller is implemented such that the operating rotational speed of the turbine can be adjusted once per day. This forecasting horizon is chosen because it represents a natural timescale for the wind turbine application. For example, one needs to consider the practical cost trade-off associated with changing the rotational speed of the turbine too frequently because of the temporary interruption in energy capture during adjustment that translates into lost energy production. In addition, it is reasonable to expect diurnal fluctuations in the wind due to the inherent heating/cooling cycles of the atmosphere over the course of a day. Therefore, the shortest forecasting horizon one might entertain is likely to be

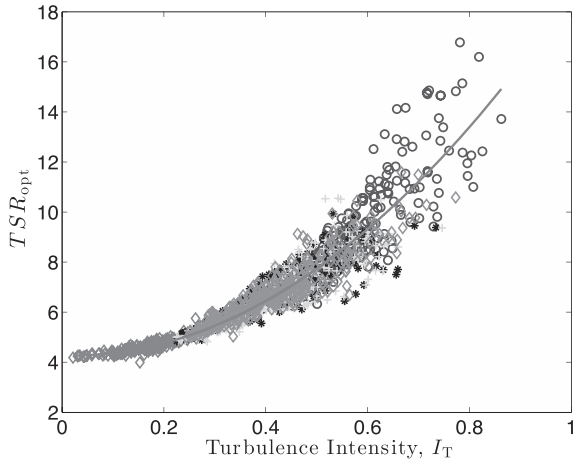

FIG. 2. Influence of turbulence intensity on the optimal TSR for a constant speed controller. Each marker type represents data from a different site. The solid line represents the curve-fit relation given in (1).

12 h, while the longest might be a couple of days. A forecasting horizon of 24 h was thus selected, as an average over this interval. To evaluate this choice, the effect of the forecasting horizon on the total amount of energy captured by the wind turbine over a full year was examined at one of the sites. Three forecasting horizons of 12 h, 24 h, and 48 h were investigated. The amount of energy captured by the wind turbine using forecasting horizons of 12 and 24 h was nearly equivalent, while that using a forecasting horizon of 48 h was slightly less (by approximately 6.2%). Based on this result, a forecasting horizon of 24 h was used for all test cases in the present study.

Figure 3 illustrates the control strategy, showing that an optimal rotational speed ω_{opt} exists for each particular day based on the measured mean wind speed $\bar{V}$ and standard deviation σ_V. Given $\bar{V}$ and $I_T\,(=\sigma_V/\bar{V})$, the relation in (1) can be used to determine TSR_{opt}, which then yields $\omega_{\text{opt}}\,(=TSR_{\text{opt}}/\bar{V})$. This ensures that the maximum amount of energy is captured each day. The problem with the above strategy lies in the fact that $\bar{V}$ and σ_V must be known in advance in order to set the optimal overspeed at the beginning of each day. Different forecasting methods were examined to estimate $\bar{V}$ and I_T for the next day. An alternative approach of forecasting the optimal rotation speed directly using knowledge of the past values of ω_{opt} was also investigated. Results from both approaches are presented.

A. Wind turbine performance model

The present study utilizes the Blade Element Momentum (BEM) theory to simulate the aerodynamic performance of the VAWT. The turbine is modeled using a single actuator disk. A detailed description of the model can be found in our preceding paper, including a validation that shows good agreement between the model and experimental data (Nguyen and Metzger[29]). The BEM model is used to calculate the power coefficient (C_p) and aerodynamic torque (Q) at each time step in the simulation. Since the turbine is operated at a constant rotational speed ($d\omega/dt = 0$), inertia effects are negligible and a balance exists at all times between the aerodynamic torque and the applied loading torque from the generator (T_L),

$$Q = T_L\,. \tag{2}$$

The total energy captured by the turbine is then simply the mechanical power integrated over the time period of interest, $E = \int \omega \cdot T_L(t)\,dt = \int \omega \cdot Q\,dt$. The choice of rotational speed ω impacts the value of Q (via the BEM model) as well as E. In the present study, different forecasting methods are examined to predict the best rotational speed (ω) of the turbine to use for the next day, based only on information from the current and previous days. Once ω is selected, the BEM model is run for the next day using the exact wind data as input to

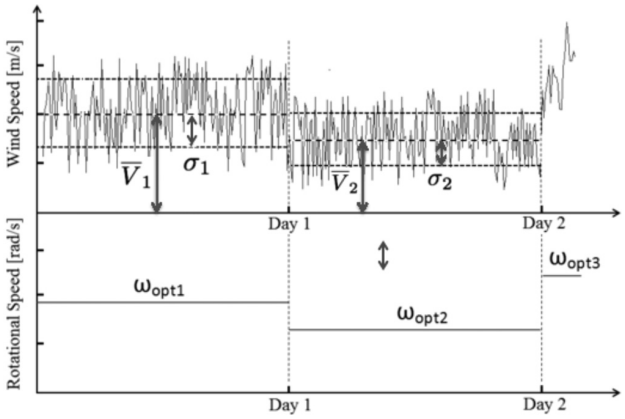

FIG. 3. Illustration of the constant-ω controller with daily adjustment of the optimal rotational speed, ω_{opt}, based on the daily averaged mean wind speed, $\bar{V}$, and turbulence intensity, $\sigma/\bar{V}$.

determine the resultant energy captured by the turbine. This procedure is repeated daily over the full year of operation.

III. FORECASTING MODELS

Four methods of forecasting the wind condition were examined in the present research: Persistence Model (PM), Modified Persistence Model (MPM), Autoregressive Moving Average (ARMA) model, and Weather Research and Forecasting (WRF) Model. In all cases, three parameters (wind speed, turbulence intensity, and rotational speed of the turbine) were forecasted for the next day using the available data from previous days, except for the WRF model which can only predict future wind conditions. For each of the different forecasting methods, the forecasting parameters were input into the numerical model for the turbine, as described in Section II A, in order to calculate the amount of energy captured during unsteady winds. Note that this model does not account for the jump discontinuities expected at the beginning of each day when the rotational speed is adjusted; instead, the numerical model assumes that the adjustment occurs instantaneously. A full year of data were analyzed to yield good statistical convergence of the results. The output from each model is compared against the ideal case where the wind time series is known exactly in advance.

A. Persistence model

The Persistence Model (PM), also referred to as the "Native Predictor" model, uses the simple assumption that the forecasted variable at any future time will have the same value as the present time.[40] The model is governed by the simple equation

$$Y_k = Y_{k-1}, \tag{3}$$

where Y is the variable of interest to be forecasted (i.e., mean wind speed, turbulence intensity, and optimal rotational speed of the turbine). In this context, the future time is expressed as $t_k = t_{k-1} + \Delta t$, where t_{k-1} represents the present time and $\Delta t = 24$ h in the current study. Note that with PM there are no additional model parameters that need to be determined. Results from PM are used as a benchmark for testing the improvement of the other forecasting models.

B. Modified persistence model

Results from several initial tests indicated that the energy captured could be enhanced if the turbine was operated at a rotational speed that was slightly above the forecasted rotational speed obtained from PM. This led to the development of the modified persistence method (MPM). In MPM, an adjustment factor, AF, is introduced as follows:

$$\omega_{\mathrm{MPM}} = \omega_{\mathrm{PM}}(1 + AF), \tag{4}$$

where ω_{PM} denotes the rotational speed derived from PM, and ω_{MPM} denotes the new updated rotational speed. This formulation of MPM is somewhat similar to the forecast model studied by Nielsen *et al.*,[30] in that both models introduce a tuned parameter into the Persistence Model equation. The tuned parameter in the work of Nielsen *et al.*[30] represents a weighting factor between the current and mean value of the forecasting variable and can be calculated from the correlation coefficient of the training data, whereas the adjustment factor AF appearing in (4) represents a multiplicative scaling factor, and, as will be shown, is linearly proportional to the value of the annual average wind speed. Note that the rationale behind the present formulation of MPM stems from an observation that the forecasted value for ω_{PM} consistently underpredicts the optimal rotational speed ω_{opt} during highly unsteady wind conditions. Therefore, an additional scaling factor is used to increase the rotational speed above that predicted by PM. Note that AF constitutes a model parameter, the value of which must be determined prior to

forecasting. In the present study, AF was tuned based on the annual average wind speed at each site as described later in Section V B 2.

C. Autoregressive moving average

The Autoregressive Moving Average (ARMA) model is the most popular type of model in the times-series-based approach to predicting future values of wind speed or power.[40] Given a random, discrete time series with zero mean value, Y_k (describing, for example, wind speed data as a function of time from an anemometer), the ARMA(p, q) method assumes that the time series can be modeled as

$$Y_k = \sum_{i=1}^{p} \phi_i Y_{k-i} + \sum_{j=1}^{q} \theta_j \epsilon_{k-j} + \epsilon_k, \tag{5}$$

where ϵ represents the residual, p represents the order of the autoregressive (AR) process, q represents the order of the moving average (MA) processes, and $(\phi_1, \ldots, \phi_p)$ and $(\theta_1, \ldots, \theta_q)$ denote the AR and MA model parameters, respectively. The model parameters are determined by performing a nonlinear curve fit of (5) to a set of *training* data, $\{y_1, \ldots, y_n\}$, that minimizes the sum of the square residual,

$$R_2 = \sum_{k=1}^{N} \epsilon_k^2 = \sum_{k=1}^{N} \left[y_k - (\phi_1 y_{k-1} + \cdots + \phi_p y_{k-p}) - (\theta_{k-1}\epsilon_{k-1} + \cdots + \theta_q \epsilon_{k-q}) \right]^2, \tag{6}$$

where N denotes the sample size of the training data. The numerical method is described in further detail in the study by Chatfield.[6] The parameters $\{\phi_i, \theta_j\}$ were calculated for a large set of (p, q) orders up to (5, 5). From this, the *optimal* order of the ARMA model was selected based on the Akaike Information Criterion (*AIC*) that seeks a model order, yielding a good fit to the observed data with preference toward low order and few parameters.[6] *AIC* is calculated as follows:

$$AIC(p,q) = -N \ln\left(\frac{R_2}{N}\right) + 2\,(p+q+1)\left(\frac{N}{N-p-q-2}\right). \tag{7}$$

The best (p, q) order that minimized the *AIC* (p, q) value was the one used for that particular time series. This process was then repeated for each forecasted variable and each time series. Note, even though the optimization strategy considered orders up to $p = 5$ and $q = 5$, the fit giving the least *AIC* value typically consisted of an ARMA model of order 1.

Other details regarding the ARMA models used in the present study are described below. A rolling-origin evaluation with recalibration over the fit period was used, with the initial origin being set at January 1. A constant fit period equal to the length of the training period was used for the entire duration of the forecast. Note, the training period varied slightly depending on site. In this manner, the hold-in samples representing the training data continuously slide toward the end of the data set, one day at a time, with the last value of the origin being set at December 30. After each forecasting horizon, the rolling window is updated with the new data, while the oldest data are pruned from the new window. The least squares regression is performed to calculate the new autoregressive and moving average parameters and orders for the new window.

One of the most important decisions in optimizing the ARMA model is the selection of the training period and forecasting horizon. To assist in this selection, a range of training periods (10–60 days) and forecasting horizons (1–30 days) was examined. The mean absolute error *(MAE)* was used to evaluate the quality of the forecast for each combination of training period and forecasting horizon,

$$MAE = \frac{1}{\tilde{N}} \sum_{k=1}^{\tilde{N}} \frac{|Y_{F_k} - Y_{T_k}|}{|Y_{T_k}|}, \tag{8}$$

where Y_T denotes the true (observed) value, Y_F denotes the forecasted value, and $\tilde{N}$ denotes the forecasting horizon. Note that (8) was calculated using only hold-out samples. Furthermore, to obtain an accurate value of *MAE* representative of the entire time series, 200 realizations were used by randomly selecting the origin with a random number generator. The reported *MAE* value is then an average over the 200 realizations. The minimum *MAE* was used as a criterion to identify the optimal training period and forecasting horizon for each given time series. Example results are shown in Section V B 3. Once the final order (p, q) and corresponding parameters, $\{\phi_i, \theta_j\}$ for $i = 1, \ldots, p$ and $j = 1, \ldots, q$, were determined for the optimal training period, the ARMA forecast model (5) could be used to predict the future values of the forecasted variable over its optimal forecasting horizon.

As shown in Figure 2, the turbulence intensity of the wind should be considered when setting the optimal rotational speed of a small VAWT. This means that both the mean value of the wind and the turbulence intensity need to be forecasted. In order to do this, one can construct separate ARMA models for the mean wind and turbulence. Another option is to couple an ARMA model with an Autoregressive Conditional Heteroskedasticity (GARCH) model to account for stochastic volatility as described by Taylor *et al.*[42] Neither of these strategies was used in the present study. Instead, the optimal rotational speed was forecasted directly. In addition to simplifying the forecasting model, it was observed that this approach yields less forecasting error as discussed further in Section V A.

D. Weather research and forecasting model

The Weather Research and Forecasting (WRF) model used in this study is WRF Model Version 3.7.1. The technical description of this model version is explained in a NCAR technical report by Skamarock *et al.*[39] The WRF model used the North American Regional Reanalysis (NARR) input forcing data and United States Geological Survey (USGS) land use dataset with 24 land use categories. The WRF modeling schemes used in this WRF model version are described in Table II. Four-Dimensional Data Assimilation (FDDA) in the mother domain (12-km) using upper air and surface observations was used for nudging of the horizontal (U and V) winds in the planetary boundary layer (PBL) and U, V, T, and Q at the surface, including soil moisture nudging for the land surface model. Two domains were used in this study with the outermost domain covering the continental United States (12-km horizontal grid resolution) and a two-way nested inner domain covering the western U.S. (4-km resolution).

IV. ECONOMIC ANALYSIS MODEL

The Levelized Cost of Energy (LCOE) was used in this research to evaluate the economic viability of using small VAWTs in Oklahoma City. The LCOE represents the price at which

TABLE II. WRF modeling schemes.

Model physic	Model scheme	References
Microphysics	Morrison double-moment scheme	28
Shortwave radiation	Dudhia shortwave radiation scheme	10
Longwave radiation	Rapid radiative transfer longwave radiation scheme	26
Cumulus parameterization	Kain-Fritsch scheme	16
Planetary boundary layer	Asymmetric convective model of version 2	33
Land surface	Pleim-Xiu scheme	46 and 34
Surface layer	Pleim-Xiu scheme	32

energy must be sold in order to achieve a break-even investment over the lifetime of the deployed technology. The LCOE can be calculated as

$$LCOE\,(\$/\mathrm{kWh}) = \frac{[\text{Project Cost}] - [\text{ITC}] + \sum_{n=1}^{N} \frac{AO}{(1+DR)^n} - \frac{RV}{(1+DR)^n}}{\sum_{n=1}^{N} \frac{E_a(1-SDR)}{(1+DR)^n}} - [\text{PTC}], \tag{9}$$

where ITC represents investment tax credit, PTC represents the production tax credit, *AO* represents the annual operating and maintenance cost, *RV* represents the residual value of the system based on its end-of-life asset, *DR* represents the discount rate, E_a represents the annual energy production of the system, *SDR* represents the system degradation rate, and *n* represents the number of years of the system lifetime. The project cost mainly consists of the cost associated with the wind turbine system and the Balance of System (BOS) equipment. In this study, the wind turbine technology is assumed to be connected to an off-grid system also referred to as a stand-alone system. Off-grid systems are not connected to the electric grid and require the use of battery tank storage. In this study, the BOS equipment consisted of an electrical controller, a turbine generator, an inverter, a battery tank, and a forecasting system including instrumentation to collect wind speed data.

The present LCOE analysis considered a small VAWT designed and manufactured by QingDao Bofend Wind Power Generator Co. with a rated power of 1 kW. This turbine has a similar size and equivalent rated power to the turbine used in the rest of the study. The costs associated with the wind turbine system and BOS were obtained from the wind turbine manufacturer and are provided in Table III. The system has an expected lifetime of 20 years. The annual energy production of the system (E_a) was calculated using the MPM method as described in Section III B. The residual value of the system at the end of its lifetime is estimated to be 10% of its original price. The system degradation rate is estimated to be 1% of its efficiency, which is equivalent to the degradation rate of the large HAWT system found in a study performed by Staffell and Green.[41] The discount rate used in the analysis is 3.1%, a standard discount rate used in many projects related to energy conservation, water conservation, and renewable energy.[20] The Department of Energy (DOE) projects a longterm nominal inflation rate of 0.1% for the 30-year period between 2015 and 2045.[20] It is worth mentioning that the discount rate of 3.1% used in the analysis accounts for the nominal inflation rate over the next 20 years representing the expected lifetime of the system.

The operating and maintenance cost (*AO*) used in this analysis is estimated to be equal to the average *AO* cost of large HAWTs.[27] However, in reality, it is expected that the *AO* of small VAWTs would be slightly less than the *AO* cost of large HAWTs due to the simplicity of the system. The investment tax credit (ITC) allows consumers to claim back 30% of the total

TABLE III. Description of system project cost.

Component	Cost
Wind turbine and generator	$1366
Electrical controller	$190
Electrical inverter	$202
Battery storage	$320
Forecasting system	$450
Residual value	10% of original value
System lifetime	20 years
Degradation rate	1% efficiency/year
Discount rate	3.1%
AO cost	$0.01/kW h

investment, while the production tax credit (PTC) allows consumers to claim back \$0.023/kWh of the energy production.[3] The investment tax credit is subtracted from the total project cost, while the production tax credit is deducted from the LCOE of the system, as done in Ref. 3.

V. RESULTS

A. Sensitivity analysis

When forecasting is implemented in the operation of a wind turbine, any error in wind condition forecasting can significantly affect the performance of the turbine. A sensitivity analysis was performed to quantify the amount by which forecasting errors decrease the total energy captured by the turbine. Note that the forecasting models were not used in the sensitivity analysis. Rather, the values of mean wind ($\bar{V}$) speed, turbulence intensity (I_T), and optimal rotational speed (ω_{opt}) based on the actual measurement data were used. The true (observed) values were randomly varied, using a uniformly distributed random number generator, by a set percentage P ranging from 1% to 20% to obtain the "uncertain" data. For example, the uncertain mean wind speed on the ith day is given by

$$\tilde{V}_i = \bar{V}_i(1 + P\,\epsilon_i\,\bar{V}_i), \tag{10}$$

where $\sim$ denotes the uncertain variable and ϵ represents a random number between -1 and 1. Similar expressions can be written for the uncertain turbulence intensity ($\tilde{I_T}$) and optimal rotational speed ($\tilde{\omega}$). The relation in (10) is meant to mimic errors of a prescribed magnitude in the forecasted variables. Two test cases were examined for the present wind turbine configuration to quantify the sensitivity in energy captured to the uncertain variables $\tilde{V}$, $\tilde{I_T}$, and $\tilde{\omega}$.

In test case 1, $\tilde{V}$, and $\tilde{I_T}$ for each day were input into the empirical relation (1) in order to calculate the effective rotational speed ($\tilde{\omega}$) of the turbine, as described in Section II. This rotational speed was then used in the numerical model of the wind turbine in order to calculate the total amount of energy captured by the wind turbine. Importantly, when running the numerical model, the turbine is subjected to the true (observed) wind data, but its rotational speed is non-optimal due to the artificial errors that were introduced into the values of the mean wind speed and turbulence intensity used to set its rotational speed. Results from test case 1 are shown in Figure 4(a) for eight different test sites in Oklahoma City. A full year's worth of data were used to calculate each data point in the figure. The sensitivity is expressed as an energy ratio, $\tilde{E}/E_{\text{true}}$, where $\tilde{E}$ represents the energy captured using the non-optimal rotational speed ($\tilde{\omega}$) based on the uncertain wind data, and E_{true} represents the maximum amount of energy that can be captured using ω_{opt} based on the true (observed) values of the wind data. The figure depicts a clear trend independent of site; namely, as uncertainty increases, the amount of energy captured by the turbine decreases. For a 10% uncertainty in both the mean wind speed and the turbulence intensity,

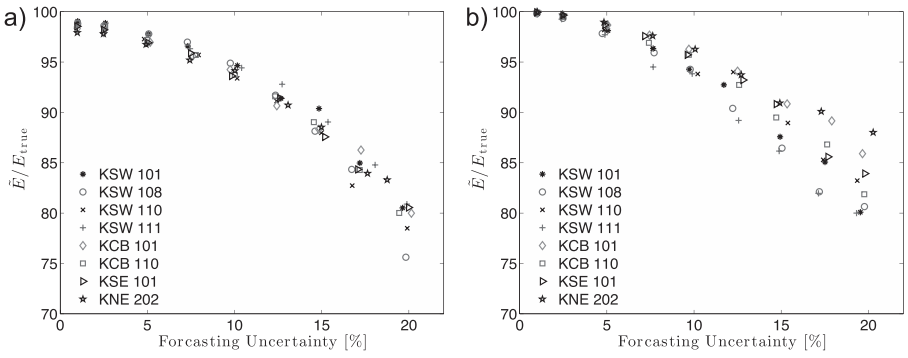

FIG. 4. Sensitivity of forecasting errors on the amount of energy captured by the wind turbine. (a) Test case 1: artificial errors are introduced into the mean wind speed and turbulence intensity. (b) Test case 2: artificial errors are introduced into the value of the optimal rotation speed.

the amount of energy captured, compared to the maximum possible, has dropped by 6%. When the uncertainty is increased to 17%, the energy captured drops to about 15%. These results are encouraging for forecasting in the case of small VAWTs operating in unsteady wind conditions, especially if the actual forecasting error can be maintained at 10% or less.

In test case 2, the optimal rotational speed ω_{opt} is first calculated based on the true (observed) $\bar{V}$ and I_T. An artificial error is subsequently introduced into the optimal rotational speed based on (10) to obtain the uncertain rotational speed ($\tilde{\omega}$). This non-optimal rotational speed $\tilde{\omega}$ was then used in the transient response model of the wind turbine in order to calculate the total amount of energy captured by the wind turbine, similar to test case 1. Again, when running the numerical model, the turbine is subjected to the true (observed) wind data. Results from test case 2 are shown in Figure 4(b). The trend looks nearly identical to that for test case 1, except with more scatter between the different test sites as the uncertainty increases. In addition, the sensitivities are noticeably less, meaning that the magnitude of the energy ratio $\tilde{E}/E_{\text{true}}$ remains closer to 100. The results suggest that forecasting the rotational speed directly may provide better accuracy and more energy captured than forecasting the wind condition.

B. Forecasting models

1. Persistence model

The ultimate goal of the forecasting model is to enhance the energy captured by the wind turbine by better forecasting the wind condition and wind turbine's operating condition. Therefore, the total energy captured by the turbine is used as a criterion in the research to evaluate the quality of the forecasting models. Five out of the fifteen data sets listed in Table I were selected and analyzed with the Persistence Model (PM). Two test cases were performed identical to those used in the sensitivity analysis from Section V A. In test case 1, the daily average wind speed and turbulence intensity were forecasted, while in test case 2, the rotational speed of the turbine was forecasted directly. Table IV summarizes the amount of energy captured by the wind turbine during 2009 for the two test cases using the PM forecasting approach. The percent difference given in the fourth column of Table IV is defined as $\text{Diff} = (E2_{\text{PM}} - E1_{\text{PM}})/E1_{\text{PM}} * 100\%$, where $E1$ and $E2$ are the total energies obtained from test cases 1 and 2, respectively. The results indicate that the approach used in test case 2 yields about 5% more energy captured, on average over the five different test sites examined. This would suggest that for the case of unsteady winds, the optimal rotational speed of the turbine should be forecasted directly, rather than forecasting the wind condition. This result is somewhat expected. In the approach of test case 1, two variables defining the wind condition (mean speed and turbulence intensity) must be forecasted simultaneously in order to determine the optimal rotation speed, whereas in test case 2 only one variable (the optimal rotation speed) is forecasted, which likely results in a lower value of the overall forecasting error. For this reason, only the approach used in test case 2 will be studied for the remaining forecasting models. In addition, since there are no tuned model parameters in the PM implementation, results from PM will be used as the benchmark for testing the improvement of the other forecasting models discussed in the subsequent Sections V B 2–V B 4.

TABLE IV. Total amount of energy captured by the wind turbine in 2009 using the persistence model of forecasting for test cases 1 and 2.

Site	Test case 1, $E1_{PM}$ (GJ)	Test case 2, $E2_{PM}$ (GJ)	Diff. (%)
KSW 101	2.669	2.760	3.41
KSW 109	1.318	1.411	7.06
KCB 101	0.714	0.772	8.12
KNW 104	2.643	2.878	5.45
KSE 101	1.334	1.399	4.87

2. Modified persistence model

When implementing the Modified Persistence Model (MPM) in conjunction with the constant-ω controller, one needs to determine an appropriate value for the speed adjustment factor (AF). A systematic approach was used in the present study in order to find the optimal AF value, yielding the largest amount of energy captured. In this approach, AF values were varied from 2% to 30% as discussed in Section III B. Wind data from all of the 15 sites listed in Table I were examined, which represented a wide range of mean wind speeds and turbulence intensity values. Figure 5 shows the sensitivity of the energy ratio $E_{\mathrm{MPM}}/E_{\mathrm{true}}$ to the AF value. Here again, E_{true} represents the maximum amount of energy that could be captured by the turbine if the actual wind conditions were known in advance. As illustrated, a parabolic curve with a clear maximum value is observed for each data set, suggesting that an optimal site-specific AF value exists in the MPM model. The results further indicate that MPM can improve wind turbine performance and enhance the amount of energy captured by as much as 7% when compared to the PM method of forecasting.

Figure 6 presents a plot of the annual average wind speed versus the optimal AF factors for each of the 15 test sites. Note that the values of AF_{opt} were selected based on the location of the peak of each curve in Figure 5. The data appear to follow a linear trend. A linear least-squares curve fit to the data yields the following empirical relationship:

$$AF_{\mathrm{opt}} = 7.37\,[V] - 17.82, \tag{11}$$

where $[V]$ denotes the annual average wind speed. This empirical relationship allows users to operate the wind turbine at its optimal operating condition when the MPM forecasting model is implemented. One only needs to estimate the average annual wind speed of the advanced year, and the optimal AF can be determined from Equation (11). One fixed AF_{opt} value is used for the entire year. It is worth mentioning that the average annual wind speed of the advanced year can be estimated using the Persistence Model on the data from the current year or by examining the wind speed history from previous years, if those data are available.

3. Autoregressive moving average

In both the PM and MPM methods, the implied forecasting horizon is one day in advance, and only conditions from the previous day are used to make the forecast. The ARMA model, on the other hand, can utilize the time history of the forecasting variable, and the forecasting horizon remains to be determined. Therefore, when employing the ARMA model, not only

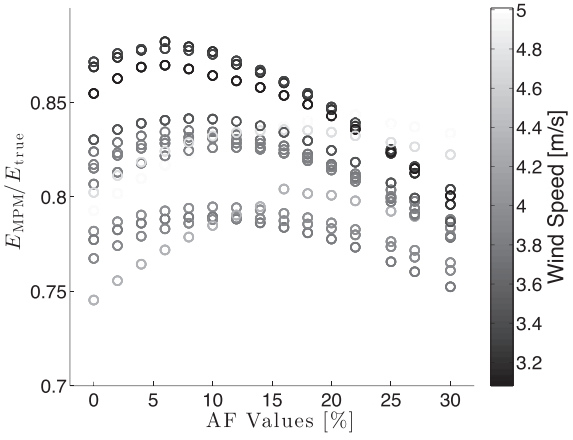

FIG. 5. The influence of rotational speed adjustment factor (AF) on the amount of energy captured by the wind turbine when the MPM forecasting method is used. Each set of curves represents a different test site, color-coded based on the annual average wind speed for 2009 at that site.

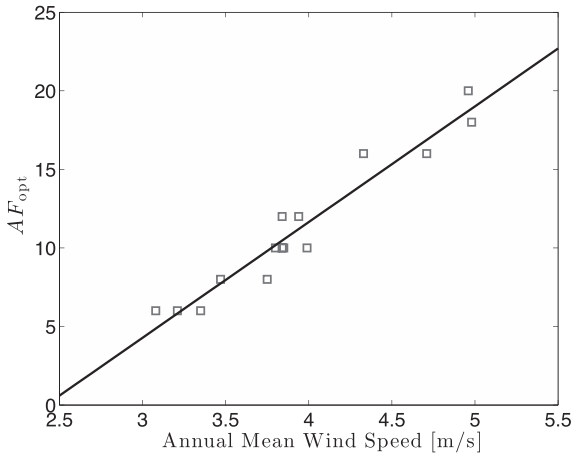

FIG. 6. Optimal rotational speed adjustment factor as used in MPM versus annual average wind speed from 2009 at each of the 15 test sites.

must the (p, q) order of the model be specified, as described in Section III C, but also one needs to decide on the training period and the forecasting horizon. Figure 7 illustrates the approach used in the present study to determine reasonable values for the training period and forecasting horizon at two test sites: KSW 101 and KSW 109. In both cases, the rotational speed of the turbine is the forecasting variable of interest. A wide range of training periods and forecasting horizons was examined, spanning from 10 to 60 days with a 5-day increment and 1–30 days with a 1-day increment, respectively. For each training period and forecasting horizon setting, the mean absolute error (*MAE*) of the rotational speed as averaged over the full year of data was calculated.

As illustrated in Figure 7, a trough in the contour plot (dark band) exists where the ARMA model has the lowest *MAE* value. It is clear from the figure that the response of the ARMA model to the amount of training data and forecasting horizon is site dependent. At the KSW 101 site, a training period of 25 days and a forecasting horizon of 5 days (as indicated by the ⋆ marker) were selected as "optimal." Note that this "optimal" training period corresponds to the time period over which the data are correlated, as verified from calculating the autocorrelation function of the training data (not shown).

Note that because of the way that the daily adjustment of rotational speed was performed in the numerical model, only integer values (in units of days) for the training period and forecasting horizon could be used. At the KSW 109 site, a training period of 30 days and a

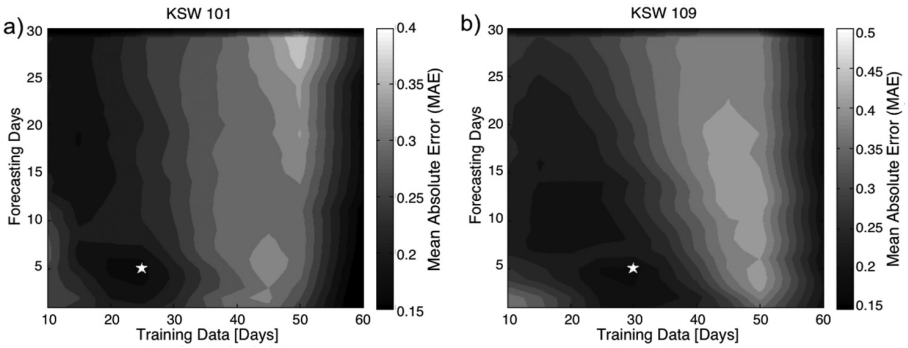

FIG. 7. Contour plot of the mean absolute error as a function of both training period and forecasting horizon for the ARMA model used to predict the rotational speed of the turbine. (a) Test site KSW 101 and (b) test site KSW 109. The ⋆ marker indicates the "optimal" training period and forecasting horizon selected for further analysis in the present study.

forecasting horizon of 5 days were selected. Both selections have *MAE* values near 18%. Also noticeable in the contour plots are regions of high *MAE* in both the lower left corner (short training period and short forecasting horizon) and upper right corner (long training period and long forecasting horizon). These results are somewhat expected. When minimal training data are used, the model is unable to represent the essential features of the forecasting variable, thus leading to high error in the forecasting result. On the other hand, when the training period is too long, the model becomes "overtrained," which tends to smooth out essential features in the behavior of the forecasting variable, leading to large errors in the forecast. The amount of energy captured using the ARMA model is shown in Section V B 5 in comparison to the other forecasting methods.

4. Weather research and forecasting model

Results from the WRF model with 4 km grid resolution were used in the forecasting analysis. Horizontal wind data from the WRF model were obtained at 40.7656° latitude, −111.8427° longitude, and 1531 m elevation above sea level, whereas the location of the actual wind data (and assumed placement of the wind turbine) is on the roof of the William Browning Building (WBB) having coordinates 40.7663° latitude, −111.8477° longitude, and 1465 m elevation above sea level. This corresponds to differences of approximately 0.34 km on the ground and 66 m in elevation. Figure 8 shows the comparison of wind speed from WRF with that from a cup and vane anemometer on the roof of WBB over a sample 30-day period in June 2013. Note that the data from WRF are available in 1-h averaged intervals. There is significant discrepancy in the wind speed magnitude between the data and model. For example, the annual average wind speed from the anemometry data at WBB in 2013 is 2.66 m/s, while the WRF model predicts an annual average of 3.24 m/s. In addition, the daily average turbulence intensity calculated from WRF was 33% lower than that calculated from the anemometer data. The difference in mean wind speeds is likely due to boundary layer effects, since the first grid point in WRF resides much higher from the surface than the actual location of the data. While the difference in turbulence intensity reflects the fact that the turbulence intensity from WRF was calculated based on the hourly averaged wind speeds, rather than instantaneous wind speed, it is worth mentioning that the WRF model tends to capture the fluctuating trends of the data relatively well. This suggests that a constant scaling factor could be applied to the WRF output to compensate for the mismatch in wind speed magnitude. The scaling factor was calculated based on the ratio of the annual average wind speeds. The scaled WRF winds were then used to compute the daily averaged wind speed ($\tilde{V}$) and turbulence intensity ($\tilde{I}_T$), which were input into the empirical relation in (1) to obtain the effective rotational speed ($\tilde{\omega}$) of the turbine for each day. Note that since the scaling factor does not change the turbulence intensity, $\tilde{\omega}$ forecasted by WRF tends to be consistently underestimated. Importantly, as with the other forecasting models,

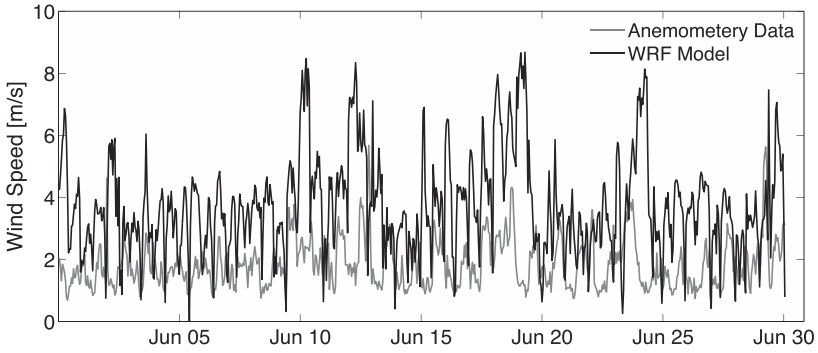

FIG. 8. Comparison of the forecasted wind speed from the WRF model with the actual data measured on the roof of the William Browning building on the University of Utah Campus over a 30-day period in June, 2013.

the performance of the turbine was calculated using the numerical model of the turbine subjected to the wind time series as measured by the anemometer data.

5. Forecasting model comparison

Figure 9 shows the comparison of different forecasting models over a sample 30-day period at test site KSW 101. The "Optimal Value" represents the optimal rotational speed at which the wind turbine would be operated if the actual wind condition was known in advance. Note that the behavior of the forecasted rotational speed produced by the PM and MPM methods is identical to the one observed using the Optimal values with a one-day phase shift. The MPM method used an optimal AF value of 18.6% as determined from (11). The ARMA model used a training period of 25 days and a 5-day forecast interval, as determined from the analysis in Section V B 3. The data suggest that for small variations in the rotational speed of the turbine the PM method provides a better forecast than the MPM and ARMA models. This is as expected since PM does not require any training data but assumes that the future value will be the same as the present value. Therefore, as long as variations in the rotational speed remain small, PM will yield fairly accurate forecasting. For large variations in the rotational speed, the ARMA model appears to outperform both the PM and MPM methods. It was observed that although the ARMA model might not be able to accurately forecast the exact value of the turbine's rotational speed, it tended to capture the trend of the rotational speed relatively well.

Although forecasting accuracy, as measured by the mean absolute error of the turbine's rotational speed, provides a useful assessment of the different forecasting methods, ultimately one would like to know how well each forecast method performs in terms of the total amount of energy captured by the turbine during a given time period of interest. This was done using the full year of 2009 data at three different Oklahoma test sites (KSW 101, KSW 109, and KNW 104) plus the full year of 2013 data at the William Browning Building (WBB) of the University of Utah Campus. The results are shown in Figure 10. The four forecasting models discussed herein (PM, MPM, ARMA, and WRF) were compared against results using no forecasting as well as results using the optimal ω settings assuming that the wind conditions were known perfectly in advance every day. The optimal ω case provides the ideal amount of energy that can be captured by a constant-ω controller. For the case of no forecasting, the turbine was rotated at a constant speed for the entire year (i.e., daily adjustment was not performed). The constant ω was determined independently at each site using the empirical relation in (1) to obtain the optimal TSR, which was then divided by the annual average wind speed and turbine radius to obtain the optimal ω for the year. The actual values of the annual average wind speed and yearly averaged turbulence intensity were used for convenience. In practice, however, these would not be known in advance and would need to be forecasted. As such, the values of total energy captured shown in Figure 10 for the "no forecasting" case overestimate what would be

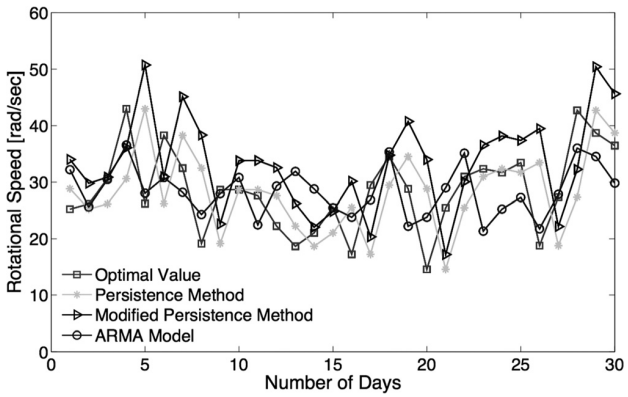

FIG. 9. Sample comparison of different forecast models over a 30-day period at test site KSW 101.

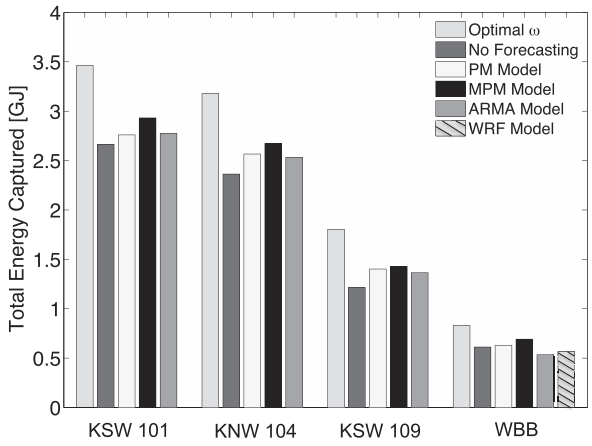

FIG. 10. Total energy captured by the turbine at four different test sites.

expected in practice. As can be seen, the MPM method consistently produces significantly more energy than the case of no forecasting, exceeding the latter by as much as 17.3% (at the KNW 104 site). Note that comparison of the WRF model with the other forecasting models was only available for the WBB site. In the results shown, the MPM models used the optimal *AF* value determined from (11) assuming that the average annual mean speed is accurately estimated at each site. The ARMA models incorporate appropriate values for the training period and forecasting horizon using the analysis outlined in Section V B 3. For the WRF model, a scaling factor was applied to the modelled horizontal wind speed prior to its analysis as discussed in Section III D.

The results in Figure 10 indicate that the MPM method outperforms the PM, ARMA, and WRF models in terms of the amount of energy captured by about 2%–6% depending on the site. Note that these percentages are only slightly sensitive to the value of the adjustment factor (*AF*) used in the MPM model. In the present study, an *AF* value appropriate for the actual annual average wind speed at each site was used, based on the empirical relation in (11). Given a 10% uncertainty in the annual average wind speed at site KSW 101, for example, and modifying the *AF* value accordingly, the total amount of energy captured from the MPM model would decrease to 2.887 GJ, compared to 2.933 GJ as shown in Figure 10. Even with the 10% uncertainty in *AF*, MPM still captures about 4.3% more energy than the PM and ARMA models at KSW 101. There is not an appreciable difference in energy captured between the PM, ARMA, and WRF models. However, it is expected that the WRF model could perform better if the vertical resolution was improved such that the predicted winds were obtained at an equivalent elevation as that of the turbine. In addition, the present results indicate that the wind turbine operating with the MPM forecast method could capture as much as 85% of the ideal amount of energy harvested using the optimal-ω.

C. Economic analysis

The economic analysis of the wind turbine was studied using the full year of wind speed data in Oklahoma City in 2009. The levelized cost of energy (LCOE) method outlined in Section IV was used to compute the LCOE price for a small stand-alone, off-grid VAWT system. Figure 11 shows the dependence of the LCOE price on the annual average wind speed for all of the fifteen test sites in Oklahoma City. The results indicate a nearly quadratic dependence of LCOE on the annual average wind speed. Note that, in the present economic analysis, the annual energy production at each test site is assumed to be the same as in year 2009. The error bars on each data point in Figure 11 represent the LCOE variation when the annual energy production is varied between $\pm 10\%$ of that calculated for 2009. Higher error bars are observed at

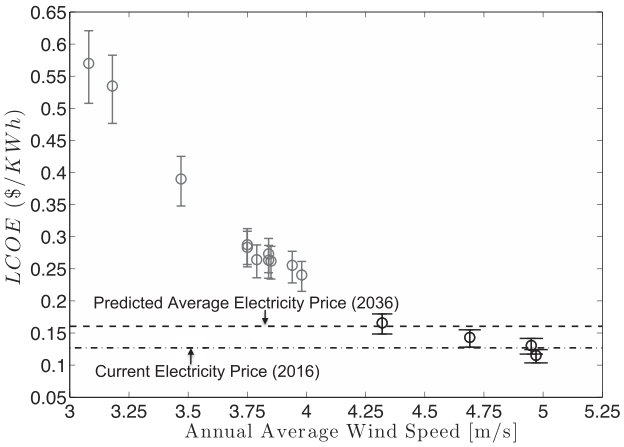

FIG. 11. Comparison of the LCOE price of the implemented system at different sites in Oklahoma City based on its projected operation during the year of 2009. The lower horizontal dashed line represents the national electricity unit price as of August 2016. The higher horizontal dashed line represents the predicted average national electricity price in 2036.

higher LCOE values, which suggests that the LCOE is more sensitive to the amount of energy produced for sites with lower annual average wind speeds.

According to the U.S. Energy Information Administration's Electric Power Monthly Report for August 2016 (Table 5.6.A in the report), the local (Oklahoma) and national electricity unit price for the residential sector for August 2016 are \$0.1051/kWh and \$0.1290/kWh, respectively.[12] Note that Oklahoma is one of the few states that have the lowest selling electricity unit price in the U.S. It is well known that the price of electricity tends to increase annually. According to a review by the U.S. Energy Information Administration in 2014, the U.S. electricity price for the residential sector increased by 17% since 2006 to 2013, which is equivalent to a 2.43% increase annually.[11] Using this annual increase rate and the present electricity price of \$0.1290/kWh, the average electricity price in the next 20 years is predicted to be \$0.1597/kWh, as illustrated in Figure 11. In fact, it only makes sense to compare the LCOE price to this future average electricity price when evaluating whether the VAWT system is economically viable.

The LCOE of turbines located at sites KSW 101, KSW 108, and KNW 104 is competitive with the national electricity unit price. The annual average wind speeds at these sites are relatively high, measuring between 4.7 m/s and 5 m/s. The LCOE of turbines located at KSW 102, KSW109, KSW 110, KCB110, KSE 102, and KNW 103, however, is double that of the national electricity unit price. The annual average wind speed at these locations ranges from 3.7 m/s to 4 m/s. The results also indicate that the LCOE for the turbine is sensitive to changes in the annual average wind speed. For example, a 20% decrease in the annual average wind speed could double the LCOE of the system. This clearly has ramifications for wind turbine siting in the urban/suburban area.

The present study examined sites covering an approximate 560 km^2 area. The LCOE of the turbine located at site KSW 102 is almost double the LCOE of the turbine located at test site KSW 101 even though these two sites are only 14 km apart. The annual wind speed and turbulence intensity at site KSW 101 are 4.95 m/s and 0.363, respectively, while those at site KSW 102 are 3.98 m/s and 0.423, respectively. The site KSW 101 lies at the western most location in the network and is characterized by open fields with trees and residential houses in the distance about 1 km from the measurement location, whereas site KSW 102 lies closer to the city center at a busy intersection off of Highway 40. Several commercial buildings (1–4 story) are located around the intersection, and a large strip mall exists approximately 1–2 blocks north. Therefore, the increased atmospheric surface roughness at site KSW 102 is the likely reason for the observed reduction in annual average wind speed and increase in turbulence intensity. The results from the economic analysis suggest that, in order for the present VAWT to be economical, the system should only be deployed at locations where the average annual wind speed

measures 4.3 m/s or higher. For test sites including KSW 102, KSW 109, KSW 110, KCB 110, KSE 102, and KNW 103, where the annual average wind speeds are about 3.75 m/s, the project cost of the deployed system would have to decrease by about 45% of the current project cost in order for the technology to exhibit a LCOE cost competitive with the national electricity unit price. It should be mentioned that the measurements, on which the present economic analysis was based, were acquired from instrumentation mounted to the street light signal at each site (approximately 9 m above ground level). It would be more realistic for a turbine to be placed on the roof of a building instead. Further work is necessary to determine the extent to which this change in height would result in a significant reduction in the LCOE at the various sites.

VI. CONCLUSION

The present study investigates different forecasting methods to improve the overall performance of a small VAWT operating in an urban/suburban area. Performance is measured in terms of the total amount of energy captured over a full year of operation. Wind data acquired in 2009 at fifteen different locations in Oklahoma City were used to drive the developed numerical models. In all cases, a constant rotational speed controller is used. The rotational speed of the turbine is adjusted daily to account for changes in the wind speed. This is especially important during unsteady/gusty wind conditions characteristic of most urban/suburban areas in order to correctly set the overspeed of the turbine. The economic viability of the VAWT is also examined by comparing the LCOE for the VAWT with the national electricity unit price.

Wind data from the combined sites in Oklahoma City demonstrate that forecasting uncertainty has a significant impact on the amount of energy captured by the wind turbine. The results indicate that a 5% increase in forecasting accuracy could increase the total amount of energy captured by the VAWT by as much as 13%. The results also showed less sensitivity to error when the rotational speed of the turbine was forecasted directly as opposed to the wind condition. Four forecasting strategies were examined in the present study: Persistence Model (PM), Modified Persistence Model (MPM), Autoregressive Moving Average (ARMA) model, and Weather Research and Forecasting (WRF) model. The three statistical approaches (PM, MPM, and ARMA) were used to forecast the optimal rotational speed of the VAWT. Since WRF represents a physical model of the atmosphere, it can only be used to predict the future wind condition. PM is the simplest approach since it does not involve any tuned model parameters. MPM involves one parameter, an adjustment factor (AF), that was found to be site-independent and linearly correlated with the annual average wind speed. This result has a potential practical application. If one can estimate the average annual wind speed of the advanced year, then the appropriate AF value may be calculated and applied to the controller. The ARMA model is a complex forecasting model that requires optimization of many parameters. The optimal training period and forecasting horizon in ARMA were found to be site-dependent.

With regard to forecasting the optimal rotational speed of the VAWT, results suggest that the PM model outperforms MPM and ARMA for small variations, while for large variations in the optimal rotational speed, ARMA appears to outperform both PM and MPM. However, in terms of the total amount of energy captured, MPM improved wind turbine performance the most, capturing as much as 6% more energy compared to PM and ARMA. Both PM and ARMA exhibited nearly equivalent performance. Across all test cases, the forecasting models allow the VAWT to capture approximately 78%–85% of the ideal amount of energy that could be captured by a constant speed controller (with daily adjustment), assuming that the actual wind data were known in advance. Compared to the case of no forecasting, MPM improved the total amount of energy captured over the full year of operation by as much as 17.3%. The WRF model performed as well as the ARMA model. It is expected that the WRF model could perform better with enhanced grid resolution, especially in the vertical direction. Including a model of the turbulent kinetic energy might also improve the WRF-based forecast of the daily average turbulence intensity needed to set the optimal rotational speed of the turbine. However, even with these improvements in the WRF model, it is not clear whether the additional computational cost would be worthwhile considering the simplicity and performance of the MPM

model, for example. Note that, in all cases, the present study only considers a forecasting horizon of 1 day. Preliminary analyses (not shown) indicate that this forecasting horizon yields the best results in terms of maximizing the energy captured over the full year of operation. It is suggested that future work could be done to examine in more detail the effect of forecasting horizon on energy captured by the turbine.

In order for VAWTs to become a viable alternative in urban/suburban areas, the LCOE from the turbine must be competitive with the average price of electricity to the residential sector. Results show that the LCOE from the present turbine decreases quadratically with annual average wind speed. At the sites where the annual average wind speed was 4.3 m/s or higher, the LCOE from the turbine was competitive with the national electricity unit price. It is surmised that the LCOE could be reduced by implementing larger VAWT systems and/or connecting multiple VAWTs together to a single controller and battery tank. It remains to be determined whether connecting the VAWT directly to the electrical grid would significantly change the LCOE.

ACKNOWLEDGMENTS

The first author was supported by a University of Utah Graduate Fellowship during the course of this work. The authors gratefully acknowledge the help of Dr. Jeff Basara of the University of Oklahoma for providing the Micronet wind data in Oklahoma City in 2009. A special thank-you goes to Marcela Loria-Salazar and Dr. Heather Holmes of the University of Nevada, Reno, for providing the WRF model results for Salt Lake City in 2013.

[1]T. Ayodele, A. Jimoh, J. Munda, J. Agee, and G. M'boungui, "Economic analysis of a small scale wind turbine for power generation in Johannesburg," in *2013 IEEE International Conference on Industrial Technology (ICIT)* (IEEE, 2013), pp. 1728–1732.
[2]J. B. Basara, B. G. Illston, C. A. Fiebrich, P. D. Browder, C. R. Morgan, A. McCombs, J. P. Bostic, R. A. McPherson, A. J. Schroeder, and K. C. Crawford, "The Oklahoma City micronet," Meteorol. Appl. **18**(3), 252–261 (2011).
[3]M. Bolinger, "An analysis of the costs, benefits, and implications of different approaches to capturing the value of renewable energy tax incentives.," Technical Report No. LBNL-6610E, Lawrence Berkeley National Laboratory, 2014.
[4]E. Cadenas and W. Rivera, "Wind speed forecasting in the south coast of Oaxaca, Mexico," Renewable Energy **32**(12), 2116–2128 (2007).
[5]W.-Y. Chang, "A literature review of wind forecasting methods," J. Power Energy Eng. **2**(4), 161 (2014).
[6]C. Chatfield, *Time Series Analysis: An Introduction*, 6th ed. (Chapman & Hall, 2004).
[7]K. T. Clifford, "WRF model performance for wind power forecasting in the coast ranges of central California," M.S. thesis (San Jose State University, 2011).
[8]A. J. Deppe, W. A. Gallus, Jr., and E. S. Takle, "A WRF ensemble for improved wind speed forecasts at turbine height," Weather Forecasting **28**(1), 212–228 (2013).
[9]G. Drisya, D. Kiplangat, K. Asokan, and K. S. Kumar, "Deterministic prediction of surface wind speed variations," Ann. Geophys. **32**, 1415–1425 (2014).
[10]J. Dudhia, "Numerical study of convection observed during the winter monsoon experiment using a mesoscale two-dimensional model," J. Atmos. Sci. **46**(20), 3077–3107 (1989).
[11]U.S. Energy Information Administration (EIA), http://www.eia.gov/todayinenergy/detail.php?id=18851 for European residential electricity prices increasing faster than prices in united states, 2014.
[12]U.S. Energy Information Administration (EIA), "Electric Power Monthly with data for August 2016," Technical Report, October 2016, U.S. Department of Energy, 2016; available at https://www.eia.gov/electricity/monthly/current_year/october2016.pdf.
[13]E. Erdem and J. Shi, "Arma based approaches for forecasting the tuple of wind speed and direction," Appl. Energy **88**(4), 1405–1414 (2011).
[14]A. Fabbri, T. G. S. Román, J. R. Abbad, and V. H. M. Quezada, "Assessment of the cost associated with wind generation prediction errors in a liberalized electricity market," IEEE Trans. Power Syst. **20**(3), 1440–1446 (2005).
[15]International Renewable Energy Agency (IRENA), "Renewable energy technologies: Cost analysis series," in *Power Sector* (IRENA, 2012), Vol. 1, Issue 5/5; available at https://www.irena.org/DocumentDownloads/Publications/RE_Technologies_Cost_Analysis-WIND_POWER.pdf.
[16]J. S. Kain, "The Kain-Fritsch convective parameterization: An update," J. Appl. Meteorol. **43**, 170–181 (2004).
[17]J. Kaldellis, "Optimum autonomous wind–power system sizing for remote consumers, using long-term wind speed data," Appl. Energy **71**(3), 215–233 (2002).
[18]R. G. Kavasseri and K. Seetharaman, "Day-ahead wind speed forecasting using f-Arima models," Renewable Energy **34**(5), 1388–1393 (2009).
[19]J. Klemp, "Advances in the wrf model for convection-resolving forecasting," Adv. Geosci. **7**, 925–929 (2005).
[20]P. D. Lavappa and J. D. Kneifel,"Energy price indices and discount factors for life-cycle cost analysis," Technical Report No. NISTR 85-3273-30, National Institute of Standards and Technology, U.S. Department of Commerce, 2015.
[21]M. Lei, L. Shiyan, J. Chuanwen, L. Hongling, and Z. Yan, "A review on the forecasting of wind speed and generated power," Renewable Sustainable Energy Rev. **13**(4), 915–920 (2009).

[22]L. Ling-ling, J.-H. Li, P.-J. He, and C.-S. Wang, "The use of wavelet theory and Arma model in wind speed prediction," in *2011 1st International Conference on, Electric Power Equipment-Switching Technology (ICEPE-ST)* (IEEE, 2011), pp. 395–398.
[23]J. Michalakes, J. Dudhia, D. Gill, T. Henderson, J. Klemp, W. Skamarock, and W. Wang,"The weather research and forecast model: Software architecture and performance," in *Proceedings of the 11th ECMWF Workshop on the Use of High Performance Computing in Meteorology* (2005), pp. 156–168.
[24]M. Milligan, M. Schwartz, and Y-H. Wan, "Statistical wind power forecasting for US wind farms," National Renewable Energy Laboratory, Report No. NREL/CP-500-33956, 2004, p. 1617.
[25]M. R. Milligan, A. H. Miller, and F. Chapman,"Estimating the economic value of wind forecasting to utilities," in *Wind Power 1995*, Washington, DC (1995), pp. 285–294.
[26]E. J. Mlawer, S. J. Taubman, P. D. Brown, M. J. Iacono, and S. A. Clough, "Radiative transfer for inhomogeneous atmospheres: RRTM, a validated correlated-k model for the longwave," J. Geophys. Res. **102**(D14), 16663–16682, doi:10.1029/97JD00237 (1997).
[27]C. Mone, A. Smith, B. Maples, and M. Hand, "2013 Cost of wind energy review," Technical Report No. NREL/TP-5000-63267, NREL National Renewable Energy Laboratory, 2013.
[28]H. Morrison, G. Thompson, and V. Tatarskii, "Impact of cloud microphysics on the development of trailing stratiform precipitation in a simulated squall line: Comparison of one-and two-moment schemes," Mon. Weather Rev. **137**(3), 991–1007 (2009).
[29]L. Nguyen and M. Metzger, "Enhanced energy capture by a vertical axis wind turbine during gusty winds in an urban/suburban environment," J. Renewable Sustainable Energy **7**(5), 053118 (2015).
[30]T. S. Nielsen, A. Joensen, H. Madsen, L. Landberg, and G. Giebel, "A new reference for wind power forecasting," Wind Energy **1**(1), 29–34 (1998).
[31]J. Palomares-Salas, J. De la Rosa, J. Ramiro, J. Melgar, A. Aguera, and A. Moreno,"Arima vs. neural networks for wind speed forecasting," in *IEEE International Conference on Computational Intelligence for Measurement Systems and Applications, 2009, CIMSA'09* (IEEE, 2009), pp. 129–133.
[32]J. E. Pleim, "A simple, efficient solution of flux-profile relationships in the atmospheric surface layer," J. Appl. Meteorol. Climatol. **45**(2), 341–347 (2006).
[33]J. E. Pleim, "A combined local and nonlocal closure model for the atmospheric boundary layer. Part I: Model description and testing," J. Appl. Meteorol. Climatol. **46**(9), 1383–1395 (2007).
[34]J. E. Pleim and A. Xiu, "Development of a land surface model. Part II: Data assimilation," J. Appl. Meteorol. **42**(12), 1811–1822 (2003).
[35]C. W. Potter and M. Negnevitsky, "Very short-term wind forecasting for Tasmanian power generation," IEEE Trans. Power Syst. PWRS **21**(2), 965 (2006).
[36]B. F. Ragnarsson, G. V. Oddsson, R. Unnthorsson, and B. Hrafnkelsson, "Levelized cost of energy analysis of a wind power generation system at Búrfell in Iceland," Energies **8**(9), 9464–9485 (2015).
[37]I. Sanchez, "Short-term prediction of wind energy production," Int. J. Forecasting **22**(1), 43–56 (2006).
[38]A. Sfetsos, "A comparison of various forecasting techniques applied to mean hourly wind speed time series," Renewable Energy **21**(1), 23–35 (2000).
[39]W. C. Skamarock, J. B. Klemp, J. Dudhia, D. O. Gill, D. M. Barker, W. Wang, and J. G. Powers,"A description of the advanced research wrf version 3," Technical Report No. NCAR/TN-475+STR, DTIC Document, 2008.
[40]S. S. Soman, H. Zareipour, O. Malik, and P. Mandal, "A review of wind power and wind speed forecasting methods with different time horizons," in *North American Power Symposium (NAPS), 2010* (IEEE, 2010), pp. 1–8.
[41]I. Staffell and R. Green, "How does wind farm performance decline with age?," Renewable Energy **66**, 775–786 (2014).
[42]J. W. Taylor, P. E. McSharry, and R. Buizza, "Wind power density forecasting using ensemble predictions and time series models," IEEE Trans. Energy Convers. **24**(3), 775–782 (2009).
[43]J. L. Torres, A. Garcia, M. De Blas, and A. De Francisco, "Forecast of hourly average wind speed with Arma models in Navarre (Spain)," Sol. Energy **79**(1), 65–77 (2005).
[44]S. Watson, L. Landberg, and J. Halliday, "Application of wind speed forecasting to the integration of wind energy into a large scale power system," IEE Proc., Gener. Transm. Distrib. **141**, 357–362 (1994).
[45]WRF, http://www.wrf-model.org/index.php, URL http://www.wrf-model.org/index.php for weather research and forecasting model, 2016.
[46]A. Xiu and J. E. Pleim, "Development of a land surface model. Part I: Application in a mesoscale meteorological model," J. Appl. Meteorol. **40**(2), 192–209 (2001).
[47]X. Zhu and M. G. Genton, "Short-term wind speed forecasting for power system operations," Int. Stat. Rev. **80**(1), 2–23 (2012).

CHAPTER 4

OPTIMIZATION OF A VERTICAL AXIS WIND TURBINE FOR APPLICATION IN AN URBAN/SUBURBAN AREA

This chapter has been submitted to the Journal of the Renewable and Sustainable Energy as "Optimization of a Vertical Axis Wind Turbine for Application in an Urban/Suburban Area," Lam Nguyen and Meredith Metzger, March 2017.

The goal of the present study is to investigate the effect of various design parameters on the performance of a Vertical Axis Wind Turbine (VAWT) subjected to realistic unsteady wind conditions. Thirteen turbine design configurations are examined to determine if an optimal VAWT exists for application in an urban/suburban environment. The four design parameters of interest include height-to-diameter aspect ratio ($0.83 \leq H/D \leq 1.34$), blade airfoil shape (NACA 0012, 0015, 0018), turbine solidity ($12 \leq S \leq 25\%$), and turbine moment of inertia. The height and diameter of the turbine varied between 1.89–2.54 m, depending on the aspect ratio. The turbine moment of inertia was calculated using a computer-aided design drawing of the turbine, along with realistic material properties for the blades, shaft, and supports. The energy generated by each VAWT design configuration is simulated using a full year of actual wind speed data collected in 2009 at 9 different locations around Oklahoma City spanning an approximate 500 km^2 area. The wind data were acquired from the top of traffic light posts at a height of about 9 m above the ground. In all cases, an active control strategy is used that allows the turbine to continuously adjust its rotational speed in response to the fluctuating wind. Results suggest that, for the case of operation in unsteady winds, the optimal power coefficient (C_p) versus tip speed ratio (TSR) curve is not necessarily the one exhibiting the

highest peak C_p value, but rather the broadest shape. Of the thirteen configurations examined, the optimal wind turbine design capable of harvesting the most energy from the gusty winds was found to have an aspect ratio of $H/D = 1.2$, solidity of $S = 12\%$, and blade shape using the NACA 0015 airfoil. This design also displayed the lowest moment of inertia. However, when the effects of weight were removed, this design still performed the best. The site-to-site variation in terms of energy captured relative to the available energy in the gusty winds was only about 5% on average, and increased slightly with turbine moment of inertia. Four of the suburban sites studies were deemed economically viable locations for a small-scale VAWT. Results further indicate, at one of these sites, the Levelized Cost of Energy (LCOE) associated with the top performing turbine designs examined in the study was about 10% less than the national electricity price, meaning that wind energy provides a cheaper alternative to fossil fuel at this location. It is surmised that VAWTs could economically harvest wind energy in the urban center as well, if the turbines were located higher than 9 m, such as on the rooftops of commercial/residential buildings.

4.1 Introduction

Wind energy harvesting has increased rapidly in the past few decades due to considerable advancements in wind turbine technology (Ackermann and Söder, 2002; Kaldellis, 2002; Leung and Yang, 2012). The U.S. Department of Energy predicts that wind energy will provide about 20% of the electricity in the U.S. by the year of 2030 (Lindenberg, 2009). Along with the increasing number of wind farms containing large horizontal axis wind turbines (HAWTs), an upsurge in small-scale wind turbines including vertical axis wind turbines (VAWTs) has also occurred in recent years (Azau, 2010; Stefan Gsnger, 2015). The ability of small VAWTs to operate effectively in the presence of highly fluctuating, turbulent flow makes them ideal energy harvesting devices in the urban/suburban environment, where winds are typically unsteady and gusty (Fiedler and Tullis, 2009; Bertényi et al., 2010; Nguyen and Metzger, 2015). In addition, because the generator and electrical components mount at the base, VAWTs provide a more suitable design solution, compared to the traditional HAWT, for small-scale urban installation such as on the rooftops

of residential/commercial buildings (Armstrong et al., 2012). Although small-scale wind turbines are certainly limited in the amount of overall energy that can be produced due to size constraints, one major benefit of locating technology where the demand is highest stems from reduced capital investment on transmission lines. The presence/visibility of renewable energy technology in densely populated areas may also have the added potential benefit of encouraging better conservation practices by the people living in those areas. One of the motivations for our work is the idea of a net-zero energy building or a net-zero energy city, wherein the total amount of energy used locally on an annual basis is roughly balanced by the amount of renewable energy generated on site. Economically viable renewable energy technologies are an important aspect of this mission. The present study provides results indicating that an optimally designed VAWT system can be financially competitive with fossil-fuel-based power plants, at least in one particular urban/suburban area (Oklahoma City), and represents a steppingstone toward evaluating the feasibility of the net-zero energy building/city.

A considerable amount of research has been conducted toward optimizing the power performance of VAWTs (Templin, 1974; Islam et al., 2008; Mohamed, 2012; Bedon et al., 2013). Design parameters affecting the performance of a VAWT include the turbine type, airfoil shape, turbine solidity, number of blades, and height to diameter ratio. Common types of VAWTs are the eggbeater Darrieus turbine, straight-blade Darrieus turbine, Savonius turbine, and helical turbine (Blackwell et al., 1976; McIntosh et al., 2007; Islam et al., 2008; Mahmoud et al., 2012; Bedon et al., 2013). Each wind turbine type poses its own advantages and disadvantages. In a review of different VAWT configurations, Mohamed (2012) concluded that the eggbeater Darrieus tubines provide lower bending stresses on the blades. However, the difficulty in manufacturing this type of wind turbine translates into high production cost, making the eggbeater Darrieus turbine less preferable compared to its straight-blade counterpart. The current study focuses exclusively on the performance of the straight-blade Darrieus turbine.

Airfoil shape is another important design parameter of the VAWT. In 1981, Sheldahl and Klimas (1981) performed wind tunnel tests on seven symmetrical

airfoil sections (NACA 00XX) to evaluate the lift and drag coefficients through 180° angle of attack at low Reynolds number. The results have been extensively used in many numerical models for predicting VAWT power performance (Paraschivoiu, 2002; Nguyen and Metzger, 2015). Roh and Kang (2013) performed a study to investigate the effect of airfoil blade profile on the performance of a straight-blade VAWT. The results suggest that high digit NACA 00XX airfoils provide higher power in the low tip speed ratio (TSR) regime, compared to the low digit NACA 00XX and vice versa. The study of McIntosh (2009) revealed that turbines with thinner airfoil sections tend to produce higher power coefficients than those with thicker airfoil sections. Paraschivoiu et al. (1983) performed a parametric analysis to study the effects of the blade geometry and airfoil selection on the aerodynamic performance of the Darrieus wind turbine. Three different airfoil sections were examined including NACA 0012, NACA 0015, and NACA 0018. The results showed that at low TSR, the NACA 0015 and NACA 0018 blades perform better than the NACA 0012, which is more efficient at high TSR. Paraschivoiu et al. (1983) concluded that while the symmetrical NACA 0015 is recommended for small-scale Darrieus wind turbines since it exhibits a more favorable stall characteristic, the NACA 0018 is suggested for use based on structural considerations, especially for large-scale turbines. Note the NACA 0018 has a larger maximum thickness (18% of the chord length) compared to the NACA 0015 (15% of the chord length), and thus is easier to manufacture albeit possibly more expensive due to the increase in material required.

Turbine solidity describes the ratio of the area of the rotor blades to the swept area of the rotor, and can significantly influence the performance of a VAWT. Templin (1974) conducted one of the first investigations regarding the impact of solidity on wind turbine performance using the single streamtube model. The results showed that turbine solidity affects the shape of the power performance curve (power coefficient, C_p, versus tip speed ratio, TSR). Specifically, the power performance curve of a turbine with low solidity is broad and wide while that of a turbine with higher solidity is narrow and sharp. As the turbine solidity increases, the peak value in the power performance curve shifts toward lower TSR. In addition, the results showed that, for a VAWT, an optimal solidity exists yielding the highest peak C_p value.

Other researchers have used the multiple streamtube model (Strickland, 1975) and free vortex model McIntosh (2009) to study the effect of turbine solidity on VAWT performance, with similar results observed.

The influence of the number of turbine blades on VAWT performance has also been documented in the literature (Castelli et al., 2012; Tirkey et al., 2014). Castelli et al. (2012) examined VAWTs with 3–5 turbine blades on a straight-blade Darrieus type wind turbine. The results indicated that the turbine with three blades had the best performance, with a wide and broad power performance curve. The results also showed that the number of turbine blades is correlated linearly with the turbine solidity. Tirkey et al. (2014) performed a numerical analysis, adopting the multiple streamtube method to examine the effect of number of blades (3–5 blades) on turbine performance. The results showed that as the number of blades increase, the peak power coefficient (C_p) decreases. The turbine with 3 blades has the highest power coefficient curve. The most commonly used wind turbines in the industry have three blades (Tirkey et al., 2014). For these reasons, the current study focuses exclusively on the performance of VAWTs having three blades.

The height-to-diameter ratio (often referred to as aspect ratio) is an important design parameter of the VAWT. Templin (1974) performed a numerical analysis using the single streamtube model to examine the effect of aspect ratio on the power performance of VAWTs with curved blades. Four wind turbine models with aspect ratios H/D of 0.5, 1.0, 1.5, and 2.0 were examined. The results showed that the turbine model with aspect ratio of 0.5 has the lowest peak power coefficient. The power performance curves of turbine models that have aspect ratios of 1.0, 1.5, and 2.0 are nearly identical. However, the wind turbine models with aspect ratios of 1.5 and 2.0 have slightly higher peak C_p values (by about 2%) than that of the turbine model with an aspect ratio of 1.0. Brusca et al. (2014) performed a numerical analysis based on the multiple streamtube model to evaluate the influence of aspect ratio on wind turbine performance for the case of a VAWT with symmetrical straight blades. Two turbine models with aspect ratios of 1.0 and 0.2 were examined. The peak power coefficients were 0.46 and 0.47 for the turbine models with aspect ratio of 1.0 and 0.2, respectively. Brusca et al. (2014) concluded that the difference in the

peak power coefficient of these two models was mainly attributed to the effect of Reynolds number. It was found that the height-to-diameter aspect ratio influenced the Reynolds number, and as a consequence affected the power coefficient of the wind turbine.

Despite the number of studies aimed at predicting and optimizing the performance of VAWTs, the majority of the research to date has been based on an examination of the power performance curves in the case of ideal wind conditions (namely, incoming winds with a constant speed). It remains to be determined whether the optimal wind turbine configuration for ideal wind conditions would perform as effectively if the turbine were deployed in an environment with turbulent winds, such as that expected in many urban/suburban areas. The present study utilizes a numerical modeling approach to investigate the effect of various VAWT design configurations on the overall energy captured from turbines subjected to realistic gusty wind conditions. The total energy captured by each turbine configuration is calculated using one year of actual wind data. Nine different locations in the metropolitan area surrounding Oklahoma City are examined with a large range of annual average wind speeds and turbulence intensities. The goal of this work is to determine if an optimal VAWT turbine configuration exists for application in urban/suburban neighborhoods, and if such an optimal design is site-independent. The results will have a significant impact on assessing the viability of implementing wind energy technology in the built environment.

4.2 Numerical Models

4.2.1 Turbine Power Performance Model

Various numerical models have been developed over the years to predict and optimize the power performance of VAWTs (Strickland et al., 1980; Paraschivoiu and Delclaux, 1983; Islam et al., 2008; Bedon et al., 2013; Alaimo et al., 2015). For example, Alaimo et al. (2015) developed a CFD model to predict the aerodynamic performance of a VAWT by solving the Reynolds Average Navier Stokes equations. While CFD models provide detailed information about the flow field around the wind turbine, computational expense remains a major drawback. For this reason,

many wind turbine designers prefer numerical models based on the Blade Element Momentum (BEM) theory to predict the power performance of VAWTs (Templin, 1974; Strickland, 1975; Paraschivoiu and Delclaux, 1983; Beri et al., 2011). BEM theory utilizes the conservation of momentum law to determine the momentum deficit across the VAWT, in combination with blade element theory based on known lift and drag coefficients of the blades, in order to calculate the power performance of a turbine subjected to a constant incoming wind speed (Paraschivoiu, 2002). BEM theory is a common feature underlying many existing numerical models of VAWTs, including, for example, the single streamtube model (Blackwell et al., 1976), the double streamtube model (Paraschivoiu, 2002), the multiple streamtube model (Strickland, 1975; Beri et al., 2011; Chong et al., 2013) and the 2D vortex model (McIntosh et al., 2008). In the present implementation of BEM, static lift and drag coefficient data are used from two different sources: Jacobs and Sherman (1937) for angles of attack less than 28°, and Sheldahl and Klimas (1981) for angles of attack greater than 28°.

Due to its simplicity and computational speed, the present study employs the single actuator disk model based on BEM theory to simulate the aerodynamic performance of the wind turbine. This particular model has shown good agreement with experimental data for the Darrieus turbine (Nguyen and Metzger, 2015). In addition, uncertainties in the generated power performance curves due to the simplicity of the BEM model are not expected to have a significant impact on the main conclusions of the study. The present study is primarily comparative in nature, comparing the total energy captured by different turbine designs subjected to the same unsteady wind conditions. Inaccuracies due to the BEM model should be present across all design configurations in a likely equitable fashion, and thus should not appreciably skew the observed differences in performance between designs. The main consideration was computational speed because of the number of different configurations investigated, and the fact that the simulation was run using a full year's worth of wind data for each configuration.

4.2.2 Turbine Transient Response Model

Understanding the transient response of a wind turbine operating under gusty wind conditions is critical to accurately estimating the amount of energy that can be generated by the wind turbine in an urban environment (Nguyen and Metzger, 2015). The transient response of the wind turbine is impacted by many different factors, namely the moment of inertia of the turbine, the unsteady nature of the applied loading torque, the temporal response of the controller, and the unsteady aerodynamic forces acting on the turbine blades. In this study, the transient response of a VAWT is modeled as

$$I \frac{d\omega}{dt} = Q - T_L, \tag{4.1}$$

where I is the moment of inertia of the wind turbine, Q is the aerodynamic torque of the turbine, T_L is the applied loading torque from the generator, and ω is the rotational speed of the turbine. In the transient response model, the aerodynamic torque Q varies according to the tip speed ratio and incoming wind speed. The aerodynamic torque used in (4.1) is calculated from the BEM model.

The ideal tip speed ratio (ideal–TSR) controller is utilized in the present study, similar to our previous work (Nguyen and Metzger, 2015). The ideal–TSR controller tries to maintain the wind turbine at its ideal TSR setting (peak C_p value) by continuously adjusting the rotational speed (ω) in response to variations of the incoming wind speed, when the wind speed remains below the rated wind speed of the turbine. In this manner, the ideal-TSR controller provides active control that allows the turbine to harvest the maximum amount of energy available from the wind. When the wind speed is between the rated and cut-out wind speeds, the controller limits the rotor speed such that the turbine operates at its rated power output. The turbine power curve is discussed further in Section 4.3. In practice, the controller consists of power electronics that continuously switch the connection between the generator and grid to change the synchronous speed of generator independently of the frequency of the grid (Nguyen and Metzger, 2015). The digital control signal to the power electronics is supplied by a microprocessor that has been programmed with the response characteristics of the turbine.

In the ideal–TSR control method, the rotational speed of the turbine is regulated continuously to maintain an ideal TSR setting that yields the maximum C_p of the turbine at every given moment in time. In this study, the electronics are modeled using a simple proportional feedback control strategy, represented by a proportional gain constant K_p in the model. Due to the gain constant (K_p) of the controller and the moment of inertia (I) of the turbine, the realistic controller exhibits a time lag, which prevents instantaneous tracking of the fluctuations in the wind speed. To model this time lag response of the turbine, the dynamics of the system (controller and turbine) are written in the Laplace domain as follow

$$\frac{\omega(t)}{\tilde{\omega}} = \frac{K_p}{Is + K_p}, \tag{4.2}$$

where $\omega(t)$ is time varying rotational speed of the turbine and $\tilde{\omega}$ is the ideal rotational speed of the turbine (for the case of zero time lag). At each time step in the numeric model, the turbine is subjected to the real wind speed according to the data. Based on this, the ideal rotational speed $\tilde{\omega}$ and aerodynamic torque of the turbine Q can be determined from the wind turbine aerodynamic performance model as described in Section 4.2.1. Given the ideal rotational speed $\tilde{\omega}$, the time-varying rotational speed of the turbine $\omega(t)$ is calculated following the dynamic model of the controller (4.2). The loading torque $T_L(t)$ is subsequently calculated by solving (4.1), and multiplied by the actual rotational speed $\omega(t)$ to obtain power as a function of time t. The total energy captured by a VAWT is calculated by integrating the power over the time period of interest.

In the present study, the turbine transient response model is subjected to actual wind speed time series as measured at nine different sites in Oklahoma City, USA in 2009 (see Figure 4.1 and Table 4.1). These nine locations are in the metropolitan area surrounding Oklahoma City and exhibit a large range of annual average wind speeds and turbulence intensities. Here, turbulence intensity is defined as the standard deviation of the wind speed divided by the mean wind speed averaged over the time period of interest ($I_T = \sigma_U/\overline{U}$). Wind speed data were acquired from sonic anemometers mounted directly to traffic signals at a height of 9 m. Data were quality assured in near real time at an interval of 1 minute. A detailed description of the experiments

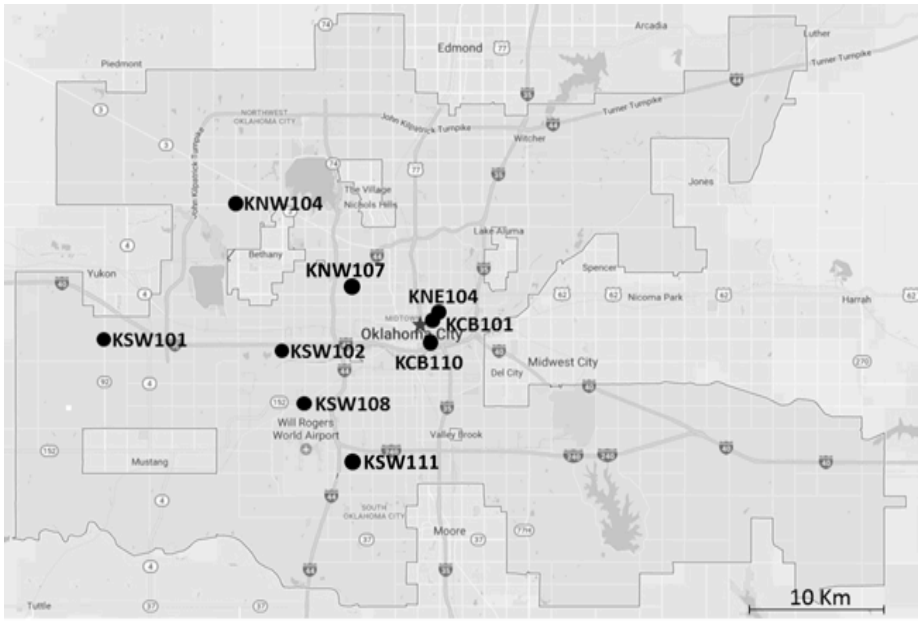

Figure 4.1: Location of sites in Oklahoma City where wind data were acquired.

Table 4.1: Location of sites in Oklahoma City where wind data were acquired. The corresponding annual average wind speed and turbulence intensity are for year 2009.

Site Name	Street Address	Annual-Average Wind Speed [m/s]	Annual-Average Turbulence Intensity
KSW 101	W Reno Ave & S Cemetery Rd	4.95	0.363
KSW 102	SW 5th St &S MacArthur Blvd	3.98	0.423
KSW 108	Amelia Earhart Ln & Terminal Dr	4.97	0.349
KSW 111	J Lee Keels Blvd & S May Ave	4.32	0.401
KCB 101	NE 5th St &N Oklahoma Ave	3.18	0.404
KCB 110	E Reno Ave & S Lincoln Blvd	3.84	0.392
KNE 104	NE 10th St & N Phillips Ave	3.75	0.353
KNW 104	River Bend Blvd & N Council Rd	4.69	0.372
KNW 107	NW 30th St & N May Ave	3.47	0.422

can be found in the study of Basara et al. (2011). Figure 4.2 shows a sample time segment of the instantaneous wind speed over two months of operation during July and August, 2009 at site KSW 101. As illustrated in Figure 4.2, the wind speed exhibits large fluctuations with a wide range of characteristic frequencies. The mean wind speed ($\overline{U}$) over the two-month period is 4.25 m/s, with a standard deviation (σ) of 2.28 m/s. The corresponding turbulence intensity over this two-month period is equal to 0.538.

4.2.3 Economic Analysis

One important aspect that needs to be considered when deploying wind technology is economic feasibility. In the present study, an economic analysis is performed to evaluate the cost effectiveness of implementing small-scale VAWTs at each of the nine sites in Oklahoma City. The Levelized Cost of Energy (LCOE) is used for this purpose, and can be calculated as

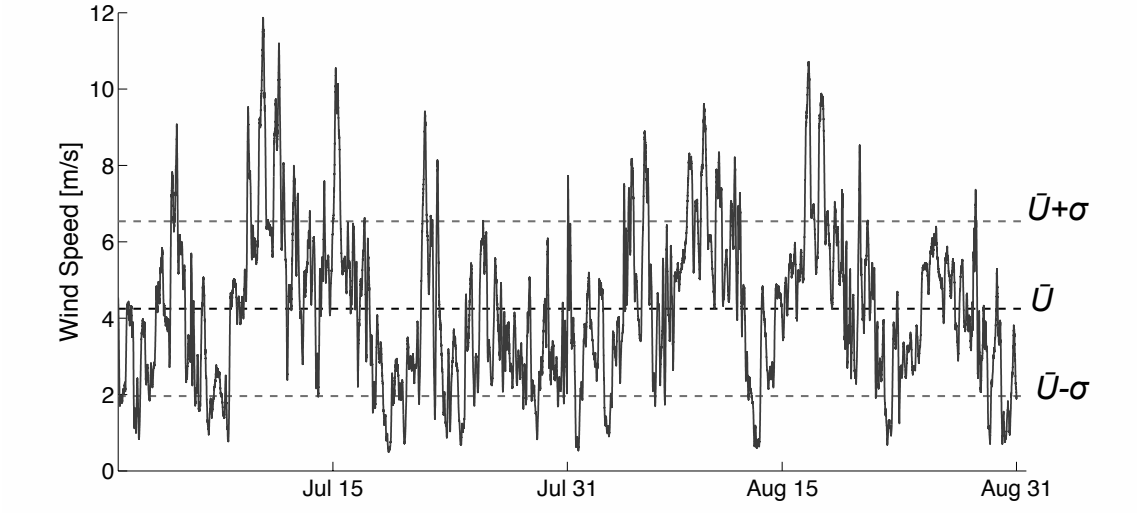

Figure 4.2: Sample time segment of the instantaneous sonic anemometry data collected at site KSW 101 during the months of July and August in 2009. $\overline{U}$ and σ represent the average wind speed and standard deviation calculated over the two-month time period shown.

$$LCOE\ (\$/\text{kWh}) = \frac{[\text{Project Cost}] - [\text{ITC}] + \sum_{n=1}^{N} \frac{AO}{(1+DR)^n} - \frac{RV}{(1+DR)^n}}{\sum_{n=1}^{N} \frac{E_a(1-SDR)}{(1+DR)^n}} - [\text{PTC}], \quad (4.3)$$

where ITC represents the investment tax credit, PTC represents the production tax credit, AO represents the annual operating and maintenance cost, RV represents the residual value of the system based on its end-of-life asset, DR represents the discount rate, E_a represents the annual energy production of the system, SDR represents the system degradation rate, and N represents the number of years of the system lifetime. The project cost mainly consists of the cost associated with the wind turbine system and the balance of system (BOS) equipment. In this study, the wind turbine is connected to an on-grid system. The BOS equipment consists of the electrical controller, turbine generator, inverter, and wind data instrumentation.

The present LCOE analysis considered a small VAWT designed and manufactured by QingDao Bofend Wind Power Generator Co. with a rated power of 2.2 kW. The cost associated with the wind turbine system and balance of the system equipment were estimated based on two quotes for 1 kW and 3 kW turbines from the wind turbine manufacturer. The costs are provided in Table 4.2. The total project cost of the system is $4979, of which the BOS equipment makes up about 45%. The system has an expected lifetime of 20 years. The residual value of the system at the end of its lifetime is estimated to be 10% of its original value. The system degradation

Table 4.2: System project costs

Component	Cost
Wind Turbine & Generator	$2740
Electrical Controller	$615
Electrical Inverter	$1174
Wind Data Instrumentation	$450
Residual Value	10% of Original Value
System Lifetime	20 years
Degradation Rate	1% Efficiency/year
Discount Rate	3.1%
AO Cost	$0.01/kW·hr

rate is estimated to be 1% of its efficiency, which is equivalent to the degradation rate of large HWAT systems Staffell and Green (2014). The discount rate used in the analysis is 3.1%, which is a standard discount rate used in many projects related to renewable energy (Lavappa, 2015). It is worth mentioning that the discount rate of 3.1% used in the analysis accounts for the nominal inflation rate over the next 20 years representing the expected lifetime of the system. The operating and maintenance cost (AO) is estimated to be \$0.01/kW·hr, which is equivalent to the AO cost of large HAWT systems. In addition, the analysis also incorporates the investment tax credit (ITC) and production tax credit (PTC) that are available for wind energy. According to the latest update of the American Wind Energy Association, the investment tax credit (ITC) allows consumers to claim back 24% of the total investment while the production tax credit (PTC) allows consumers to claim back \$0.018/kWh of the energy production(A.W.E.A., 2017).

4.3 Turbine Design Configurations

The main objective of the present study is to determine whether an optimal VAWT configuration exists for wind turbine applications in an urban/suburban environment. In all cases, a straight-blade Darrieus type VAWT (also referred to as an H-rotor turbine) with three blades is utilized. The present study examines the effects of turbine solidity, airfoil section, height-to-diameter aspect ratio, and moment of inertia on the overall performance of the wind turbine when it is subjected to actual gusty wind conditions. Only blades comprised of low-digit, symmetric NACA 00XX airfoil sections are considered in the present study. The last two digits of the airfoil section represent the ratio of airfoil maximum thickness to chord length, e.g., the maximum thickness of the NACA 0015 airfoil is 15% of the chord length.

A total of thirteen turbine design configurations are investigated, as listed in Table 4.3, where S, c, H, D, and I denote the solidity, chord length, turbine height, turbine diameter, and moment of inertia of the turbine about the axis of rotation, respectively. Design #1 serves as the baseline case. It is worth mentioning that all designs share the same frontal area ($A_t = HD$) of 4.8 m^2. To explicitly study the influence of each design parameter on VAWT performance, only one design parameter was typically varied

Table 4.3: Turbine design configurations examined in the present study.

Design #	Airfoil	S [%]	c [cm]	H [m]	D [m]	H/D	I [kg·m^2]
1	0015	18	12.0	2.40	2.00	1.20	31.02
2	0015	18	11.4	2.54	1.89	1.34	27.25
3	0015	18	13.1	2.19	2.19	1.00	35.90
4	0015	18	14.3	2.00	2.40	0.83	44.77
5	0015	19	12.0	2.54	1.89	1.34	29.15
6	0015	16	12.0	2.19	2.19	1.00	31.89
7	0015	15	12.0	2.00	2.40	0.83	35.70
8	0018	18	12.0	2.40	2.00	1.20	34.80
9	0012	18	12.0	2.40	2.00	1.20	27.21
10	0015	12	8.00	2.40	2.00	1.20	18.07
11	0015	15	10.0	2.40	2.00	1.20	25.23
12	0015	21	14.0	2.40	2.00	1.20	37.86
13	0015	25	16.7	2.40	2.00	1.20	51.43

relative to the baseline case in each configuration. Imposed constraints, however, prevent this approach in some instances. For example, varying the aspect ratio H/D while keeping S constant sets limits on the values of H and D, and also constrains the chord length c, as can be seen in designs #2–4, where both c and H/D must be varied in order to maintain a constant solidity of 18%.

With the ideal tip-speed-ratio controller, inertial effects play an important role in the wind turbine response behavior. In order to obtain a realistic value for the moment of inertia I of each turbine design configuration, a Computer-Aided Design (CAD) model of each VAWT was created using Solidworks 3D 2016. Figure 4.3 illustrates the CAD model for design #13. The turbine blades are assumed to be made of carbon fiber, whereas the turbine shaft and blade supports are assumed to be made of Aluminum 2024. The same materials were used in all of the design configurations. Note, since the bulk of the mass is concentrated in the blades, design configurations with smaller diameters necessarily exhibit lower values for I. In addition, designs with a lower chord length have less total mass in the blades, and hence a smaller value of I. Similarly, the designs with lower NACA airfoil sections (e.g., 0012 compared to 0015) have a lower percentage of thickness to chord length ratio, which translates into less total mass in the blades and lower I values as well.

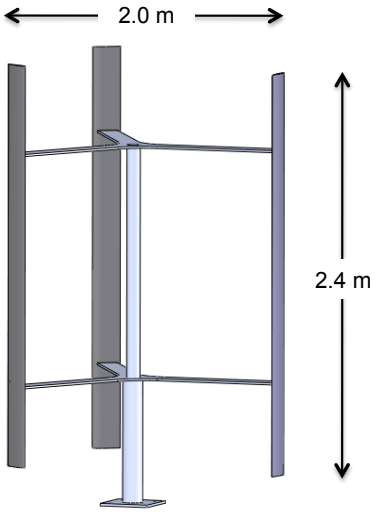

Figure 4.3: CAD model of VAWT design configuration #13.

All of the wind turbine configurations examined in this study are assumed to have similar wind power curves as illustrated in Figure 4.4. In particular, each turbine model is assumed to have a cut-in speed of 3 m/s and a cut-out speed of 24 m/s. In addition, every turbine is assumed to have an identical rated wind speed of 12 m/s and rated power of 2.2 kW. As shown in Figure 4.4, for wind speeds greater than the cut-in speed, the turbine power rises monotonically until the rated speed is

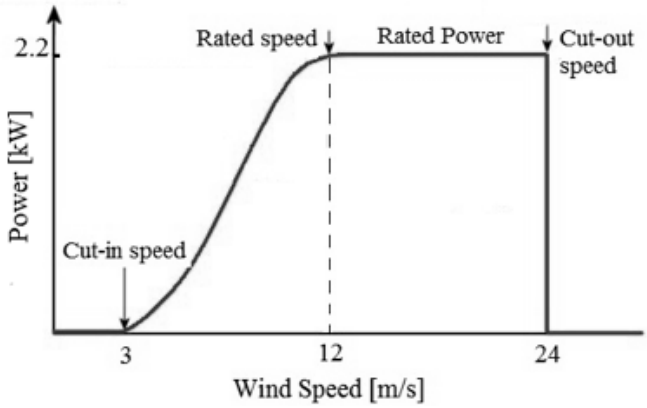

Figure 4.4: Illustration of the wind turbine power curve highlighting the important characteristics used for all of the design configurations.

reached. In this range, the active controller instantaneously adjusts the rotor speed according to the incoming wind so that the turbine operates at its optimal TSR setting. For wind speeds beyond the rated speed, the turbine power is limited by the capacity of the electric generator. In this regime, the controller actively maintains the turbine at its rated power setting. At wind speeds above the cut-out speed, the turbine is shut off to prevent the rotor and blades from damage due to the applied load on the turbine. In practice, a braking system is employed to bring the rotor to standstill. It is worth mentioning that due to variations in design parameters, the turbine configurations will necessarily exhibit differences in terms of structural integrity, which may slightly impact how the turbines perform when operated under the wind power curve illustrated in Figure 4.4. However, for the purpose of this study, which is to determine an optimal wind turbine design configuration based on its power performance, all turbine configurations are assumed to behave the same structurally.

4.4 Results

4.4.1 Wind Turbine Performance

4.4.1.1 Power Coefficient Versus Tip Speed Ratio Curves

A common method to characterize wind turbine performance is via the power coefficient versus tip speed ratio curve (C_p–TSR curve). Wind turbine design parameters (e.g., airfoil shape, solidity, height to diameter aspect ratio, etc.) affect the shape and magnitude of the C_p–TSR curve in different ways. Figure 4.5 shows the C_p–TSR curves for the thirteen wind turbine configurations investigated in the present study (refer to Table 4.3). These curves were generated using the Turbine Power Performance Model described in Section 4.2.1 with a constant incoming wind speed of 7 m/s. Note, because the C_p–TSR curves are generated using a constant wind speed, the results in Figure 4.5 are not influenced by the moment of inertia of the turbine.

Figure 4.5a shows the effect of height-to-diameter aspect ratio (H/D) at a constant turbine solidity (S=18%), corresponding to turbine designs #1–4. Note, in order to achieve a constant solidity, the chord length had to be adjusted as indicated in the

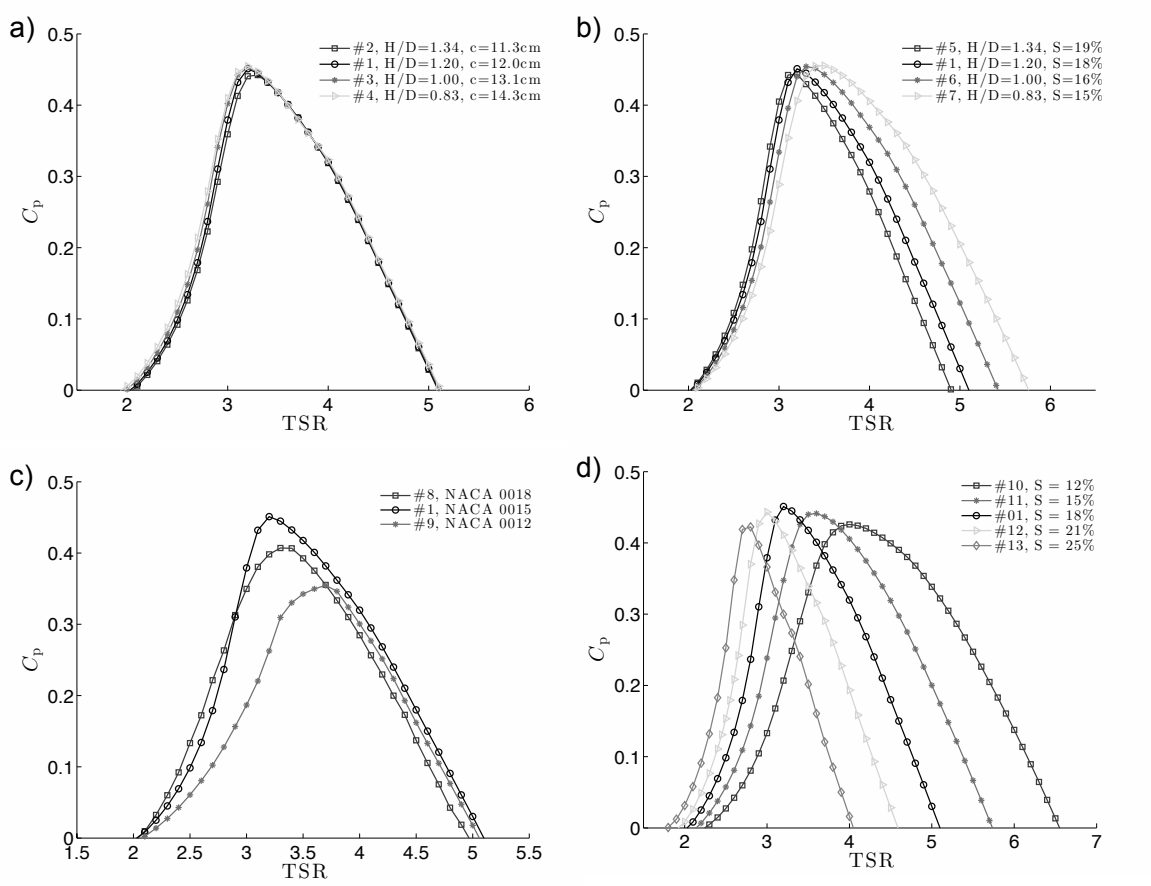

Figure 4.5: Power coefficient curve versus tip speed ratio for all thirteen turbine designs. In all subplots, the baseline design configuration #1 is given by the black line. (a) constant solidity ($S = 18\%$) and airfoil shape (NACA 0015), with varying aspect ratio and chord length; (b) constant chord length ($c = 12$ cm) and airfoil shape (NACA 0015), with varying aspect ratio and solidity; (c) constant aspect ratio ($H/D = 1.2$), chord length ($c = 12$ cm), and solidity ($S = 18\%$), with varying airfoil shape; (d) constant aspect ratio ($H/D = 1.2$), chord length ($c = 12$ cm), and airfoil shape (NACA 0015), with varying solidity. The power coefficient curves shown are all simulated at a wind speed of 7 m/s.

legend. As illustrated, the C_p–TSR curves of these four configurations are almost identical, especially in the high TSR regime (TSR values greater than the peak C_p). Turbine solidity represents the amount of flow blockage due to the presence of the turbine, and as such directly correlates with the momentum deficit in the wake of the wind turbine. Since all four turbine configurations have the same solidity, it is expected that the momentum deficit will be nearly identical, thus resulting in similar C_p–TSR curves. A noticeable difference, however, does exist at low TSR. The results indicate that turbines with lower aspect ratios produce slightly larger C_p values, compared to those with higher aspect ratios at the same TSR. These results are consistent with the observations of Brusca et al. (2014). The reason for this behavior may be attributed to Reynolds number (Re) effects at low TSR. Lowering the aspect ratio requires an increase in chord length of the turbine blade in order to maintain the same solidity. The slight increase in the turbine chord length raises the operating Reynolds number of the turbine blade, thus allowing the turbine blade to generate higher lift forces, translating into higher power or C_p for a given incoming wind speed.

Figure 4.5b illustrates the C_p–TSR curves for turbine designs #5–7 that have different aspect ratios, but the same turbine chord length (c = 12 cm). Note, the turbine solidity must be varied accordingly in order to maintain a constant chord length for each H/D setting. As apparent in the figure, the peak C_p value increases slightly with decreasing aspect ratio and shifts to higher TSR. The difference in peak C_p between the four configurations is only 2.7%. A similar result was shown by Templin (1974), who found an approximate 2.0% difference in peak C_p values when comparing eggbeater-type Darrieus turbines with aspect ratios of 1.0, 1.5, and 2.0. Another important feature observed from the figure pertains to the shape of the C_p–TSR curves. Decreasing the turbine aspect ratio causes the C_p–TSR curve to broaden and shift toward higher TSR values. For example, the maximum TSR value for the case of H/D = 0.83 is 5.7, compared to 4.9 for the case of H/D = 1.34. This result can be attributed mainly to solidity effects. At a lower aspect ratio, the solidity is smaller, meaning the turbine creates less flow blockage, thus producing less momentum deficit in the wake of the wind turbine. As a result, the C_p–TSR curve is

broader and wider. For the four cases examined in Figure 4.5b, the C_p–TSR curves nearly overlie at the low TSR regime.

Figure 4.5c shows the influence of airfoil shape on the power coefficient curves. Three different airfoil shapes are examined: NACA 0012, NACA 0015, and NACA 0018, representing the three turbine designs #9, 1, and 8, respectively. All other design parameters are the same. The results suggest that airfoil shape has a significant impact on the power coefficient curve of the wind turbine. The three configurations have nearly the same operating TSR range. The turbine with the NACA 0015 airfoil shape, however, outperforms the others, since it exhibits a much higher peak C_p value of 0.45, compared to 0.41 for NACA 0018 and 0.35 for NACA 0012. Note, the NACA number here indicates the maximum airfoil thickness to chord length ratio. The results suggest that an optimum thickness to chord length ratio exists for the case of the symmetric airfoil blades; and that this optimum ratio is around 15%. The results are in a good agreement with the study performed by Paraschivoiu et al. (1983) that also examined the same three airfoil shapes as in this study. A significant difference in C_p values in the low TSR regime is observed, with the NACA 0015 and 0018 configurations exhibiting similar slopes, but the NACA 0012 configuration displaying much lower C_p values at the same TSR. In the low TSR regime, one may conclude that thicker airfoil blades appear to yield higher C_p values compared to thinner airfoils. This agrees with the studies performed by Paraschivoiu et al. (1983) and Roh and Kang (2013).

Figure 4.5d illustrates the effect of turbine solidity on the power coefficient curves for five turbine designs #1, 10, 11, 12, and 13. The range of solidity examined here is 12% (design #10), 15% (design #11), 18% (design #1), 21% (design #12), and 25% (design #13). As shown in the figure, the peak C_p varies slightly between the different cases with a solidity of 18% exhibiting the highest peak C_p of 0.45. The difference in peak C_p values between the five configurations is approximately 6.5%. Another important feature observed is the shape of the C_p–TSR curves. Decreasing the turbine solidity causes the curve to widen, thereby expanding the TSR operating range, and also shifting the entire curve to the right (higher TSR values). For example, in the case of S = 12%, the operating range of the turbine is $2.3 \leq TSR \leq 6.5$, while for

$S = 25\%$, the operating range is $1.8 \leq TSR \leq 4.1$. Similar trends were observed in the studies performed by (Strickland, 1975) and Templin (1974). The result is expected, as discussed earlier, due to flow blockage effects associated with increasing the solidity.

Under steady wind conditions, one would select the optimum turbine design solely based on whichever C_p–TSR curve displayed the highest peak power coefficient (C_P). According to the results from Figure 4.5, turbine #7 (NACA 0015, $S = 15\%$, $H/D = 0.83$) satisfies this criterion. The main question of the present study is whether this same turbine design yields the best performance during unsteady wind conditions. In fact, it will be shown that turbine #7 performs the worst of all thirteen design configurations in terms of total energy captured, when the turbine is implemented in an environment with realistic gusty winds.

4.4.1.2 Total Amount of Energy Captured

Figure 4.6a shows a box plot of the energy ratio (E/E_a) for each of the thirteen turbine design configurations listed in Table 4.3 using actual wind speed data collected in 2009 from the nines sites in Oklahoma City listed in Table 4.1. Here, E represents the actual amount of energy captured by the wind turbine over the entire year of 2009, using the numerical method as described in Section 4.2.2 while E_a represents the maximum amount of energy available from the wind,

$$E_a = \tfrac{1}{2}\,\rho\,A_t \int_0^T U^3 dt\,. \tag{4.4}$$

In the above equation, ρ denotes the air density, $A_t\,(= H{\cdot}D)$ represents the turbine frontal area, and U is the time-varying wind speed as measured by the sonic anemometer. Note, in all calculations, $T = 525,600$ min., i.e., the number of minutes in the year 2009, and $A_t = 4.8$ m^2. Figure 4.6b shows a box plot of the same design configurations except with identical moment of inertia values set equal to $I = 31.0$ kg·m^2 (corresponding to that of the baseline design configuration #1). Each box in Figure 4.6 represents the variation of E/E_a over the nine different sites examined in Oklahoma City. The horizontal line in each box represents the median value between the sites; while the lower and upper lines on each box represent the 25% quartile and 75% quartile of the data, respectively. The two extended vertical error bars from each box represent the minimum and maximum values in each data set. In Figure 4.6a,

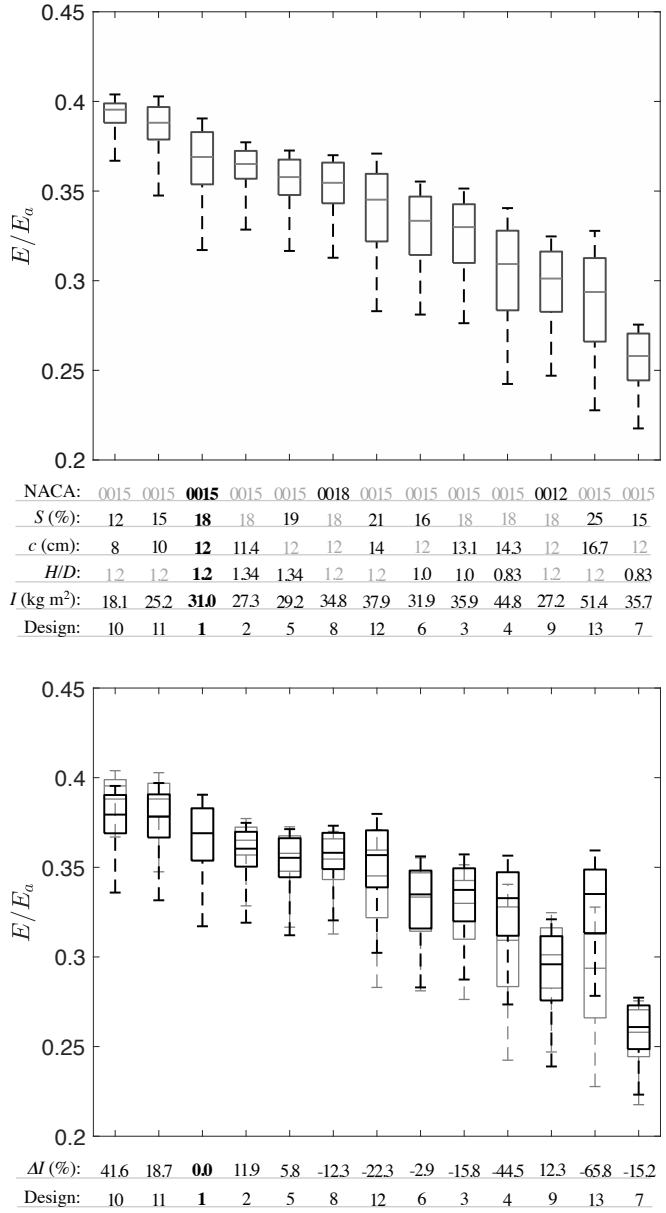

Figure 4.6: Box plot of the energy ratio for the thirteen different turbine designs examined in the study. (a) realistic moment of inertia used for each design (b) black boxes: moment of inertia set to the same value of I = 31.0 kg·m^2 for each design; gray boxes: same data as the black boxes in plot (a). Each box represents statistics calculated over the nine sites in Oklahoma City. The labels on the horizontal axis provide details regarding the design parameters for each configuration. The bold black text denotes the reference (baseline) configuration (Design #1). For the other design configurations, the black text highlights the design parameters that were varied with respect to the baseline case, whereas the grey text represents the parameters that remained the same with respect to the baseline case. In plot (b), ΔI represents the percent change in moment of inertia relative to the baseline design.

the results are plotted so that the median values of E/E_a decrease monotonically. To facilitate interpretation of the results, the turbine design configuration corresponding to each box is given on the x-axis in terms of its NACA airfoil, solidity, chord length, aspect ratio, moment of inertia, and design number following Table 4.3. One immediate conclusion from Figure 4.6b is that moment of inertia cannot be used to explain the discrepancy in performance amongst the various design configurations. In fact, except for two configurations (#3 and #13), the rank ordering of the turbines with respect to the energy ratio remains unchanged when moment of inertia is eliminated as a design parameter.

The top two performing turbine design configurations #10 and 11 have median values for the energy ratio of 0.395 and 0.388, respectively. Both designs share the same blade shape (NACA 0015) and aspect ratio (H/D = 1.2), but have different solidity. The top performing turbine design (#10) has the lowest solidity (S = 12%) of all of the configurations examined in the present study. Physically, this corresponds to a turbine with shorter, thinner blades, and hence a lower moment of inertia, which is desirable for responding quickly to fluctuating winds. The broad shape of the C_P–TSR curve for design #10 is also advantageous during unsteady wind conditions. During a gust event, for example, the actual rotational speed ω of the turbine lags behind its ideal value (due to turbine inertia and controller gain) and thus temporarily operates off the peak C_p value. In the case of a broadly shaped power coefficient curve, though, the actual operating C_p of the turbine at any given time does not stray too far from its peak value, allowing the turbine to operate more efficiently and capture more energy during the gusts. It is also not surprising that the top performing configurations utilize blades based on the NACA 0015 airfoil, since the peak C_p value for this case (Figure 4.5c) is significantly higher than either those using the NACA 0012 or 0018 airfoil blades.

Figure 4.6a also reveals some interesting behavior regarding the effect of aspect ratio on the amount of energy captured by the turbine. Two sets of design configurations were generated to examine H/D effects. In the first set (designs #1, 2, 3, 4), the solidity remains the same while the chord length is varied; in the second set (designs #1, 5, 6, 7), the opposite is true. In both sets, the aspect ratio ranges

between H/D = 0.83 to 1.34. The first set of designs is described in this paragraph, and the second set in the following paragraph. With designs #1, 2, 3, 4, the solidity and blade shape remain constant at S = 18% and NACA 0015, respectively. The corresponding C_p–TSR curves (shown in Figure 4.5a) are nearly identical; however, the energy captured by these different turbines are quite disparate. For example, designs #1 (H/D = 1.2) and #2 (H/D = 1.34) are able to capture comparable amounts of energy with a E/E_a ratio of about 0.37, ranking them the third and fourth highest performing turbines, whereas designs #3 (H/D = 1.0) and #4 (H/D = 0.83) have much smaller energy ratios. This might suggest that turbines with $H/D > 1$ are more efficient at capturing energy from gusty winds. However, one must also consider the moment of inertia of the turbine. Designs #3 and #4 have relatively high moments of inertia (23% and 53% higher, respectively, than the average moment of inertia between designs #1 and #2). This means that they are not able to respond as quickly to wind fluctuations, and thus are not expected to be as efficient in gusty wind conditions despite having similar C_p–TSR curves. Note, the differences in moment of inertia arise from two factors. First of all, the frontal area of the turbines is constrained to be the same, which necessarily dictates the D and H values of the turbine for a given aspect ratio. Turbines with larger diameters will clearly have a larger moment of inertia. Secondly, for the particular case of designs #1–4, the solidity is also constrained to be the same, which means that the chord length must vary according to the aspect ratio. Increasing the chord length results in a larger moment of inertia as well.

The second set of configurations used to examine the effect of aspect ratio on energy captured by the turbine (E/E_a) is given by designs #1, 5, 6, 7. In these four designs (see Table 4.3), the aspect ratio varies from H/D = 0.83 to 1.34, whereas the chord length remains the same (c = 12 cm). This necessarily means the solidity changes slightly between the four designs, as well as the moment of inertia. The energy ratio is highest for design #1 (E/E_a = 0.369, H/D = 1.2), followed by design #5 (E/E_a = 0.358, H/D = 1.34), #6 (E/E_a = 0.333, H/D = 1.0), and #7 (E/E_a = 0.258, H/D = 0.83). Note, design #7 displayed the lowest energy ratio of all the thirteen configurations examined in the present study, and coincidentally had a relatively

high moment of inertia (16% higher than the average between designs #1, 5, and 6). These results would be somewhat unexpected based solely on the behavior of the corresponding C_p–TSR curves for these four designs, as shown in Figure 4.5b. Design #7 displays the broadest C_p–TSR curve, while design #5 exhibits the narrowest. It was argued earlier that a broad C_p–TSR curve allows the wind turbine to operate more closely to its optimal TSR setting, and thus capture more energy from the fluctuating wind. This advantage, however, is negated by the slow response time of design #7 due to its higher moment of inertia, and hence inability to closely track variations in the fluctuating wind speed. On the other hand, design #5 exhibits a narrower C_p–TSR curve, but its lower moment of inertia permits more energy to be captured during wind gusts. Because of this complicated interplay involving moment of inertia, results from Figure 4.6a for designs #1, 5, 6, and 7 are inconclusive in terms of the effect of aspect ratio on energy captured.

In order to unravel the effects of moment of inertia on energy captured, the simulations used to generate Figure 4.6a were repeated using the same moment of inertia for each design configuration ($I = 31.02$ kg·m^2, i.e., the value representative of baseline design #1). The results are presented in Figure 4.6b showing the energy ratio assuming the same I in each design (black boxes) overlaid on top of the previous results from Figure 4.6a (grey boxes) using the realistic I values. The ordering of the design configurations along the x-axis is the same in plot (b) as that of plot (a). Also displayed along the x-axis of plot (b) is the percent relative change in moment of inertia (ΔI) from its original value to the set value of $I = 31.02$ kg·m^2. For example, the change in moment of inertia associated with design #10 (having an original moment of inertia of 18.1 kg·m^2) is given by $\Delta I = (31.02 - 18.07)/31.02 * 100 = -41.6\%$. The results in Figure 4.6b indicate a clear effect of turbine aspect ratio (H/D) on energy captured (E/E_a). The designs having an aspect ratio greater than unity (# 1, 2, 5, 8, 10, 11, 12) outperform those with $H/D \leq 1.0$ (#3, 4, 6, 7, 9, 13). In addition, when solidity or chord length are held constant, the design with an aspect ratio of $H/D = 1.2$ (design #1) yields the highest energy ratio compared to the other designs. This would suggest that an optimum aspect ratio exists of about 1.2, irrespective of the moment of inertia of the turbine.

The effect of airfoil shape on the amount of energy captured by the wind turbine can be examined by comparing designs #1, 8, and 9 in Figure 4.6. In these three designs, the NACA airfoil type is varied while the other design parameters are held constant. Note, because the airfoil types have different thickness to chord length ratios, the moment of inertia of the three designs is not the same. Of the three, turbine design #1 has the highest energy ratio (NACA 0015, $E/E_a = 0.367$), followed by design #8 (NACA 0018, $E/E_a = 0.353$) and #9 (NACA 0012, $E/E_a = 0.295$). This result is somewhat expected based on the power coefficient curves shown in Figure 4.5c, with the NACA 0015 design displaying a significantly higher peak C_p value (10% larger than 0018 and 27% larger than 0012). Despite the fact that design #9 (NACA 0012) has the lowest moment of inertia of the three designs due to thinner blades, the magnitude of C_p measures much lower than the other power coefficient curves, rendering design #9 uncompetitive in terms of energy captured. The moment of inertia of design #8 (NACA 0018) is larger than that of design #1 (NACA 0015) by about 12% due to its thicker blades; however, the median energy ratio of design #1 is only 4% more than that of design #8. When accounting for moment of inertia effects (Figure 4.6b), the difference in E/E_a between designs #1 and 8 drops to less than 3%. This is a little surprising given the relatively large difference in peak C_p values (10%) between the two designs. It remains to be determined why design #8 performs as well as it does, despite its inferior power coefficient curve.

In order to examine the effect of turbine solidity on the amount of energy captured, turbine designs #1, 10–13 are compared. In these five designs, the aspect ratio is held constant at $H/D = 1.2$ as well as the airfoil shape (NACA 0015), whereas the solidity ranges from $S = 12\%$ to 25%. Physically, this is achieved by varying the chord length linearly proportional to S, resulting in a range of chord lengths from $c = 8$ cm to 16.7 cm, which also translates into a wide range of values for the turbine moment of inertia (18.07–51.43 kg·m^2 across the five designs). As apparent from Figure 4.6a, when isolating these five designs, the energy ratio clearly decreases with increasing solidity. Specifically, design #10 ($S = 12\%$) exhibits the highest energy ratio, measuring 55% higher than that of design #13 ($S = 25\%$) with the lowest energy ratio. The same trend is observed in Figure 4.6b when moment of inertia

remains constant. Therefore, one can definitively conclude that lower solidity turbine designs yield superior performance in terms of the amount of energy captured during unsteady wind conditions.

Figure 4.6 also reveals a connection between the moment of inertia of the turbine and the spread in E/E_a between the various sites. To highlight this, Figure 4.7 shows the standard deviation of the energy ratio (σ_{E/E_a}) calculated over the nine sites in Oklahoma City as a function of the moment of inertia (I) of the turbine for each design configuration. Smaller values of σ_{E/E_a} indicate less site dependence in the energy ratio. As can be seen, there is a general trend toward increasing σ_{E/E_a} with increasing I. This makes sense because turbines with higher moment of inertia will not respond as quickly to wind fluctuations, and thus will tend to not operate at their ideal TSR (peak C_p) value. This means the turbine response is more susceptible to the nature of the wind fluctuations (velocity spectra), resulting in site-specific behavior.

4.4.1.3 Effect of Blade Material

During operation, the turbine blades are the components that experience the highest applied force due to wind loading. To ensure their structural integrity, wind turbine blades are often made of materials characterized by high strength, high stiffness, and long fatigue life (Babu et al., 2006). Material selection of the blades plays an important role in wind turbine design. Technical considerations include material properties, material reliability, safety, and performance characteristics. Other factors are important as well, such as the response of the material to environmental conditions and the disposability/recyclability of the material. Finally, the economic aspects of material selection such as availability, raw material cost, and manufacturing costs will have a significant impact on the practical viability of the turbine. The present study examined four different materials that are commonly used for wind turbine blades to determine how material selection (density, specifically) affects power performance, in terms of the amount of energy that can be captured over a full year of operation during realistic wind conditions. The four materials considered are: Aluminum 2024, E glassfiber, Carbonfiber, and Aramid fiber. Aluminum is a low price metal that has good reliability but low tensile strength and stiffness. Glassfiber has good stiffness,

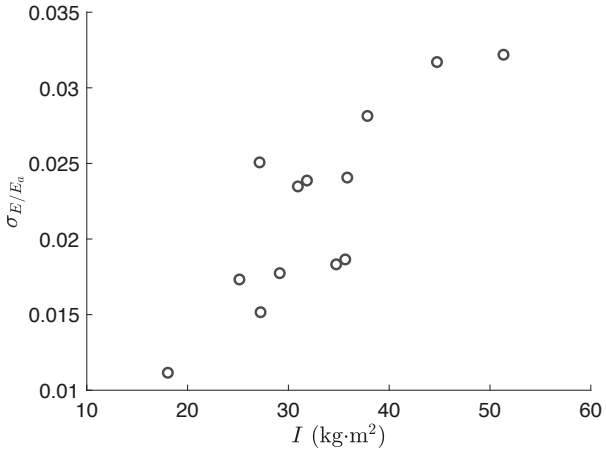

Figure 4.7: Standard deviation of the energy ratio E/E_a between the nine sites in Oklahoma City as a function of moment of inertia of the turbine design.

high strength, and moderate density, whereas Carbonfiber is commonly used because of its high stiffness, high strength, and light weight (Babu et al., 2006). Aramid fiber has good static and dynamic fatigue resistance as well as high strength and an extremely low density, all of which are favorable characteristics for wind turbine blade applications. In each case, the turbine shaft and supporting bars still utilize Aluminum 2024 as in the rest of the study.

Figure 4.8 shows the box plot of the energy ratio (E/E_a) calculated for the baseline turbine design #1 using the four different blade materials as discussed above. Each box represents statistics calculated over the nine sites in Oklahoma City using wind data spanning the entire year of 2009. The disparity in performance is attributed to differences in the mass moment of inertia of each turbine, arising from differences in the density of each blade material. The mass moment of inertia (I) of each turbine is given in parenthesis in the x-axis label of Figure 4.8. In order of highest to lowest I are Aluminum 2024 (41.91 kg·m^2), Glass fiber (40.52 kg·m^2), Carbon fiber (31.02 kg·m^2), and Aramid fiber (27.58 kg·m^2). This corresponds to a variation in I of about 40% between the four cases. As can be seen, the energy captured by the turbine decreases with increasing moment of inertia as expected. The variation in the median E/E_a

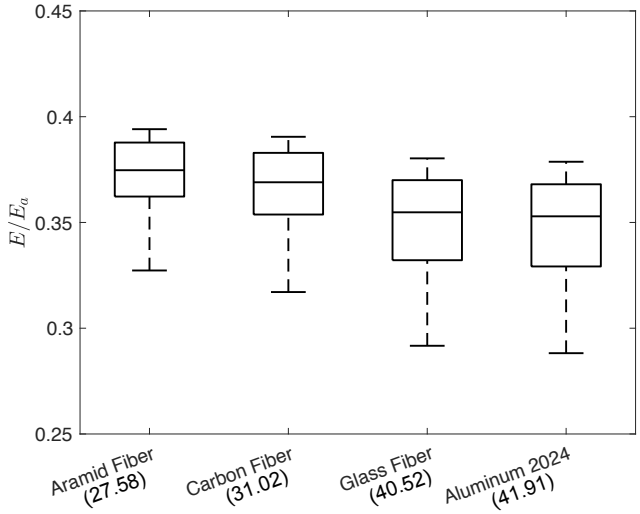

Figure 4.8: Box plot of the energy ratio for the baseline test case (turbine design #1) as a function of turbine blade material. Statistics for each box are calculated over the nine test sites in Oklahoma City. The moment of inertia of the turbine is shown in parenthesis for each material type in units of kg·m^2.

over the four cases is 6%. A greater spread in E/E_a over the nine sites is also noticeable for the two turbines with higher moments of inertia, similar to what was observed in Figure 4.6. The present study only considers the effect of blade material on power performance. A full strengths evaluation, using Finite Element Analysis (FEA), for example, should be performed to assess how the structural performance of the turbine varies with blade material. Finally, implications related to the expense of each material should also be considered before making a final design decision.

4.4.1.4 Structural Considerations

Wind turbine blades and their supports experience different types of loadings during operation, such as stochastic load, inertia load, and aerodynamic load, the latter of which plays a critical role in many wind turbine blade failures (Jureczko et al., 2005; Schubel and Crossley, 2012). Aerodynamic load is generated by the lift and drag forces acting on the turbine blades, and is dependent on the incoming wind speed, airfoil shape, rotor speed, and angle of attack. Due to the change in orientation

of the blades with respect to the incoming wind as the rotor spins, the magnitude and direction of the lift and drag forces vary significantly over the period of revolution of the turbine. The component of aerodynamic load that primarily causes turbine blade failure is the thrust (normal force). Therefore, understanding the response characteristics of the normal forces (F_N) acting on the turbine blades during realistic operating conditions is crucial for making informed design decisions.

Figure 4.9 shows the normal force acting on a single turbine blade for designs #1, 10, and 13 as a function of azimuth angle during one full period of revolution for the case of a constant 7 m/s incoming wind speed. Design #1 constitutes the baseline case, whereas designs #10 and #13 were selected for comparison, because these two configurations exhibit the lowest and highest normal forces, respectively, of all of the designs examined in the present study. As can be seen in Figure 4.9, F_N follows a nearly sinusoidal trend with an amplitude in the range 78–90 N. The maximum and minimum forces are observed at azimuth angles around 70°–90° and 270°–290°, respectively. At these azimuth angles, the turbine blades are nearly perpendicular to the incoming flow. Note, all three of the turbine designs examined in Figure 4.9 (#1, 10, 13) have the same design parameters, except for solidity (chord length). For design #10, c = 8 cm, whereas for designs #1 and 13, c = 12 cm and 16.7 cm, respectively. Since all three designs utilize the same airfoil shape (NACA 0015), the blades share identical characteristics for the lift and drag coefficients. The dimensional lift and drag forces, therefore, are expected to be linearly proportional to the chord length. The normal forces in Figure 4.9 were then normalized by the turbine blade chord length and turbine blade weight, respectively. The normalized F_N forces in Figure 4.9 did not collapse into a single curve, suggesting that the observed differences in F_N between the three designs cannot entirely be attributed to the blade chord length.

Design #13 experiences the highest F_N (89.5 N); however, this design may also be the strongest structurally due to its larger blades. The increased weight, though, unfavorably affects power performance, as design #13 displayed the second lowest energy ratio of all of the designs examined in the present study. The opposite can be said about design #10. In fact, there likely exists a trade-off between power performance and structural performance in VAWT design. The study of Paraschivoiu

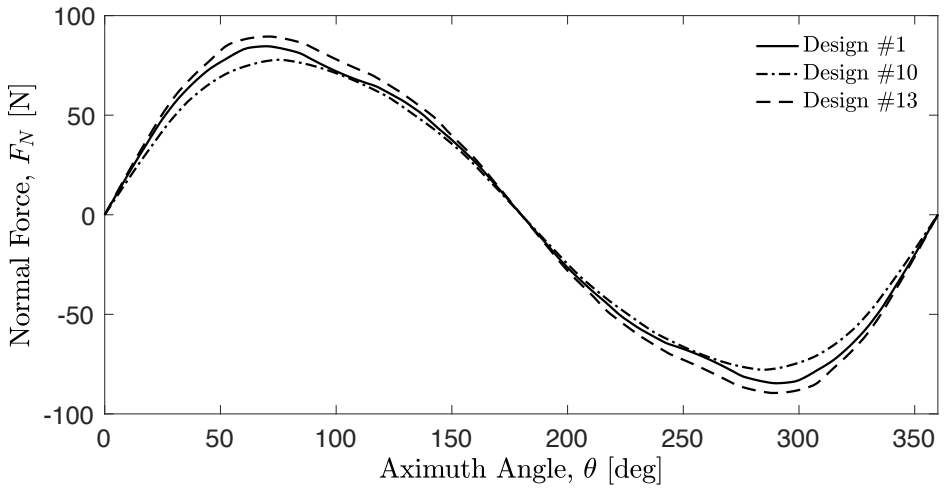

Figure 4.9: Normal force acting on a single turbine blade as a function of azimuth angle during one period of revolution for the case of a constant incoming wind speed of 7 m/s.

et al. (1983) recommends the symmetrical NACA 0015 for small-scale wind turbines, due to its favorable stall characteristic, and, the NACA 0018 for large wind turbines, to enhance the structural performance. A detailed FEA analysis should be considered for future work in order to assess the structural viability of the designs considered in the present study.

Figure 4.10a shows the probability density function (PDF) of the wind speed at site KSW 101 in Oklahoma City in 2009. Also indicated are the cut-in and rated speeds. The median value of 4.7 m/s remains close to the annual average of about 5 m/s. The solid black line in Figure 4.10a represents the best-fit gamma distribution to the data. Figure 4.10b shows the corresponding PDF of the amplitude of the normal force ($\overline{F}_N$) acting on a single turbine blade for the baseline design case #1 during the full year of operation at site KSW 101 in 2009. The amplitude is determined as the peak normal force obtained over each revolution of the turbine. The minimum and maximum $\overline{F}_N$ over the year is 15.8 N and 503.9 N, respectively. The annual average amplitude is 69.6 N; and, the median is 51 N. The solid black line in Figure 4.10b represents the best-fit lognormal distribution to the data. Note, a gamma distribution did not fit the PDF of $\overline{F}_N$ as well as a lognormal distribution. Since the stochastic processes governing the normal force acting on the turbine blades and the incoming

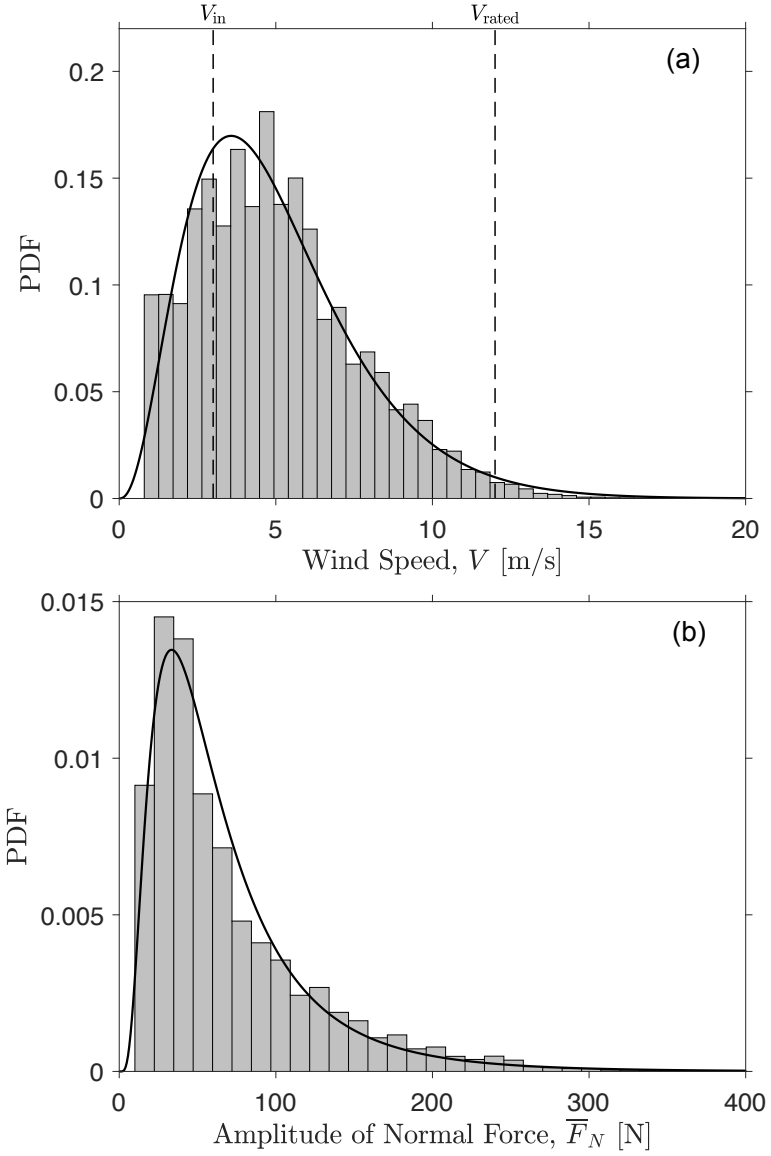

Figure 4.10: Probability density functions at site KSW 101 in Oklahoma City based on data acquired over the full year of 2009: (a) wind speed and (b) amplitude of the normal force acting on a single turbine blade for design #1. Also indicated are the cut-in and rated wind speeds, V_{in} and V_{rated}, respectively. The black solid line in (a) denotes the best-fit gamma distribution to the wind data; whereas the solid black line in (b) represents the best-fit lognormal distribution to the force data.

wind speed appear to be different, it is not clear that one could predict the expected load on the turbine blades using a simple relationship based on the PDF of the wind speed.

4.4.2 Economic Analysis

The performance of the thirteen turbine designs are studied from an economic perspective by evaluating the levelized cost of energy (LCOE) using the method outlined in Section 4.4.2. The economic analysis utilizes the full year of wind speed data from 2009 at site KSW 101 to determine which turbine design configurations offer a viable economic solution for harvesting wind in the urban/suburban area surrounding Oklahoma City. Figure 4.11 shows the LCOE (in \$/kWh) calculated for each design. The designs are arranged using the same ordering as in Figure 4.6. One can observe a direct correlation between the energy ratio results presented in Section 4.4.1.2 and LCOE, whereby more energy produced translates into lower overall LCOE price as expected. Note, the analysis assumes the same project cost for each design. This may not be entirely accurate since some design configurations consist of larger blades, which may augment the material costs slightly compared to designs with smaller blades. Therefore, the observed differences in LCOE between the various designs can be attributed to the disparity in energy production (E/E_a). The two horizontal dashed lines in Figure 4.11 represent the current electricity price (as of August 2016) and the predicted national electricity price in the next 20 years. These values are taken as \$0.1290/kWh and \$0.1597/kWh, respectively, following Nguyen and Metzger (2017). The results indicate that seven of the designs (#1, 2, 5, 8, 10, 11, 12) exhibit LCOE values at or below the current electricity price, making them economically viable solutions. The most effective design (#10) has an LCOE equal to 0.116 \$/kWh, which means that electricity produced by this turbine is 10% cheaper than that currently generated from fossil-fuel-based power plants. The remaining designs, except for design # 7, may become economically viable in the future as the price of electricity increases.

The error bars on each data point in Figure 4.11 represent the uncertainty in LCOE due to ±10% variation in the annual energy production at site KSW 101 in

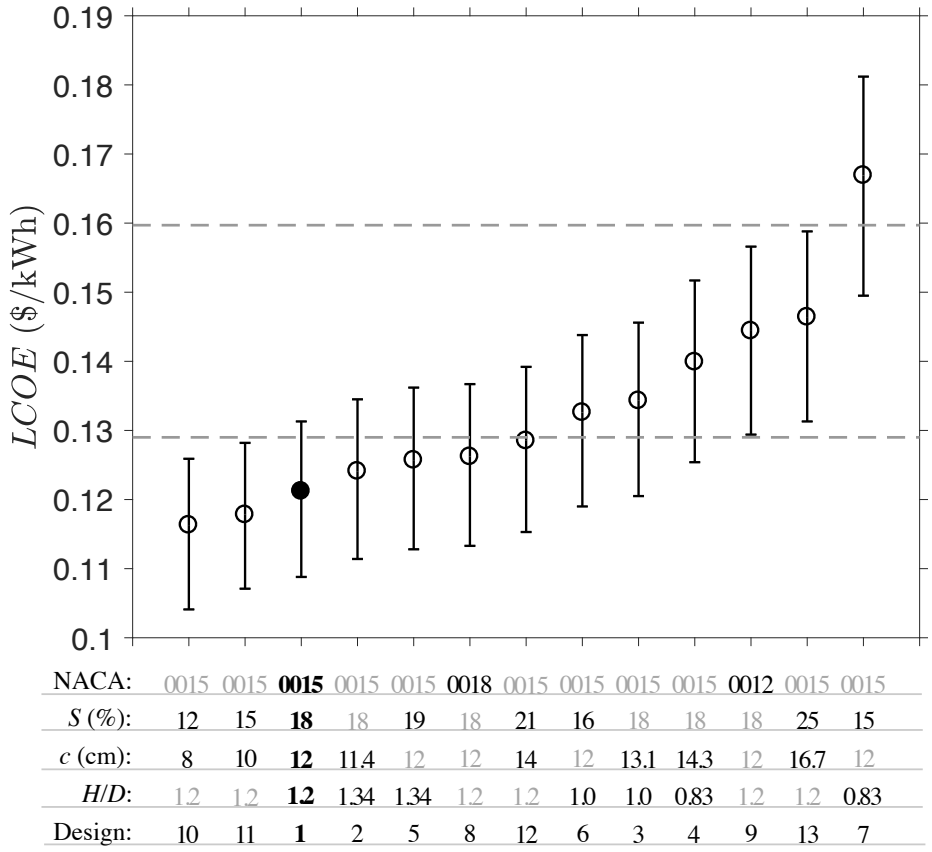

Figure 4.11: Comparison of the LCOE price for the thirteen turbine designs implemented at site KSW 101 in Oklahoma City based on their projected operation during the year of 2009. The lower horizontal dashed line represents the national electricity unit price as of August 2016, whereas the higher horizontal dashed line represents the predicted average national electricity price in 2036. The designs are plotted left to right in the same order as in Figure 4.6.

Oklahoma City. Sonic anemometry data do not exist to compare projected wind energy production over multiple consecutive years, so the value of ±10% used here should be considered arbitrary and only for illustrative purposes. Slightly longer bars are noticeable in turbine designs exhibiting higher LCOE values, which suggests that the LCOE is more sensitive to uncertainties in energy production in cases with higher LCOE prices.

Note, the results shown in Figure 4.11 are only valid at test site KSW 101. Nguyen and Metzger (2017) showed that the LCOE can vary considerably at different sites depending on the local annual average wind speed. Figure 4.12 presents the LCOE for each of the nine sites in Oklahoma City using turbine design #1 plotted versus the annual average wind speed at each site. The horizontal dashed lines again represent the current electricity price and the predicted electricity price for year 2036. The error bars represent the uncertainty in LCOE due to ±10% variation in the annual energy production at each site. The present data in black are compared against the data from Nguyen and Metzger (2017) in grey calculated for the same turbine design configuration but implemented using a constant-ω controller with daily adjustment of turbine rotational speed set according to the modified persistence forecasting method. As apparent, continuous adjustment of the turbine rotation speed by active control via the ideal-TSR controller outperforms the constant-ω controller in every case, producing lower LCOE prices. The LCOE values at sites KSW 101, KSW 108, KSW 111, and KNW 104 are lower than the average electricity price predicted between years 2016–2036, which suggests that a wind turbine based on design configuration #1 installed at these locations would produce electricity at a cost competitive with that charged by public utilities. These sites exhibit annual average wind speeds greater than 4.3 m/s, and are all located in suburban areas on the western side of the metropolis. Because the present wind data were acquired at relatively low heights (9 m, corresponding to the height of typical traffic signals), further work is necessary to determine whether installation of the turbines at higher elevations, such as on building or home rooftops, would yield more economically viable results at sites within the urban area.

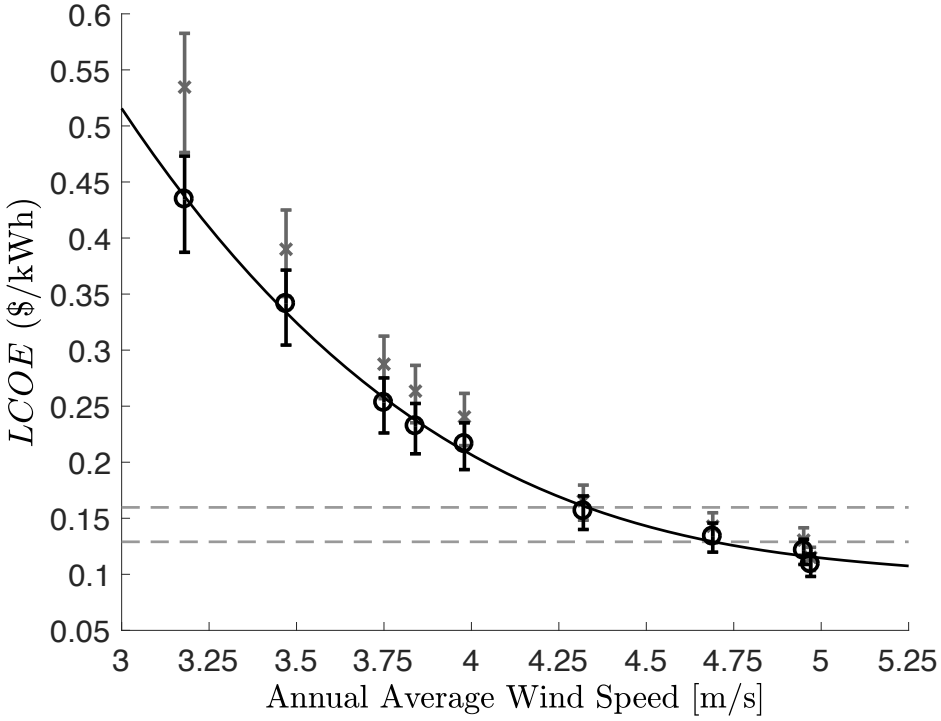

Figure 4.12: Comparison of the LCOE price for design #1 implemented at different sites in Oklahoma City based on the projected operation during the year 2009. Error bars represent the uncertainty in LCOE due to ±10% variation in the annual energy production. Gray crosses: results from our preceding paper (Nguyen and Metzger, 2017), based on using a constant-ω controller with daily adjustment of rotational speed set according to the modified persistence forecasting method. Black circles: present results based on continuous active adjustment of the rotational speed using the ideal-TSR controller. Black line: cubic polynomial fit to the current data. Gray dashed lines: current average national electricity price (lower horizontal line) and projected average national electricity price for 2036 (upper horizontal line).

By inspecting Figure 4.12, one can determine the cost reduction necessary to achieve an economically viable design at test sites where the annual average wind speed remains below the critical value of about 4.3 m/s. For example, test site KNE 104 has an annual average wind speed of 3.75 m/s compared to 4.32 m/s at KSW 111. Because of this, the LCOE value at site KNE 104 is nearly double that at site KSW 111. However, only a 13% increase in the annual average wind speed at site KNE 104 is necessary in order to reduce the LCOE to a value equivalent to that of KSW 111. This clearly has ramifications for wind turbine siting in urban/suburban areas. The LCOE may also be reduced by decreasing project costs. For test sites such as KNE 104 and KCB 110 where the annual average wind speed measures about 3.75 m/s, the project cost of the deployed system would have to decrease by about 40% of the current project cost in order for the technology to be economically viable. This provides an impetus for finding ways to diminish manufacturing expenses. It is also worth mentioning that the present economic analysis utilized the baseline design (#1), whereas Figures 4.6 and 4.11 both demonstrate that designs # 10 and 11 exhibit superior performance. If design configuration #10 were installed at site KSW 102, for example, instead of design #1, then the LCOE would drop 5.63% from 0.213 $/kWh to 0.201 $/kWh. An additional reduction in the LCOE may also be realized with design #10 due to the smaller blades; however, this remains to be verified.

The results in Figure 4.12 suggest a cubic relationship between LCOE and annual average wind speed. This is expected since the LCOE depends strongly on the annual energy production. Energy production, in turn, is equal to the energy ratio (E/E_a) multiplied by the available energy, which is proportional to the cube of the velocity, as noted in (4.4). The difference in LCOE prices between the two types of controllers noticeably increases with increasing LCOE (or decreasing annual average wind speed). The sensitivity of LCOE at low wind speeds may be related to the fact that, at low wind speeds, the turbine blades spend more time (larger percentage of the rotational cycle) at unfavorable angles of attack beyond stall. Thereby, any lag in response, leading to operation off of the ideal TSR (peak C_p) value, is expected to have a more pronounced effect on performance in the low wind speed regime.

4.5 Conclusion

The present study investigates whether an optimal Vertical Axis Wind Turbine (VAWT) design exists for application in gusty wind conditions characteristic of an urban/suburban area. The new aspect of this work is the use of actual time-resolved wind speed data as input to drive a numerical simulation that calculates the total amount of energy captured by the turbine over a full year of operation. Nine different sites, in both urban and suburban neighborhoods, spanning an approximate 500 km^2 region surrounding Oklahoma City were interrogated. At each site, wind data from the year 2009 were obtained from 3D sonic anemometers mounted on the top of traffic light posts at a height of about 9 m above the ground. An ideal control strategy was utilized that provides active control of the turbine rotational speed, allowing the turbine to continuously adjust to fluctuations in wind speed. A total of thirteen wind turbine design configurations were examined, all of them being straight-blade Darrieus type with three blades. The baseline design consisted of the following features: height H = 2.4 m, diameter D = 2.0 m, solidity S = 18%, blade shape comprised of the NACA 0015 airfoil, and chord length c = 12 cm. Each of the remaining twelve turbine design configurations were obtained by varying one or more design parameters relative to the baseline case. The following parameter ranges were investigated: three airfoil blade shapes (NACA 0012, 0015, 0018), four aspect ratios ($0.83 \leq H/D \leq 1.34$), five solidities ($12 \leq S \leq 25\%$), and eight different chord lengths ($8 \leq c \leq 16.7$). In each design configuration, the turbine moment of inertia used in the simulation was a realistic value based on a computer-aided-design drawing of the turbine with appropriate material properties for the various components. The main performance measure used to identify the optimum design configuration was the percent of energy captured by the turbine over the course of the year relative to the available energy in the gusty wind during the same time period.

In the case of steady incoming winds, turbine performance is typically characterized via the power coefficient (C_p) versus tip speed ratio (TSR) curve. Based on a comparison of the C_p–TSR curves at a fixed incoming wind speed of 7 m/s, the turbine with an aspect ratio of H/D = 0.83 exhibited the maximum peak C_p value of all the thirteen design configurations examined. In addition, for a fixed aspect ratio

and solidity, the turbine with the NACA 0015 airfoil blades produced a higher peak C_p value than those using the NACA 0012 or 0018 airfoils. Finally, for a fixed aspect ratio and blade shape, the turbine with a solidity of S = 18% displayed the highest peak C_p value compared to the other solidities. Further observations include the fact that solidity had the greatest effect on the TSR operating range of the turbine, and the turbine with the lowest solidity (S = 12%) exhibited the broadest C_p–TSR curve with the largest TSR range. Results from the C_p–TSR curves were found to be somewhat misleading, however, in determining an optimum turbine design for operation during unsteady winds. When subjecting each of the thirteen design configurations to the actual wind data from the nine test sites, it was discovered that the optimal turbine design was the one with the following features: H/D = 1.2, NACA 0015 airfoil blades, S = 12%, and c = 8 cm. This design configuration was able to extract the most energy at each site, and therefore is considered to be a site-independent optimal design solution. Note, this optimal design had the lowest moment of inertia of all of the configurations studied. Importantly though, when the moment of inertia was eliminated as a design parameter, this optimal design configuration still performed the best. From the perspective of VAWT power performance in unsteady gusty winds, the results suggest that an optimal turbine design should possess these three characteristics: (i) low mass moment of inertia, (ii) high peak C_P value, and (iii) broad C_P–TSR curve. Future work aims to validate these results with experimental performance data.

The optimal turbine design identified in the present study considers power performance as the only metric. Structural performance, however, also plays an important role in wind turbine design. The turbine must be designed to withstand the high forces encountered due to applied wind loading on the turbine blades and supports. This is particularly critical for turbines implemented in urban/suburban areas that experience highly fluctuating wind speeds. The present study illustrates the range of forces that can be expected to act on the turbine during a full year of operation. Future work aims to utilize this information to analyze the structural behavior of various turbine designs. For example, increasing turbine solidity (bigger chord length) or using a thicker airfoil shape might enhance structural integrity,

but may simultaneously degrade the power performance of the turbine. Examining the trade-off between power and structural performance is an essential next step toward understanding how best to implement wind energy technology in the built environment.

Results from an economic analysis, based on the energy produced during normal operation at one of the test sites, show that the Levelized Cost of Energy (LCOE) for the baseline turbine design decreases cubically with the annual average wind speed. The LCOE value is highly sensitive to the amount of energy produced at locations where the annual average wind speed is relatively low. At sites where the annual average wind speed was about 4.2 m/s or higher, the LCOE of the baseline turbine design was competitive with the national electricity price, which suggests that the deployed VAWT system is economically viable at these sites. The LCOE of all thirteen design configurations was calculated at one of the test sites with an annual average wind speed of 5 m/s. It was discovered that only design configurations with $H/D \geq 1.2$ were economically viable. At this site, turbine designs utilizing both the NACA 0015 and 0018 airfoil blades were found to be economically viable. Furthermore, the optimal design configuration at this site produced electricity at a cost that was 10% less than the national electricity unit price. In all cases, the project costs were assumed to be the same regardless of the turbine design configuration. Further work is necessary to understand how subtle changes in the turbine design parameters, such as solidity and airfoil thickness or chord length, might affect the project cost of the VAWT system, and ultimately the LCOE.

4.6 References

Ackermann, T. and L. Söder, 2002: An overview of wind energy-status 2002. *Renewable and Sustainable Energy Reviews*, **6 (1)**, 67–127.

Alaimo, A., A. Esposito, A. Messineo, C. Orlando, and D. Tumino, 2015: 3d cfd analysis of a vertical axis wind turbine. *Energies*, **8 (4)**, 3013–3033.

Armstrong, S., A. Fiedler, and S. Tullis, 2012: Flow separation on a high reynolds number, high solidity vertical axis wind turbine with straight and canted blades and canted blades with fences. *Renewable Energy*, **41**, 13–22.

American Wind Energy Association (A.W.E.A.), Production tax credit. Accessed: 2017-03-03. URL `http://www.awea.org/production-tax-credit`.

Azau, S., 2010: A breath of fresh air the european wind energy association annual report 2009. Tech. Rep. ISSN 2032-9024, EWEA.

Babu, K. S., N. S. Raju, M. S. Reddy, and D. N. Rao, 2006: The material selection for typical wind turbine blades using a madm approach & analysis of blades. *Proceedings of 18th International Conference on Multiple Criteria Decision Making (MCDM 2006), Chania, Greece, June*, 19–23.

Basara, J. B., et al., 2011: The oklahoma city micronet. *Meteorological Applications*, **18 (3)**, 252–261.

Bedon, G., M. R. Castelli, and E. Benini, 2013: Optimization of a darrieus vertical-axis wind turbine using blade element–momentum theory and evolutionary algorithm. *Renewable Energy*, **59**, 184–192.

Beri, H., Y. Yao, et al., 2011: Double multiple streamtube model and numerical analysis of vertical axis wind turbine. *Energy and Power Engineering*, **3 (03)**, 262.

Bertényi, T., C. Wickins, and S. McIntosh, 2010: Enhanced energy capture through gust-tracking in the urban wind environment. *48th AIAA Aerospace Sciences Meeting, Orlando, Florida, USA*.

Blackwell, B. F., R. E. Sheldahl, and L. V. Feltz, 1976: Wind tunnel performance data for the darrieus wind turbine with naca 0012 blades. Tech. rep., Sandia Labs., Albuquerque, N. Mex.(USA).

Brusca, S., R. Lanzafame, and M. Messina, 2014: Design of a vertical-axis wind turbine: how the aspect ratio affects the turbine?s performance. *International Journal of Energy and Environmental Engineering*, **5 (4)**, 333–340.

Castelli, M. R., S. De Betta, and E. Benini, 2012: Effect of blade number on a straight-bladed vertical-axis darreius wind turbine. *World Academy of Science, Engineering and Technology*, **61**, 305–3011.

Chong, W., K. Pan, S. Poh, A. Fazlizan, C. Oon, A. Badarudin, and N. Nik-Ghazali, 2013: Performance investigation of a power augmented vertical axis wind turbine for urban high-rise application. *Renewable Energy*, **51**, 388–397.

Fiedler, A. and S. Tullis, 2009: Blade offset and pitch effects on a high solidity vertical axis wind turbine. *Wind Engineering*, **33 (3)**, 237–246.

Islam, M., D. S.-K. Ting, and A. Fartaj, 2008: Aerodynamic models for darrieus-type straight-bladed vertical axis wind turbines. *Renewable and Sustainable Energy Reviews*, **12 (4)**, 1087–1109.

Jacobs, E. N. and A. Sherman, 1937: Airfoil section characteristics as affected by variations of the reynolds number. Tech. Rep. 586, National Advisory Committee for Aeronautics.

Jureczko, M., M. Pawlak, and A. Mezyk, 2005: Optimisation of wind turbine blades. *Journal of Materials Processing Technology*, **167 (2)**, 463–471.

Kaldellis, J., 2002: Optimum autonomous wind–power system sizing for remote consumers, using long-term wind speed data. *Applied Energy*, **71 (3)**, 215–233.

Lavappa, K.-J., P.D., 2015: Energy price indices and discount factors for life -cycle cost analysis. Tech. Rep. NISTR 85-3273-30, National Institute of Standards and Technology - US Department of Commerece.

Leung, D. Y. and Y. Yang, 2012: Wind energy development and its environmental impact: A review. *Renewable and Sustainable Energy Reviews*, **16 (1)**, 1031–1039.

Lindenberg, S., 2009: *20% Wind Energy By 2030: Increasing Wind Energy' s Contribution to US Electricity Supply*. Diane Publishing.

Mahmoud, N., A. El-Haroun, E. Wahba, and M. Nasef, 2012: An experimental study on improvement of savonius rotor performance. *Alexandria Engineering Journal*, **51 (1)**, 19–25.

McIntosh, S., H. Babinsky, and T. Bertenyi, 2007: Optimizing the energy output of vertical axis wind turbines for fluctuating wind conditions. *45th AIAA Aerospace Sciences Meeting and Exhibit, Reno, Nevada*.

McIntosh, S., H. Babinsky, and T. Bertenyi, 2008: Unsteady power output of vertical axis wind turbines operating within a fluctuating free-stream. *46th AIAA Aerospace Sciences Meeting and Exhibit, Reno, Nevada*.

McIntosh, S. C., 2009: Wind energy for the built environment. Ph.D. thesis, University of Cambridge.

Mohamed, M., 2012: Performance investigation of h-rotor darrieus turbine with new airfoil shapes. *Energy*, **47 (1)**, 522–530.

Nguyen, L. and M. Metzger, 2015: Enhanced energy capture by a vertical axis wind turbine during gusty winds in an urban/suburban environment. *Journal of Renewable and Sustainable Energy*, **7 (5)**, 053 118.

Nguyen, L. and M. Metzger, 2017: Comparison of forecasting methods for vertical axis wind turbine applications in an urban/suburban area. *Journal of Renewable and Sustainable Energy*, **9 (2)**, 023 302.

Paraschivoiu, I., 2002: *Wind turbine design: with emphasis on Darrieus concept*. Presses inter Polytechnique.

Paraschivoiu, I. and F. Delclaux, 1983: Double multiple streamtube model with recent improvements (for predicting aerodynamic loads and performance of darrieus vertical axis wind turbines). *Journal of Energy*, **7 (3)**, 250–255.

Paraschivoiu, I., F. Delclaux, P. Fraunie, and C. Beguier, 1983: Aerodynamic analysis of the darrieus rotor including secondary effects. *Journal of Energy*, **7 (5)**, 416–422.

Roh, S.-C. and S.-H. Kang, 2013: Effects of a blade profile, the reynolds number, and the solidity on the performance of a straight bladed vertical axis wind turbine. *Journal of Mechanical Science and Technology*, **27 (11)**, 3299–3307.

Schubel, P. J. and R. J. Crossley, 2012: Wind turbine blade design. *Energies*, **5 (9)**, 3425–3449.

Sheldahl, R. E. and P. C. Klimas, 1981: Aerodynamic characteristics of seven symmetrical airfoil sections through 180-degree angle of attack for use in aerodynamic analysis of vertical axis wind turbines. Tech. rep., Sandia National Labs., Albuquerque, NM (USA).

Staffell, I. and R. Green, 2014: How does wind farm performance decline with age? *Renewable Energy*, **66**, 775–786.

Stefan Gsnger, J. D.-P., 2015: 2015 small wind world report summary. Tech. Rep. March 2015 Report, WWEA.

Strickland, J. H., 1975: Darrieus turbine: a performance prediction model using multiple streamtubes. Tech. rep., Sandia Labs., Albuquerque, N. Mex.(USA).

Strickland, J. H., B. Webster, and T. Nguyen, 1980: Vortex model of the darrieus turbine: an analytical and experimental study. Tech. Rep. SAND-79-7058, Texas Tech Univ., Lubbock (USA).

Templin, R., 1974: Aerodynamic performance theory for the nrc vertical-axis wind turbine. *NASA STI/Recon Technical Report N*, **76**, 16 618.

Tirkey, A., Y. Sarthi, K. Patel, R. Sharma, and P. K. Sen, 2014: Study on the effect of blade profile, number of blade, reynolds number, aspect ratio on the performance of vertical axis wind turbine. *International Journal of Science, Engineering and Technology Research (IJSETR)*, **3 (12)**.

CHAPTER 5

CONCLUSION

The primary and direct impact of the work in this research is to broaden the current understanding of the transient response of a vertical axis wind turbine operating in gusty winds representative of an urban/suburban environment and examine the conditions under which the wind turbine would constitute an economically viable alternative to electricity generated from fossil-fuel power plants. The present results show that the amount of available energy in gusty wind, relative to that of the mean wind, increases quadratically with turbulence intensity. This provides motivation for striving to harness as much energy from wind gusts as possible. For both types of system controllers (constant rotational speed controller and ideal TSR controller), the efficiency of the turbine was found to be strongly dependent on the turbulence intensity of the wind condition. The effect of gust frequency on turbine efficiency was observed to be insignificant. The mean wind speed also had a significant impact on the turbine efficiency due to the Reynolds number effect on the aerodynamic flow over the turbine blades.

For the case of the constant rotational speed controller, it was shown that the turbine should be operated at an overspeed setting (ω_{opt}) based on the turbulence intensity of the incoming wind in order to harvest as much energy as possible. The optimal overspeed setting (ω_{opt}) was found to be quadratically correlated with the wind turbulence intensity. This has practical implications on VAWT installation in urban areas, as one only needs an estimate of the expected turbulence intensity of the wind in order to dial in the proper overspeed setting on the turbine to harness the maximum amount of energy possible using a constant-ω controller. Using an optimal overspeed setting allowed for significant energy to be captured, e.g., a factor of six

times greater during the year of 2013 at William Browning Building compared to the energy captured using a fixed speed based naively on the annual average wind speed.

For the case of the ideal tip speed ratio controller ($ideal - TSR$), the turbine efficiency was observed to plateau to a maximum value when the nondimensional turbine response parameter ζ drops below the critical value ζ_c. For the regime $\zeta < \zeta_c$, the turbine responds quickly to fluctuations in the wind, allowing the wind turbine to efficiently capture energy from the wind. As the turbine response parameter increases above the critical value ($\zeta > \zeta_c$), the turbine is no longer able to closely track the wind gust, and a decrease in turbine efficiency is observed. In addition, the results show that a fast response VAWT is capable of harnessing an order of magnitude or more energy during gusty wind with the $ideal - TSR$ controller, compared to simply operating the turbine at a TSR based on the corresponding mean wind speed. This is significant because the concept of an $ideal - TSR$ controller may provide the difference necessary in order to make the wind technology viable in some urban areas, whereas a wind turbine operating with a constant-ω controller would not be capable of providing enough energy to make the investment worthwhile. This would be especially true for typical wind conditions in urban areas, where the annual average wind speed is relatively low, but the wind gusts are significant.

The study also seeks to provide solutions for improving the turbine efficiency and energy captured by investigating different methods of wind condition forecasting. Wind data from the combined sites in Oklahoma City demonstrate that forecasting uncertainty has a significant impact on the amount of energy captured by the wind turbine. Specifically, a 5% increase in forecasting accuracy could increase the total energy captured as much as 13%. This increase could make a significant difference in terms of the VAWT being a viable renewable technology in many urban areas. Forecasting is only applied on the constant-ω controller as the wind condition is required to be known in advance in order to set the operating point (rotational speed) of the wind turbine. For all the test cases, the four examined forecasting models allow the VAWT to capture approximately 78% to 85% of the ideal amount of energy that could be captured assuming the actual wind data were available in real time. The modified persistence model (MPM) outperformed the persistence model (PM),

autoregressive moving average (ARMA), and weather research and forecasting model (WRF) by capturing as much as 6% more energy. When compared to the case of no forecasting, the MPM improved the total amount of energy captured over the full year of operation as much as 17.3%. The MPM method only involves one tuned parameter, an adjustment factor (AF), that was found to be site independent and linearly correlated with the annual average wind speed. This empirical relationship has a potential practical application that one can estimate the average annual average wind speed of the advanced year, and then set an appropriate AF value for the controller for the subsequent year. The amount of training data and forecasting horizon in the ARMA model was found to be site dependent. In terms of the amount of energy captured, the WRF model performed as well as the ARMA model; however, the WRF has the potential to perform even better with enhanced grid resolution, especially in the vertical direction.

The study also investigates the optimal VAWT design for application in gusty wind conditions typical of an urban/suburban environment. Thirteen turbine design configurations were examined. Four design parameters were varied, including the height-to-diameter aspect ratio, blade airfoil shape, turbine solidity, and turbine moment of inertia. Of the thirteen configurations examined, the optimal wind turbine design capable of harvesting the most energy from the gusty wind was found to have an aspect ratio of 1.2, solidity of 12%, and blade shape based on the NACA 0015 airfoil. The results suggest that the turbine configuration with the peak power coefficient (C_P) does not necessarily capture the most energy when exposed to unsteady wind speeds. From the perspective of VAWT power performance in unsteady gusty winds, the results suggest that an optimal turbine design should possess these three characteristics: (i) low mass moment of inertia, (ii) high peak C_P value, and (iii) broad $C_P - TSR$ curve. Besides the power performance, the turbine must also be designed to withstand the high forces encountered due to applied wind loading on the turbine blades and supports. This is particularly critical for turbines implemented in urban/suburban areas that experience highly fluctuating wind speeds. To increase the turbine structural integrity, the turbine solidity or airfoil thickness could be increased; however, this may simultaneously degrade the power performance

of the turbine. Examining the trade-off between the power and structural performance is essential in optimizing a VAWT design for the built environment.

An economic analysis was conducted in order to quantify the economic viability of the VAWT system and determine the conditions under which the system should be deployed. The economic analysis shows that the LCOE values decrease cubically with the annual wind speed. The LCOE value is highly sensitive on the amount of energy produced by the wind turbine at locations where the annual wind speed is relatively low. The LCOE suggests that the ideal-TSR controller is more economical and viable compared to the constant-ω controller. At the sites where the annual average wind speed is about 4.2 m/s or higher, the LCOE of the system is competitive with the national electricity price and the deployed VAWT system is economically viable at these sites.

The research presented in this dissertation has advanced scientific knowledge in the area of VAWT power performance when the turbine is deployed in realistic unsteady wind conditions. Prior to this, the literature has focused on VAWT performance under steady winds. The results provide a guide for designing small-scale VAWTs appropriate for installation on the rooftops of houses and buildings in urban/suburban areas. In addition, the investigation of different wind turbine configurations, turbine controllers, and wind forecasting methods have demonstrated that the Darrieus wind turbine is a promising (and economically competitive) renewable energy technology for harvesting wind energy in the built environment. It is hoped that the knowledge and findings from this study would be beneficial for the future of wind turbine design and motivate more investment from industry and energy consumers into vertical axis wind turbines in order to realize our vision of an energy-neutral sustainable city.

5.1 Future Works

There are certain extensions to the work presented in this dissertation that were either beyond the scope of the study, or only briefly addressed. The work presented in Chapter 4 only discussed the wind turbine optimization based on the power/energy performance of the turbines. However, structural performance of the turbine is another important factor in wind turbine design. During the operation, the turbine

experiences a significant loading, especially on its turbine blades (Jureczko et al., 2005; Schubel and Crossley, 2012). Therefore, the turbine design must be structurally sound in order to sustain this loading on its blades and supports. In a study performed by Paraschivoiu et al. (1983), airfoil shape NACA 0015 is suggested for small-scale wind turbine in terms of power performance; while NACA 0018 is recommended for structural purposes. Therefore, the full-strength structural evaluation should be performed to examine the structural performance of each wind turbine configuration. This could be performed using several available commercial software packages such as SolidWorks, Abaqus, and Comsol in combination with Fluent. In addition, some aspects of turbine configuration could be explored to improve the structural integrity of the turbine such as increasing turbine solidity or airfoil thickness or material selection of the turbine blades. However, this variation may simultaneously degrade the power performance of the turbine. Examining the trade-off between the power and structural performance is an essential next step toward understanding how best to implement wind energy technology in the built environment.

Another extension of this current work is to characterize different loading forces that act on the turbine blades during operation in gusty wind conditions. The work presented in Chapter 4 briefly studied the aerodynamic load acting on the blades in the form of the normal force (thrust). The results suggest the normal force increases rapidly with the wind speed. In addition to the aerodynamic load, the turbine also experiences different types of loading such as static load, stochastic load, and inertia load acting on the turbine blades (Jureczko et al., 2005; Schubel and Crossley, 2012). The stochastic load is derived from the wind turbulence and is relevant to the fatigue response of the wind turbine structure. In fact, these loads in combination with the aerodynamic load are the ones that can cause the most structural failure on wind turbine blades, particularly due to fatigue. Future work aimed at quantifying these applied loadings will be informative and useful in order to determine whether the optimal turbine design configuration identified herein is structurally viable for implementation in the real world.

The results from the present study suggest that the wind condition, as characterized by the mean wind speed and turbulence intensity, has a significant impact on

the overall performance of the turbine and the optimal wind turbine configuration. This is especially true for gusty wind conditions typical of the urban/suburban environment. As apparent from Figure 4.7, a nearly linear correlation between the turbine moment of inertia (I) and the standard deviation of the energy ratio (σ_E/E_a) was observed from the thirteen wind turbine configurations examined. This correlation suggests a relationship between the optimal wind turbine configuration and the incoming wind characteristics. It would be convenient and easy for a wind turbine engineer/designer if simple computational software existed that output the optimal wind turbine configuration for a particular urban application, given the desired location of installation and size constraints, for example. It is also preferred that this computational software incorporate a structural analysis and modify the optimal design accordingly, such as increasing the thickness of the airfoil or solidity, for example. An extensive study of different wind turbine configurations and wind conditions should be performed as part of this future work.

The numerical results presented in this dissertation require experimental validation. In particular, it remains to be determined whether use of static lift and drag coefficients in BEM is accurate for the transient case where winds are unsteady. Ideally, experimental validation should be performed both in the laboratory and in the field. In the laboratory, one could conduct wind tunnel tests using a scaled model of one of the VAWT configurations examined in Chapter 4. It would be important to be able to vary the incoming wind speed in a manner similar to the actual atmospheric flow observed at the Oklahoma sites. Most wind tunnel fans utilize a frequency controller that could be programmed to vary the wind speed with time according to a prescribed signal; however, it is unclear how quickly the wind tunnel fan could respond. Therefore, these laboratory experiments may not be trivial. In addition, it would be useful to conduct in situ field experiments using a rooftop-mounted VAWT. Work is currently in progress to mount a small VAWT on the rooftop of the Kennecott Building. In both cases, the aerodynamic torque generated and rotational speed of the turbine rotor should be measured simultaneously in order to calculate power as a function of time, and total energy captured by the wind turbine. Experimental validation will help increase confidence in the results produced

by the present numerical models. The experiments will also provide a benchmark database against which future numerical models may be validated.

Finally, the results presented this dissertation mainly focused on the Darrieus vertical axis wind turbine. This research should be further extended for the application on the helical wind turbine that has been studied extensively in the recent years (Berténi et al., 2010; Scheurich et al., 2010; McIntosh and Babinsky, 2012). The helical wind turbine was innovated from the Gorlov helical turbine that had its blade twisted and covered total 360° revolution (Gorlov, 1995). The helical wind turbine has gained popularity in residential and urban areas because of its low starting wind speed and fast response behavior (Berténi et al., 2010). Many wind turbine manufacturers have started manufacturing and selling helical wind turbine for the industrial use with two big manufacturers: QuietRevolution and Urban Green Energy (UGE) International. An extension of this research on the helical wind turbine would allow the engineer to determine the practicality and viability of the system operating in the gusty wind condition representative of an urban/suburban area.

5.2 References

Berténi, T., C. Wickins, and S. McIntosh, 2010: Enhanced energy capture through gust-tracking in the urban wind environment. *48th AIAA Aerospace Sciences Meeting, Orlando, Florida, USA*.

Gorlov, A., 1995: The helical turbine: A new idea for low-head hydro. *Hydro Review*, **14 (5)**.

Jureczko, M., M. Pawlak, and A. Mezyk, 2005: Optimisation of wind turbine blades. *Journal of Materials Processing Technology*, **167 (2)**, 463–471.

McIntosh, S. C. and H. Babinsky, 2012: Aerodynamic modeling of swept-bladed vertical axis wind turbines. *Journal of Propulsion and Power*, **29 (1)**, 227–237.

Paraschivoiu, I., F. Delclaux, P. Fraunie, and C. Beguier, 1983: Aerodynamic analysis of the darrieus rotor including secondary effects. *Journal of Energy*, **7 (5)**, 416–422.

Scheurich, F., T. Fletcher, and R. Brown, 2010: The influence of blade curvature and helical blade twist on the performance of a vertical-axis wind turbine. *48th AIAA Aerospace Sciences Meeting Including the New Horizons Forum and Aerospace Exposition*, 1579.

Schubel, P. J. and R. J. Crossley, 2012: Wind turbine blade design. *Energies*, **5 (9)**, 3425–3449.

APPENDIX

DYNAMIC STALL MODEL

A.1 Introduction

The majority of numerical models based on BEM theory incorporate static airfoil data to calculate lift and drag on the turbine blade elements. It is well known that lift and drag forces acting on an airfoil undergo hysteresis in unsteady wind conditions due to the phenomenon of dynamic stall. Dynamic stall is characterized by flow separation, vortex shedding, and reattachment of the flow over the upper lifting surface of the airfoil (Paraschivoiu, 2002; Schuerich and Brown, 2011). In the application of wind turbines, dynamic stall occurs because the airfoil blades undergo rapid variations in angle of attack as the blades rotate about the rotor shaft. A CFD study performed by Schuerich and Brown (2011) showed that, at moderate tip speed ratio, the use of dynamic stall data more accurately captures the behavior of the normal and tangential forces on the blades of a helical VAWT compared to that using static airfoil data. Masson et al. (1998) also showed that incorporating dynamic stall data in a multiple streamtube BEM model yielded better agreement of the power performance curves with experimental data, compared to the same BEM model using static airfoil data.

The aim of the dynamic stall model is to numerically compute the dynamic lift and drag characteristics of the airfoil from the available static coefficients. An overview of dynamic stall models adapted for VAWT applications can be found in Paraschivoiu (2002). Many of these models originate from the 1973 Gormont model (Gormont, 1973), derived from experimental data of the dynamic stall on helicopter blades. The Gormont model, however, overpredicts the effect of dynamic stall in the performance of VAWTs. Several modifications to the Gormont model have been suggested to better predict wind turbine performance (Strickland et al., 1980; Berg, 1983; Paraschivoiu

et al., 1988). Strickland et al. (1980) proposed an adaption to the Gormont model that utilized a modified angle of attack. A few years later, Berg (1983) proposed a method based on a linear interpolation between the dynamic coefficients predicted by the Gormont model and the static coefficients. Comparison with experimental data suggests Berg's modification provides a more accurate prediction of wind turbine performance (Paraschivoiu, 2002). Although incorporating the effect of dynamic stall has been shown to improve one's ability to model the power performance curves of VAWTS, it remains to answer how much this alters the prediction of total energy captured by a VAWT operating in gusty wind conditions. In the present study, we compare the output from our numerical model using both dynamic and static lift/drag coefficients. The dynamic lift/drag coefficients were determined from the static coefficients using the Gormont model with the Berg correction, as described in the next section: Numerical Model.

A.2 Numerical Model

A.2.1 Gormont Model

The Gormont model empirically mimics the hysteresis response of the airfoil blade during dynamic stall, by defining a reference angle of attack (α_{ref}) that is different than the geometric angle of attack (α). The reference angle of attack is defined as

$$\alpha_{ref} = \alpha - K\,\delta\alpha \tag{A.1}$$

where

$$K = \begin{cases} 1, & \text{for } \dot{\alpha} \geq 0, \\ -0.5, & \text{for } \dot{\alpha} < 0. \end{cases} \tag{A.2}$$

Here, $\delta\alpha$ describes the delay angle of attack, K represents a delay parameter in Gormont's Model, and $\dot{\alpha}$ is the rate of change of the angle of attack. Based on Gormont's empirical observations, the delay angle of attack is proportional to the nondimensional rate parameter S,

$$S = \sqrt{\left|\frac{c\dot{\alpha}}{2V_r}\right|} \tag{A.3}$$

where c is the chord length and V_r is the relative velocity on the airfoil blade. Gormont observed that for higher S values, dynamic stall is delayed to larger angles of attack.

This delay in angle of attack can then be calculated as

$$\delta\alpha = \begin{cases} \gamma_1 S, & \text{for } S \le S_c, \\ \gamma_1 S_c + \gamma_2 (S - S_c), & \text{for } S > S_c, \end{cases} \tag{A.4}$$

where S_c represents a critical value of S, defined as

$$S_c = 0.06 + 1.5\left(0.06 - \frac{t}{c}\right), \tag{A.5}$$

with t denoting the airfoil thickness. The parameters γ_1 and γ_2 in (A.4) are determined as follows,

$$\gamma_1 = \begin{cases} \frac{\gamma_2}{2}, & \text{for lift,} \\ 0, & \text{for drag,} \end{cases} \tag{A.6}$$

where

$$\gamma_2 = \gamma_{max} \max\left(0, \min\left[1, \frac{M - M_2}{M_1 - M_2}\right]\right). \tag{A.7}$$

M denotes the Mach number of the airfoil blade section. The Mach number is calculated as $M = V_r/V_s$, where V_s represents the speed of sound (having a value of 340.3 m/s in standard air). Other parameters, including γ_{max}, M_1 and M_2, have different specific forms for the lift and drag characteristics as listed in Table A.1.

Finally, the dynamic lift and drag coefficients are given by

$$C_D^{dyn} = C_D(\alpha_{ref}) \tag{A.8}$$

and

$$C_L^{dyn} = C_L(\alpha_o) + m(\alpha - \alpha_o) \tag{A.9}$$

where

$$m = \min\left[\frac{C_L(\alpha_{ref}) - C_L(\alpha_o)}{\alpha_{ref} - \alpha_o}, \frac{C_L(\alpha_{ss}) - C_L(\alpha_o)}{\alpha_{ss} - \alpha_o}\right] \tag{A.10}$$

Table A.1: Specific forms for the parameters in (A.7) of the Gormont model

Parameter	Lift Characteristic	Drag Characteristic
M_1	$0.4 + 5.0(0.06 - t/c)$	0.2
M_2	$0.9 + 2.5(0.06 - t/c)$	$0.7 + 2.5(0.06 - t/c)$
γ_{max}	$1.4 + 6.0(0.06 - t/c)$	$1.0 + 2.5(0.06 - t/c)$

In the above expression, α_o is any convenient angle of attack, but typically is taken as the zero-lift angle of attack, and α_{ss} is the static stall angle of attack. It is worth mentioning that the value for the reference angle of attack (α_{ref}) is different for the lift and drag characteristics. Note, the value of α_{ref} also varies with yaw angle as the wind turbine blades rotate.

A.2.2 Berg Model

The Gormont model was developed for helicopter blades, in which the maximum angle of attack reached is much lower than the angle of attack of VAWT blades during operation. Therefore, Berg hypothesized that the pure Gormont model might overpredict the dynamic lift and drag characteristic of the airfoil blades on a VAWT, thus overpredicting the dynamic stall effect on VAWT performance. To avoid this overprediction, Massé (1981) proposed a method to compute the modified dynamic coefficients (C_L^{mod} and C_D^{mod}) based on a linear interpolation between the dynamic coefficients (C_L^{dyn} and C_D^{dyn}) predicted by the Gormont model and the available static coefficients (C_L and C_D), as follows

$$C_L^{mod} = \begin{cases} C_L + \left[\frac{A_M\alpha_{ss}-\alpha}{A_M\alpha_{ss}-\alpha_{ss}}\right]\left(C_L^{dyn} - C_L\right), & \text{for } \alpha \le A_M\alpha_{ss}, \\ C_L, & \text{for } \alpha > A_M\alpha_{ss}. \end{cases} \tag{A.11}$$

$$C_D^{mod} = \begin{cases} C_D + \left[\frac{A_M\alpha_{ss}-\alpha}{A_M\alpha_{ss}-\alpha_{ss}}\right]\left(C_D^{dyn} - C_D\right), & \text{for } \alpha \le A_M\alpha_{ss}, \\ C_D, & \text{for } \alpha > A_M\alpha_{ss}. \end{cases} \tag{A.12}$$

where A_M is a Masse damping coefficient. Massé (1981) proposed a value A_M = 1.8. Starting with the above modification, Berg (1983) further proposed using A_M = 6. This new A_M value gave good agreement between numerical results and experimental data of the power performance for a 17 m Sandia eggbeater VAWT with NACA0015 airfoil blades (Shires, 2013). The optimal value of A_M seemed to be dependent on the relative thickness of the airfoil; for example, A_M=∞ was found to be more appropriate for wind turbine with NACA 0018 and SNLA 0018 airfoils (Masson et al., 1998; Shires, 2013). Berg also proposed the definition of static stall angle of attack (α_{ss}) as the angle at which the variation of the lift coefficient with respect to the angle of attack begins to depart from the linear behavior. In the present study, our numerical model uses Berg's model to calculate the dynamic lift and drag coefficients during the dynamic

stall phenomenon. The dynamic lift and drag coefficients are later incorporated in the Blade Element Momentum (BEM) model to predict the power performance of the turbine. Detailed description of the BEM model can be found in the section: Turbine Model in Chapter 2 of this dissertation.

A.3 Preliminary Results

The main objective of this appendix is to investigate the effect of the dynamic stall phenomena on the power performance of the wind turbine. This is done by comparing the C_P-TSR curve from the dynamic stall model to the one obtained using the static lift and drag coefficients. For this comparison, the turbine is subjected to a steady wind speed. A straight blade Darrieus type VAWT (also referred as an H-rotor turbine) with three blades is examined. The turbine blades have a chord length (c) of 12 cm and are based on the NACA 0015 airfoil shape. The turbine has a height (H) of 2.4 m and diameter (D) of 2.0 m. The turbine solidity (S), defined as the ratio of the area of the blades ($N \cdot c \cdot H$) to the turbine frontal area ($H \cdot D$), is 18%.

Figure A.1 shows the power coefficient versus tip speed ratio (C_P-TSR) curves of the examined turbine model using the static and dynamic stall models. The power coefficient curves are all simulated at a wind speed of 7 m/s. Different delay parameters (K_1) and Masse damping coefficients (A_M) are used in the dynamic stall model as recommended by previous studies (Berg, 1983; Masson et al., 1998; Shires, 2013). As shown in Figure A.1, in all cases, the C_P-TSR curve obtained from the static model outperforms the ones computed by the dynamic stall models. The difference between the peak C_P values between the static and dynamic stall models is approximately 36%. The results also show that the delay parameter, K_1, seems to have little impact on the overall power performance of the turbine compared to the impact of the Masse damping coefficient, A_M. Changing the delay parameter K_1 from -0.5 to 0 seems to slightly improve the power coefficient of the turbine in the low TSR regime. For K_1 = 0, changing the Masse damping coefficient from A_M = 6 to A_M = ∞ increases the peak C_P value from 0.241 to 0.288, which represents an approximate 20% increase.

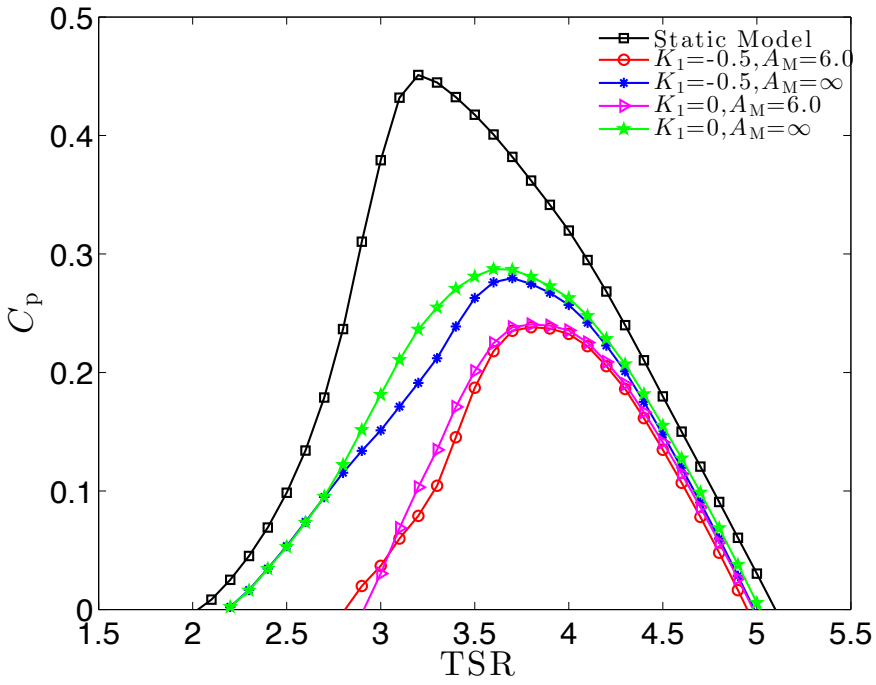

Figure A.1: Power coefficient versus tip speed ratio curve. The colored symbols represent various dynamic stall models with different delay parameters (K) and Masse damping coefficients (A_M) as indicated. In all cases, the incoming wind speed is 7 m/s.

Previous researchers have identified a need to tune the Masse damping coefficient (A_M) to better define the effect of dynamic stall on the aerodynamic lift and drag of different VAWT configurations (Shires, 2013; Berg, 1983; Masson et al., 1998). In his original study, Massé (1981) proposed the use of A_M = 1.8 for all turbine configurations. It is well known that the dynamic stall phenomena is complex and varies significantly with airfoil shape and Reynolds number (Shires, 2013). Therefore, the manner in which dynamic stall affects the overall performance of a turbine is expected to depend on the turbine configuration (blade airfoil shape, chord length, aspect ratio, and solidity). In fact, many different values of the damping coefficient have been proposed for different wind turbine configurations to account for these design variations (Berg, 1983; Masson et al., 1998; Shires, 2013).

In a study performed by Berg (1983), the results suggested that the dynamic stall model with A_M = 6.0 provided good agreement with experimental results for

the case of a 17 m eggbeater VAWT with blades in the shape of the NACA 0015 airfoil. It is questionable, however, whether this damping coefficient may be applicable to other configurations. A study performed by Masson et al. (1998) on a 24 m eggbeater VAWT with NACA 0018 airfoils suggested that a damping coefficient of A_M=∞ provided better simulation results compared to A_M = 6. Masson et al. (1998) further suggested that the damping coefficient is a function of blade airfoil geometry, particularly the airfoil thickness to chord length ratio. Similarly, the results from Shires (2013) suggested that at low rotational speed (e.g., 30 rpm), the damping coefficient, A_M = 3.6, provided good agreement with the measured power for a 24 m eggbeater VAWT. In addition, Shires (2013) also proposed further modification to the Gormont model that is more appropriate for H-rotor VAWTs, neglecting the dynamic lift and drag for negative rates of change of the angle of attack ($\dot{\alpha} < 0$). Specifically, the model proposed a modification to equation A.2 such that K_1 = 0 for $\dot{\alpha} < 0$. The results from that study indicated that the modification provided improvement of the simulated power compared to that obtained using the original Gormont model.

A.4 Conclusion

The present results show that the dynamic stall phenomenon (as modeled following Berg) tends to dramatically decrease turbine performance. Unfortunately, there are no experimental data by which to validate the present numerical findings due to the difference in the turbine configuration used here compared to those in the literature. Previous studies (e.g., Masson et al. (1998); Shires (2013)) indicate that the effect of the dynamic stall model on VAWT performance can vary significantly depending on the wind turbine configuration, including turbine solidity, chord length, and airfoil shape. In addition, a universal value for the damping coefficient (A_M) does not exist, meaning this value must be tuned according to the turbine configuration. At this time, it remains unclear how to select an appropriate A_M for a given turbine configuration.

Finally, whereas the dynamic stall models presented in this appendix account for the rate of change of the angle of attack of the airfoil, they do not allow for changing Reynolds numbers, as would be the case for a VAWT. That is, for a VAWT, both the

magnitude and direction of the resultant velocity vector acting at the center of lift of the airfoil blades can change considerably during one revolution depending on the tip speed ratio and incoming wind speed. Accounting for this unsteady effect may be needed in order to obtain the correct dynamic stall behavior on VAWT blades. Further work beyond the scope of this dissertation is necessary in order to resolve the discrepancy between the C_p–TSR curves observed using the static airfoil data and those using the dynamic stall model.

A.5 References

Berg, D. E., 1983: Improved double-multiple streamtube model for the darrieus-type vertical-axis wind turbine. Tech. Rep. SAND-82-2479C, Sandia National Labs., Albuquerque, NM (USA).

Gormont, R. E., 1973: A mathematical model of unsteady aerodynamics and radial flow for application to helicopter rotors. Tech. Rep. D210-10492-1, DTIC Document.

Massé, B., 1981: *Description de deux programmes d'ordinateur pour le calcul des performances et des charges aérodynamiques pour les éoliennes à axe vertical*. Institut de recherche de l'Hydro-Québec.

Masson, C., C. Leclerc, and I. Paraschivoiu, 1998: Appropriate dynamic-stall models for performance predictions of vawts with nlf blades. *International Journal of Rotating Machinery*, **4 (2)**, 129–139.

Paraschivoiu, I., 2002: *Wind turbine design: with emphasis on Darrieus concept*. Presses inter Polytechnique.

Paraschivoiu, I., P. Desy, and C. Masson, 1988: Blade tip, finite aspect ratio, and dynamic stall effects on the darrieus rotor. *Journal of Propulsion and Power*, **4 (1)**, 73–80.

Schuerich, F. and R. E. Brown, 2011: Effect of dynamic stall on the aerodynamics of vertical-axis wind turbines. *AIAA Journal*, **49 (11)**, 2511–2521.

Shires, A., 2013: Development and evaluation of an aerodynamic model for a novel vertical axis wind turbine concept. *Energies*, **6 (5)**, 2501–2520.

Strickland, J. H., B. Webster, and T. Nguyen, 1980: Vortex model of the darrieus turbine: an analytical and experimental study. Tech. Rep. SAND-79-7058, Texas Tech Univ., Lubbock (USA).